

Automatic Model Construction with Gaussian Processes



David Kristjanson Duvenaud

University of Cambridge

This dissertation is submitted for the degree of

Doctor of Philosophy

Pembroke College

June 2014

Declaration

I hereby declare that except where specific reference is made to the work of others, the contents of this dissertation are original and have not been submitted in whole or in part for consideration for any other degree or qualification in this, or any other University. This dissertation is the result of my own work and includes nothing which is the outcome of work done in collaboration, except where specifically indicated in the text. This dissertation contains less than 65,000 words including appendices, bibliography, footnotes, tables and equations and has less than 150 figures.

David Kristjanson Duvenaud
June 2014

Acknowledgements

I'd like to thank my supervisor, Carl Rasmussen, for so much advice and encouragement. It was wonderful working with someone who had spent many years thinking deeply about the business of modeling, who also allowed me the freedom to make my own mistakes. I'd also like to thank my advisor, Zoubin Ghahramani, for providing much encouragement and support.

Thanks to Michael Osborne, whose thesis was an inspiration, and to Roman Garnett for making research fun. Sinead Williamson and Peter Orbanz provided valuable advice early on. Philipp Hennig was a mentor to me during my time in Tübingen, and demonstrated an inspiring level of German effectiveness. Who else finishes their conference papers with entire days to spare?

I'd like to thank Andrew McHutchon, Konstantina Palla, Alex Davies and Neil Houlsby for making the lab feel like a family. I'd like to thank James Lloyd for the many endless discussions, and for keeping a level head even during the depths of deadline death-marches.

Roger Grosse demonstrated the power of deeply understanding the basics, and how much we still don't know about simple things. Josh Tenenbaum's infectious enthusiasm and broad perspective made every project much more rewarding. Christian Steinruecken constantly reminded me that amazing things are hidden all around.

My graduate study was supported by the National Sciences and Engineering Research Council of Canada, The Cambridge Commonwealth Trust, Pembroke College, and a grant from Google.

Abstract

This thesis develops a broad class of models, useful for learning and forecasting in such domains as time series, geological formations, and physical dynamics. These models are based on Gaussian processes, which can express a wide variety of statistical structure, depending on the choice of kernel. Historically, the type of kernel has been chosen by hand by experts. In this thesis, we show how to automate this task, creating an artificial statistician capable of systematically exploring a large space of models.

The introductory chapters show many types of structure, such as periodicity, change-points, additivity, and symmetries can be encoded by kernels, and that these structure can be combined by combining kernels. For example, compound kernels can produce priors over topological manifolds such as cylinders, toruses, and Möbius strips, as well as their higher-dimensional analogues.

The main contribution of this thesis is to show how this open-ended space of models can be explored automatically. To do so, we define a simple grammar over kernels, a search criterion (marginal likelihood), and a breadth-first search procedure. Combining these, we present a procedure which takes a dataset, and outputs an automatically-constructed model, along with a detailed report with graphs and automatically-generated text illustrating the qualitatively different, and potentially novel, types of structure discovered in that dataset. This system automates parts of the model-building and analysis currently performed by expert statisticians.

This thesis also explores several extensions to Gaussian process models. First, building on earlier work relating Gaussian processes and neural nets, we explore the natural extensions of these models to *deep kernels* and *deep Gaussian processes*. Second, we examine the model class consisting of the sum of functions of all possible combinations of input variables. We show a close connection between this model class and the recently-developed regularization method of *dropout*. Third, we combine Gaussian processes with the Dirichlet process to produce the *warped mixture model* – an unsupervised clustering model with nonparametric cluster shapes, and a corresponding latent space in which each cluster has an interpretable parametric form.

Contents

Contents	v
List of Figures	ix
List of Tables	xi
Notation	xii
1 Introduction	1
1.1 Gaussian Process Models	1
1.1.1 Model Selection	3
1.1.2 Prediction	4
1.1.3 Useful Properties of Gaussian Processes	4
1.1.4 Limitations of Gaussian Processes	5
1.2 Outline and Contributions of Thesis	6
2 Expressing Structure with Kernels	8
2.1 Definition	8
2.2 A Few Basic Kernels	9
2.3 Combining Kernels	10
2.3.1 Notation	10
2.3.2 Combining Properties through Multiplication	10
2.3.3 Building Flexible Multidimensional Models	12
2.4 Modeling Sums of Functions	13
2.4.1 Additivity Across Multiple Dimensions	14
2.4.2 Long-range Extrapolation through Additivity	15
2.4.3 Example: An Additive Model of Concrete Strength	15
2.4.4 Posterior Variance of Additive Components	17

2.5	Changepoints	19
2.5.1	Multiplication by a Known Function	20
2.6	Feature Representation	20
2.6.1	Relation to Linear Regression	20
2.6.2	Feature-space view of Combining Kernels	21
2.7	Expressing Symmetries and Invariants	21
2.7.1	Three Recipes for Group Invariance	22
2.7.2	Periodicity	24
2.7.3	Symmetry About Zero	24
2.7.4	Translation Invariance in Images	25
2.8	Generating Topological Manifolds	26
2.8.1	Möbius Strips	27
2.9	Kernels on Categorical Variables	28
2.10	Building a Kernel in Practice	28
3	Automatic Model Construction	29
3.1	Ingredients of an Automatic Statistician	30
3.2	A Language of Regression Models	31
3.3	A Model Search Procedure	32
3.4	A Model Comparison Procedure	34
3.5	A Model Description Procedure	35
3.6	Structure Discovery in Time Series	36
3.6.1	Mauna Loa Atmospheric CO ₂	36
3.6.2	Airline Passenger Counts	36
3.7	Related Work	37
3.8	Experiments	41
3.8.1	Interpretability versus Accuracy	41
3.8.2	Predictive Accuracy on Time Series	41
3.8.3	High-dimensional Prediction	43
3.8.4	Structure Recovery on Synthetic Data	43
3.9	Discussion	44
4	Automatic Model Description	45
4.1	Generating Descriptions of Kernels	46
4.1.1	Simplification Rules	46
4.1.2	Describing Each Kernel in a Product	47

4.1.3	Combining Descriptions into Noun Phrases	47
4.1.4	Worked Example	49
4.2	Example Descriptions	50
4.2.1	Summarizing 400 Years of Solar Activity	50
4.2.2	Describing Varying Noise Levels in Air Traffic Data	51
4.3	Related Work	53
4.4	Conclusion	55
5	Deep Gaussian Processes	56
5.1	Relating Neural Networks to Deep Gaussian Processes	57
5.1.1	Single-layer Models	57
5.1.2	Multiple Hidden Layers	58
5.1.3	Two Network Architectures Equivalent to Deep GPs	59
5.2	Characterizing Deep Gaussian Processes	61
5.2.1	One-dimensional Asymptotics	61
5.2.2	Distribution of the Jacobian	62
5.3	Formalizing a Pathology	64
5.4	Fixing the Pathology	68
5.5	Deep Kernels	71
5.5.1	Infinitely Deep Kernels	72
5.5.2	When are Deep Kernels Useful Models?	73
5.6	Related Work	73
5.7	Conclusions	75
6	Modeling Additive Interactions	76
6.1	Additive Kernels	77
6.1.1	Parameterization	78
6.1.2	Efficient Evaluation of Additive Kernels	79
6.1.3	Computational Cost	80
6.2	Non-local Interactions	80
6.3	Dropout in Gaussian Processes	81
6.3.1	Dropout on Hidden Units	82
6.3.2	Dropout on Inputs	83
6.4	Related Work	83
6.5	Experiments	86
6.5.1	Datasets	87

6.5.2	Results	88
6.5.3	Source Code	90
6.6	Conclusion	90
7	Warped Mixture Models	91
7.1	The Gaussian Process Latent Variable Model	93
7.2	The Infinite Warped Mixture Model	95
7.3	Inference	98
7.3.1	Posterior Predictive Density	99
7.4	Related Work	100
7.5	Experimental Results	102
7.5.1	Clustering Faces	102
7.5.2	Synthetic Datasets	103
7.5.3	Mixing	104
7.5.4	Density Estimation	104
7.5.5	Visualization	105
7.5.6	Clustering Performance	106
7.6	Future Work	108
7.7	Conclusion	108
Appendix A	Gaussian Conditionals	109
Appendix B	Kernel Definitions	110
Appendix C	Search Operators	112
Appendix D	Example Report	114
References		122

List of Figures

1.1	One-dimensional Gaussian process posterior	2
2.1	Examples of one-dimensional structures expressible by multiplying kernels	11
2.2	A product of squared-exponential kernels across different dimensions . . .	12
2.3	Additive kernels correspond to additive functions	14
2.4	Long-range inference in functions with additive structure	15
2.5	Decomposition of posterior into interpretable one-dimensional functions .	16
2.6	Visualizing posterior correlations between components	18
2.7	Draws from changepoint priors	19
2.8	Three ways to introduce symmetry	23
2.9	Generating 2D manifolds with different topological structures	26
2.10	Generating Möbius strips	27
3.1	A search tree over kernels	33
3.2	Progression of models as the search depth increases	34
3.3	Decomposition of the Mauna Loa model	37
3.4	Decomposition of airline dataset model	38
3.5	Comparison of extrapolation error of all methods on 13 time-series datasets.	42
4.1	Solar irradiance dataset	50
4.2	Automatically-generated descriptions of the solar irradiance data set . . .	51
4.3	A learned component corresponding to the Maunder minimum	51
4.4	ABCD isolating the part of the signal explained by a slowly-varying trend	52
4.5	Extract from an automatically-generated report	52
4.6	Short descriptions of the four components of the airline model	53
4.7	Capturing non-stationary periodicity in the airline data	54
4.8	Modeling heteroscedasticity in the airline dataset	54

5.1	Neural network architectures giving rise to GPs	59
5.2	Neural network architectures giving rise to deep GPs	60
5.3	One-dimensional draws from a deep GP prior	61
5.4	Desirable properties of representations of manifolds	64
5.5	Distribution of singular values of the Jacobian of a deep GP	65
5.6	Points warped by a draw from a deep GP	66
5.7	Visualization of a feature map drawn from a deep GP	67
5.8	Two different architectures for deep neural networks	68
5.9	Draws from a 1D deep GP prior with each layer connected to the input .	68
5.10	Points warped by a draw from an input-connected deep GP	69
5.11	Distribution of singular values of an input-connected deep GP	69
5.12	Feature mapping of an input-connected deep GP	70
5.13	Infinitely deep kernels	73
6.1	Isocontours of additive kernels in 3 dimensions	81
6.2	A comparison of different additive model classes	85
7.1	A draw from the infinite warped mixture model prior	92
7.2	One-dimensional Gaussian process latent variable model	93
7.3	Two-dimensional Gaussian process latent variable model	94
7.4	Graphical model of the infinite warped mixture model	97
7.5	Latent clusters of face images	102
7.6	Recovering clusters on synthetic data	103
7.7	A visualization of a sampler for the iWMM	104
7.8	Comparing density estimates of between the GP-LVM and the iWMM .	105
7.9	Comparison of latent coordinate estimates	105

List of Tables

2.1	Examples of structures expressible by some basic kernels	9
2.2	Examples of one-dimensional structures expressible by adding kernels	13
3.1	Some other basic kernels	31
3.2	Common regression models expressible in the kernel language	32
3.3	Kernels recovered on synthetic data	44
4.1	Descriptions of the effect of each kernel, written as a post-modifier	48
4.2	Noun phrase descriptions of each type of kernel	48
6.1	Relative variance contributed by each order of the additive model	79
6.2	Regression Dataset Statistics	87
6.3	Classification Dataset Statistics	87
6.4	Comparison of predictive error on regression problems	88
6.5	Comparison of predictive likelihood on regression problems	89
6.6	Comparison of predictive error on classification problems	89
6.7	Comparison of predictive likelihood on classification problems	89
7.1	Datasets used for evaluation of the iWMM	106
7.2	Clustering performance comparison	107
7.3	Predictive log-likelihood comparison	107

Notation

Unbolded x represents a single number, \mathbf{x} represents a vector, and \mathbf{X} represents a matrix. A individual element of a vector will be denoted with a subscript and without boldface. For example, the i th element of a vector \mathbf{x} is denoted as x_i . A bold lower-case number with an index such as \mathbf{x}_j represents a particular row of matrix \mathbf{X} .

Symbol	Description
$y \sim p(y)$	y is drawn from, or distributed according to, distribution $p(y)$
$\mathcal{O}(\cdot)$	The big-O asymptotic complexity of an algorithm.
$A \otimes B$	The Kronecker product of matrices A and B .
SE	The squared-exponential kernel, also known as the radial-basis function (RBF) kernel, or the Gaussian kernel.
RQ	The rational-quadratic kernel.
Per	The periodic kernel.
Lin	The linear kernel.
WN	The white-noise kernel.
C	The constant kernel.
σ	The changepoint kernel, $\sigma(x, x') = \sigma(x)\sigma(x')$, where $\sigma(x)$ is a sigmoidal function such as the logistic function.
$k_1 + k_2$	Addition of kernels, shorthand for $k_1(\mathbf{x}, \mathbf{x}') + k_2(\mathbf{x}, \mathbf{x}')$
$k_1 \times k_2$	Multiplication of kernels, shorthand for $k_1(\mathbf{x}, \mathbf{x}') \times k_2(\mathbf{x}, \mathbf{x}')$
$k(\mathbf{X}, \mathbf{X})$	The Gram matrix, whose i, j th element is given by $k(\mathbf{x}_i, \mathbf{x}_j)$.
\mathbf{K}	Shorthand for the Gram matrix $k(\mathbf{X}, \mathbf{X})$
$f(\mathbf{X})$	A vector of function values, whose i th element is given by $f(\mathbf{x}_i)$.
$\text{vec}(\mathbf{X})$	The vectorization operator, which concatenates each column of \mathbf{X} into a column vector.
$\text{mod}(i, j)$	The modulo operator: the remainder after dividing i by j .

Chapter 1

Introduction

“All models are wrong, but yours are stupid too.”

@ML_Hipster (2013)

Prediction, extrapolation, and induction are all examples of learning a function from data. There are many ways to learn functions, but one particularly nice way is by *inference*. Inference procedures set up a group of hypotheses – a *model*, then weight those hypotheses based on how well their predictions match the data. Keeping around all the hypotheses that match the data helps guard against over-fitting. We can also compare models to find what sorts of structure are present in a dataset.

To be able to learn a wide variety of types of structure, we’d like to have an expressive language of models of functions. We’d like to be able to represent simple kinds of functions, such as linear or polynomial ones. We’d also like to have models of arbitrarily complex functions, specified in terms of high-level properties such as how smooth they are, whether they repeat over time, or which symmetries they have.

This thesis will show how to build such a language using Gaussian processes (GPs), a tractable set of models of very different types of functions. This chapter will introduce the basic properties of GPs. The next chapter will describe the many types of functions that we know how to model using GPs.

1.1 Gaussian Process Models

Gaussian processes are a simple and general class of models of functions. To be precise, a GP is any distribution over functions such that any finite subset of function values $f(\mathbf{x}_1), f(\mathbf{x}_2), \dots, f(\mathbf{x}_N)$ have a joint Gaussian distribution (Rasmussen and Williams,

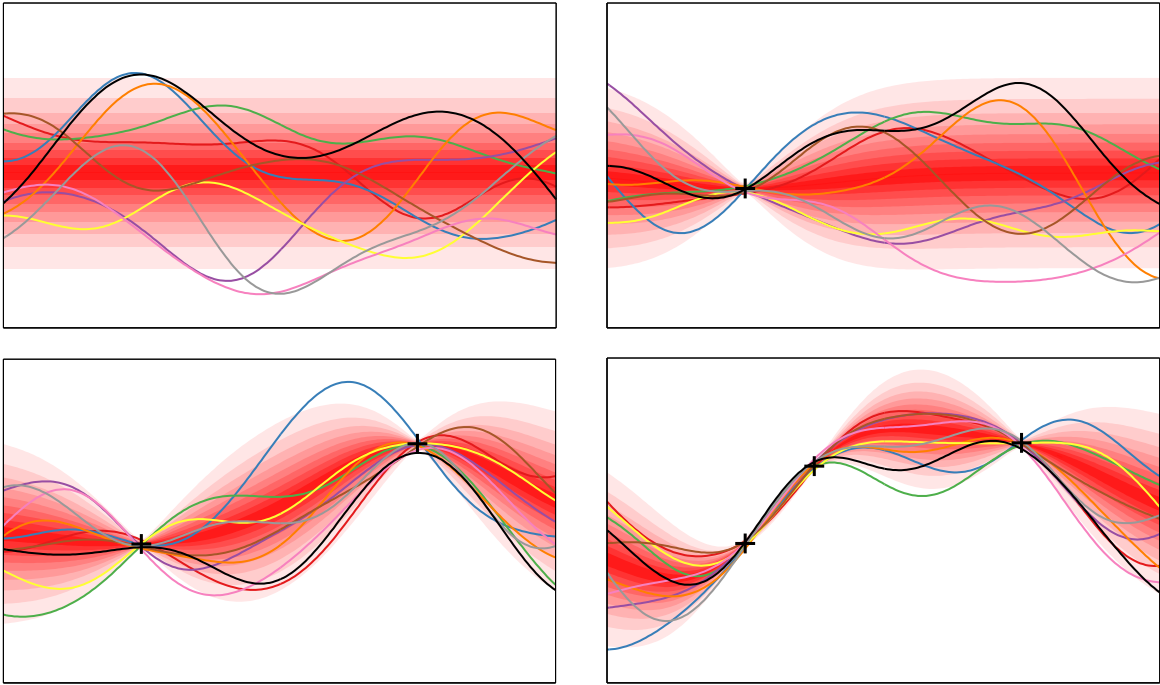


Fig. 1.1 A visual representation of a one-dimensional Gaussian process posterior. Different shades of red correspond to deciles of the predictive density at each input location. Coloured lines show samples from the process. *Top left:* A GP not conditioned on any datapoints. *Remaining plots:* The posterior after conditioning on different amounts of data.

2006). A GP model, before conditioning on data, is completely specified by its mean function,

$$\mathbb{E}[f(\mathbf{x})] = \mu(\mathbf{x}) \quad (1.1)$$

and its covariance function, also called the *kernel*:

$$\text{Cov}(f(\mathbf{x}), f(\mathbf{x}')) = k(\mathbf{x}, \mathbf{x}') \quad (1.2)$$

It is common practice to assume that the mean function is simply zero everywhere, since uncertainty about the mean function can be taken into account by adding an extra term to the kernel.

After accounting for the mean, the kind of structure which can be captured by a GP model is entirely determined by its kernel. The kernel determines how the model generalizes, or extrapolates to new data.

There are many possible choices of covariance function, and we can specify a wide range of models just by specifying the kernel of a GP. For example, linear regression, splines, and Kalman filters are all examples of GPs with particular kernels. However, these model classes barely scratch the surface of the many possible models we can express through choosing a kernel. One of the main difficulties in using GPs is constructing a kernel which represents the particular structure present in the data being modelled.

1.1.1 Model Selection

The crucial property of GPs that allows us to automatically construct models is that we can compute the *marginal likelihood* of a particular model, also known as the *evidence* MacKay (1992). The marginal likelihood allows us to compare models and automatically discover the appropriate amount of detail to use, due to Bayesian Occam's razor (MacKay, 2003; Rasmussen and Ghahramani, 2001). Choosing a kernel, or kernel parameters, by maximizing the marginal likelihood will typically select the *least* flexible model class which still captures all the structure in the data. For example, if a kernel has a parameter which controls the smoothness of the functions it models, the maximum-likelihood estimate of that parameter will usually correspond to the smoothest possible family of functions which still go through all the observed function values.

Here's the marginal likelihood under a GP of observing a set of function values $[f(\mathbf{x}_1), f(\mathbf{x}_2), \dots, f(\mathbf{x}_N)] = \mathbf{f}(\mathbf{X})$ at locations $[\mathbf{x}_1, \mathbf{x}_2, \dots, \mathbf{x}_N]^\top = \mathbf{X}$:

$$\begin{aligned}
p(\mathbf{f}(\mathbf{X})|\mathbf{X}, \mu(\cdot), k(\cdot, \cdot)) &= \mathcal{N}(\mathbf{f}(\mathbf{X})|\mu(\mathbf{X}), k(\mathbf{X}, \mathbf{X})) \\
&= (2\pi)^{-\frac{N}{2}} \underbrace{|k(\mathbf{X}, \mathbf{X})|^{-\frac{1}{2}}}_{\text{discourages flexibility}} \\
&\quad \times \underbrace{\exp \left\{ -\frac{1}{2} (\mathbf{f}(\mathbf{X}) - \boldsymbol{\mu}(\mathbf{X}))^\top k(\mathbf{X}, \mathbf{X})^{-1} (\mathbf{f}(\mathbf{X}) - \boldsymbol{\mu}(\mathbf{X})) \right\}}_{\text{encourages fit with data}}
\end{aligned} \tag{1.3}$$

This multivariate Gaussian density is referred to as the *marginal likelihood* because it implicitly integrates (marginalizes) over all possible functions values $\mathbf{f}(\bar{\mathbf{X}})$, where $\bar{\mathbf{X}}$ is the set of all locations where we haven't observed the function.

1.1.2 Prediction

Even though we don't need to consider locations other than at the data when computing the marginal likelihood, we can still ask the model which function values are likely to occur at any location, given the observations we've seen. By the formula for Gaussian conditionals (described in appendix A), the predictive distribution of a function value $f(\mathbf{x}^*)$ at a test point \mathbf{x}^* has a simple form:

$$p(f(\mathbf{x}^*) | \mathbf{f}(\mathbf{X}), \mathbf{X}, \mu(\cdot), k(\cdot, \cdot)) = \mathcal{N}\left(f(\mathbf{x}^*) | \underbrace{\mu(\mathbf{x}^*) + k(\mathbf{x}^*, \mathbf{X})k(\mathbf{X}, \mathbf{X})^{-1}(\mathbf{f}(\mathbf{X}) - \mu(\mathbf{X}))}_{\text{predictive mean goes through observations}}, \underbrace{k(\mathbf{x}^*, \mathbf{x}^*) - k(\mathbf{x}^*, \mathbf{X})k(\mathbf{X}, \mathbf{X})^{-1}k(\mathbf{X}, \mathbf{x}^*)}_{\text{predictive variance shrinks given more data}}\right) \quad (1.4)$$

These expressions may look complex, but only require a few matrix operations to evaluate.

Sampling a function from a GP is also straightforward: a sample from a GP at a finite set of locations is just a single sample from a single multivariate Gaussian distribution, given by equation (1.4). Figure 1.1 shows prior and posterior samples from a GP, as well as contours of the predictive density.

Our representation of uncertainty through probabilities does not mean that we are assuming the function being learned is stochastic or random in any way; it is simply a consistent method of keeping track of our uncertainty.

1.1.3 Useful Properties of Gaussian Processes

There are several reasons why GPs in particular are well-suited for building a language of regression models:

- **Analytic inference.** Given a kernel function and some observations, the predictive posterior distribution can be computed exactly in closed form. This is a rare property for nonparametric models to have.
- **Expressivity.** By choosing different covariance functions, we can express a very wide range of modeling assumptions.
- **Integration over hypotheses.** The fact that a GP posterior lets us exactly integrate over a wide range of hypotheses means that overfitting is less of an

issue than in comparable model classes, such as neural networks. It also removes the need for sophisticated optimization schemes. In contrast, much of the neural network literature is devoted to techniques for regularization and optimization.

- **Marginal likelihood.** A side benefit of being able to integrate over all hypotheses is that we can compute the *marginal likelihood* of the data given the model. This gives us a principled way of comparing different models.
- **Closed-form predictive distribution.** The predictive distribution of a GP at a set of test points is simply a multivariate Gaussian distribution. This means that GPs can easily be composed with other models or decision procedures.
- **Easy to analyze.** It may seem unsatisfying to restrict ourselves to a limited model class, as opposed to trying to do inference in set of all computable functions. However, simple models can be used as well-understood building blocks for constructing more interesting models.

For example, consider linear models. Although they form an extremely limited model class, they are fast, simple, and easy to analyze, and easy to incorporate into other models or procedures. Gaussian processes can be seen as an extension of linear models (Rasmussen and Williams, 2006) which retain these attractive properties.

1.1.4 Limitations of Gaussian Processes

There are, unfortunately, several issues which make usage of GPs sometimes difficult:

- **Slow inference.** Computing the matrix inverse in equations (1.3) and (1.4) takes $\mathcal{O}(N^3)$ time, making inference slow for more than about 1000 datapoints. However, this problem can be addressed by approximate inference schemes (Hensman et al., 2013; Quiñonero-Candela and Rasmussen, 2005; Snelson and Ghahramani, 2006). Most GP software packages implement several of these methods (Rasmussen and Nickisch, 2010; Vanhatalo et al., 2014).
- **Light tails of the predictive distribution.** The predictive distribution of a standard GP model is Gaussian. In order to be robust to outliers, or to perform classification, we may wish to use non-Gaussian noise models. Fortunately, mature software packages exist which can automatically perform approximate inference for a wide variety of non-Gaussian likelihoods.

- **The need to choose a kernel.** In practice, the extreme flexibility of GP models means that we are also faced with the difficult task of choosing a kernel. In fact, choosing a useful kernel is equivalent to the problem of learning a good representation of the input. Kernel parameters are usually set automatically by maximizing the marginal likelihood. However, until recently, human experts were still required to choose the parametric form of the kernel from a small set of standard kernels. Chapter 3 will show how the entire construction of kernels can be automated.

1.2 Outline and Contributions of Thesis

The main contribution of this thesis is to show how to automate the discovery and explanation of structure in functions, simply by searching an open-ended language of regression models. It also includes a set of related results showing how Gaussian processes can be extended, or composed with other models.

Chapter 2 is a tutorial showing how to build a wide variety of structured models of functions by constructing appropriate covariance functions. We'll also show how GPs can produce nonparametric models of manifolds, diverse topological structures, such as cylinders, toruses and Möbius strips.

Chapter 3 shows how to search over a general, open-ended language of models, built by composing together different kernels. Since we can evaluate each model by its marginal likelihood, we can automatically construct custom models for each dataset by a simple search. The nature of GPs allow the resulting models to be visualized by decomposing them into diverse, interpretable components, each capturing a different type of structure. Capturing this high-level structure sometimes even allows us to extrapolate beyond the range of the data.

One benefit of using a compositional model class is that the resulting models are interpretable. **Chapter 4** demonstrates a system which automatically describes the structure implied by a given kernel on a given dataset, generating reports with graphs and English-language text describing the resulting model. We'll show several automatic analyses of time-series. Combined with the automatic model search developed in chapter 3, this system represents the beginnings of an “automatic statistician”.

Chapter 5 analyzes deep network models by characterizing the prior over functions obtained by composing GP priors to form *deep Gaussian processes*. We show that, as the number of layers in such models increases, the amount of information retained about the

original input diminishes to a single degree of freedom. A simple change to the network architecture fixes this pathology. We relate these models to neural networks, and as a side effect derive different forms of *infinitely deep kernels*.

Chapter 6 examines a more limited, but much faster way of discovering structure using GPs. Specifying a kernel with many different types of structure, we use kernel parameters to discard whichever types of structure *aren't* found in the current dataset. The model class we examine is called *additive Gaussian processes*, a model summing over exponentially-many GPs, each depending on a different subset of the input variables. We give a polynomial-time inference algorithm for this model class, and relate it to other model classes. For example, additive GPs are shown to have the same covariance as a GP that uses *dropout*, a recently discovered regularization technique for neural networks.

Chapter 7 develops a Bayesian clustering model in which the clusters have non-parametric shapes - the infinite Warped Mixture Model. The density manifolds learned by this model follow the contours of the data density, and have interpretable, parametric forms in the latent space. The marginal likelihood lets us infer the effective dimension and shape of each cluster separately, as well as the number of clusters.

Chapter 2

Expressing Structure with Kernels

In this chapter, we'll show how to use kernels to build many different kinds of models of functions. By combining a few simple kernels through addition and multiplication, we'll be able to express many different kinds of structure: additivity, symmetry, periodicity, interactions between variables, and changepoints. We'll also show several ways to encode group invariants into kernels. Combining kernels in these simple ways will give us a rich, open-ended language of models.

2.1 Definition

Since we'll be discussing kernels at length, we now give a precise definition. A kernel (also called a *covariance function*), is a positive-definite function between two points x, x' in some space \mathcal{X} . Formally, $k(\mathbf{x}, \mathbf{x}') : \mathcal{X} \times \mathcal{X} \rightarrow \mathbb{R}$. In this chapter, \mathcal{X} is usually a Euclidean space, but it could just as easily correspond to the space of images, document, categories or points on a sphere.

Gaussian process models use a kernel to define the prior covariance between any two function values:

$$\text{Cov}(f(\mathbf{x}), f(\mathbf{x}')) = k(\mathbf{x}, \mathbf{x}') \quad (2.1)$$

Colloquially, kernels are often said to specify the similarity between two objects. This is a slightly misleading statement in this context, since what is actually being specified is the similarity between two values of a *function* over objects. The kernel specifies which functions are likely under the GP prior, which in turn determines the generalization properties of the model.

2.2 A Few Basic Kernels

To begin understanding the types of structures expressible by GPs, we'll start by briefly examining the types of structure encoded by a diverse set of commonly used kernels: the squared-exponential (SE), periodic (Per), and linear (Lin) kernels. These kernels are defined in Table 2.1.

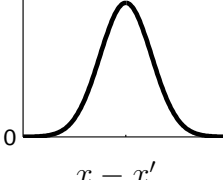
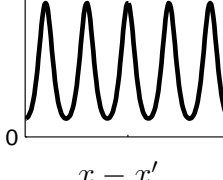
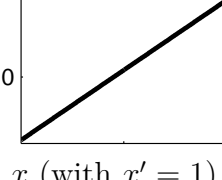
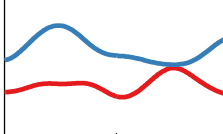
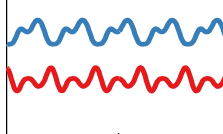
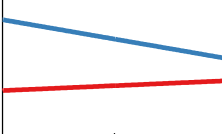
Kernel name:	Squared-exp (SE)	Periodic (Per)	Linear (Lin)
$k(x, x') =$	$\exp\left(-\frac{(x-x')^2}{2\ell^2}\right)$	$\exp\left(-\frac{2}{\ell^2} \sin^2\left(\pi \frac{x-x'}{p}\right)\right)$	$(x - c)(x' - c)$
Plot of kernel:			
	$x - x'$ ↓	$x - x'$ ↓	x (with $x' = 1$) ↓
Samples from prior:			
Type of structure:	local variation	repeating structure	linear functions

Table 2.1 Examples of structures expressible by some basic kernels.

Each covariance function corresponds to a different set of assumptions made about the function we wish to model. For example, using a squared-exp (SE) kernel implies that the function we are modeling has infinitely many derivatives. There exist many variants of “local” kernels similar to the SE kernel, each encoding slightly different assumptions about the smoothness of the function being modeled.

Kernel parameters Each kernel has a number of parameters which specify the precise shape of the covariance function. These are sometimes referred to as *hyper-parameters*, since they can be viewed as specifying a distribution over function parameters, instead of being parameters which specify a function directly.

Stationary and Non-stationary The SE and Per kernels are *stationary*, meaning that their value only depends on the difference $x - x'$. This implies that the probability of observing a particular dataset remains the same, even if we move all the \mathbf{x} values

over by some amount. In contrast, the linear kernel Lin is non-stationary, meaning that the corresponding GP model will produce different answers if the data is moved around while the kernel parameters are kept fixed.

2.3 Combining Kernels

What if the kind of structure we need isn't expressed by any existing kernel? For many types of structure, it's possible to build a "made to order" kernel with the desired properties. The next few sections of this chapter will explore ways in which kernels can be combined to create new ones with different properties. This will allow us to include as much high-level structure as necessary into our models.

2.3.1 Notation

Below, we'll focus on two ways of combining kernels: addition and multiplication. We'll often write these operations in shorthand, without arguments:

$$k_a + k_b = k_a(\mathbf{x}, \mathbf{x}') + k_b(\mathbf{x}, \mathbf{x}')$$
 (2.2)

$$k_a \times k_b = k_a(\mathbf{x}, \mathbf{x}') \times k_b(\mathbf{x}, \mathbf{x}')$$
 (2.3)

All of the basic kernels we considered in section 2.2 are one-dimensional, but kernels over multidimensional inputs can be constructed by adding and multiplying between kernels on different dimensions. The dimension on which a kernel operates is denoted by a subscripted integer. For example, SE₂ represents an SE kernel over the second dimension of \mathbf{x} . To remove clutter, we'll usually refer to a kernels without specifying their parameters.

2.3.2 Combining Properties through Multiplication

Multiplying two positive-definite kernels together always results in another positive-definite kernel. But what properties do these new kernels have? Figure 2.1 shows some interesting kernels that one can obtain by multiplying two basic kernels together.

Working with kernels rather than the parametric form of the function itself allows us to express high-level properties of functions that don't necessarily have a simple parametric form. Here, we'll discuss a few examples.

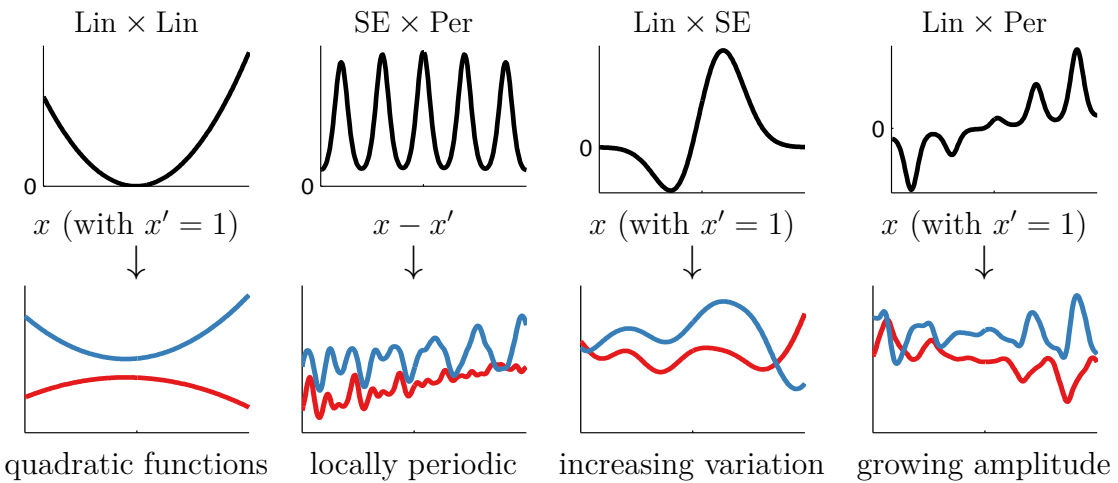


Fig. 2.1 Examples of one-dimensional structures expressible by multiplying kernels. Plots have same meaning as in figure 2.1.

Polynomial Regression

By multiplying together T linear kernels, we obtain a prior on polynomials of degree T . Column 1 of figure 2.1 shows a quadratic kernel.

Locally Periodic Functions

In univariate data, multiplying a kernel by SE gives a way of converting global structure to local structure. For example, Per corresponds to exactly periodic structure, whereas Per \times SE corresponds to locally periodic structure, as shown in column 2 of figure 2.1.

Functions with Growing Amplitude

Multiplying by a linear kernel means that the marginal standard deviation of the function being modeled will grow linearly away from the origin. Columns 3 and 4 of figure 2.1 show two examples.

More Combinations

We can multiply any number of kernels together in this way to produce kernels combining several high-level properties. For example, the kernel SE \times Lin \times Per is a prior on functions which are locally periodic with linearly growing amplitude. We'll see examples of real datasets with this kind of structure in chapter 3.

2.3.3 Building Flexible Multidimensional Models

We can build flexible models of functions of more than one input simply by multiplying kernels between the different inputs. For example, products of SE kernels, having a different lengthscale parameter for each dimension, are called the SE-ARD kernel:

$$\text{SE-ARD}(\mathbf{x}, \mathbf{x}') = \prod_{d=1}^D \exp\left(-\frac{1}{2} \frac{(x_d - x'_d)^2}{\ell_d^2}\right) = \exp\left(-\frac{1}{2} \sum_{d=1}^D \frac{(x_d - x'_d)^2}{\ell_d^2}\right) \quad (2.4)$$

Figure 2.2 illustrates the SE-ARD kernel in two dimensions.

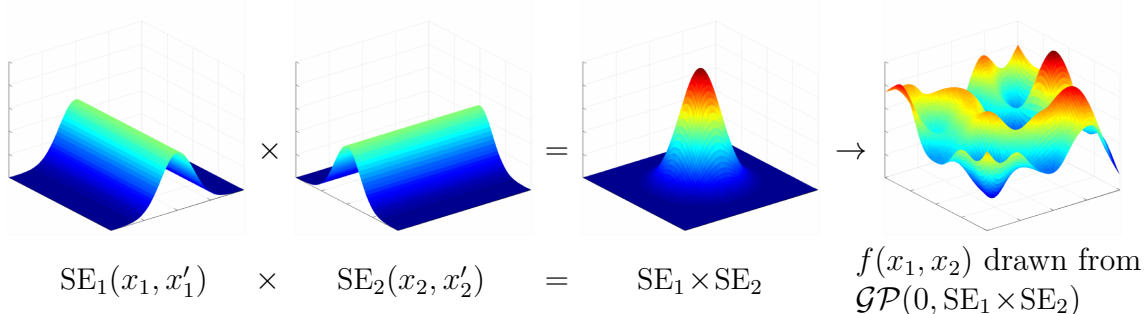


Fig. 2.2 A product of two one-dimensional kernels gives rise to a prior on functions which depend on both dimensions.

ARD stands for Automatic Relevance Determination, so named because estimating the lengthscale parameters $\ell_1, \ell_2, \dots, \ell_D$, implicitly determines the “relevance” of each dimension. Input dimensions with relatively large lengthscales indicate relatively little variation along those dimensions in the function being modeled.

SE-ARD kernels are the default kernel in most applications of GPs. This may be partly because they have relatively few parameters to estimate, and those parameters are relatively interpretable. In addition, there is a theoretical reason to use them: they are *universal* kernels (Micchelli et al., 2006), capable of learning learning any continuous function given enough data, under some conditions.

However, this flexibility means that they can sometimes be relatively slow to learn, due to the *curse of dimensionality* (Bellman, 1956). In general, the more structure we account for in the data, the less data we'll need - the *blessing of abstraction* (Goodman et al., 2011) counters the curse of dimensionality. Below, we'll investigate ways to encode more structure into our kernels.

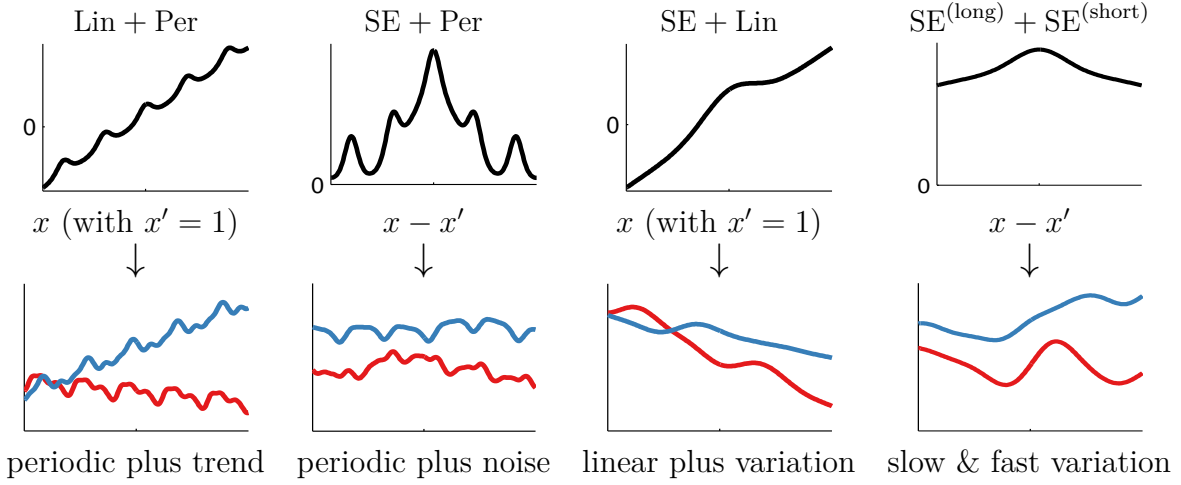


Table 2.2 Examples of one-dimensional structures expressible by adding kernels. Rows have the same meaning as in table 2.1. $\text{SE}^{(\text{long})}$ denotes a SE kernel whose lengthscale is long relative to that of $\text{SE}^{(\text{short})}$

2.4 Modeling Sums of Functions

An additive function is one which can be expressed as $f(\mathbf{x}) = f_a(\mathbf{x}) + f_b(\mathbf{x})$. Additivity is a very useful modeling assumption in a wide variety of contexts, especially if it allows us to make strong assumptions about the individual component which make up the sum. Restricting the flexibility of the component functions often aids in building interpretable models, and sometimes enables extrapolation in high dimensions.

Fortunately, it's easy to encode additivity into GP models. Suppose functions f_1, f_2 are drawn independently from GP priors:

$$f_a \sim \mathcal{GP}(\mu_a, k_a) \quad (2.5)$$

$$f_b \sim \mathcal{GP}(\mu_b, k_b) \quad (2.6)$$

Then the sum of those functions is simply another GP:

$$f_a + f_b \sim \mathcal{GP}(\mu_a + \mu_b, k_a + k_b). \quad (2.7)$$

Kernels k_a and k_b can be kernels of different types, allowing us to model the data as a sum of independent functions, each possibly representing a different type of structure. We can also sum any number of components this way.

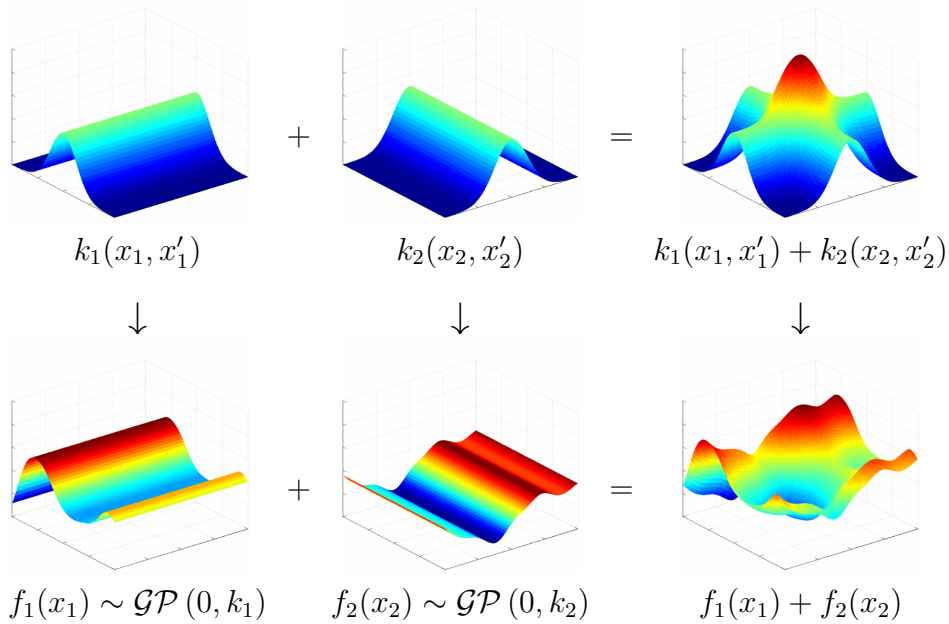


Fig. 2.3 A sum of two orthogonal one-dimensional kernels. *Top row:* An additive kernel is any sum of kernels. *Bottom row:* A draw from an additive kernel corresponds to a sum of draws from independent GP priors, each having the corresponding kernel.

2.4.1 Additivity Across Multiple Dimensions

When modeling functions of multiple dimensions, summing kernels can give rise to additive structure across different dimensions. To be more precise, if the kernels being added together are functions only of a subset of input dimensions, then the implied prior over functions decomposes in the same way. For example, if

$$f(x_1, x_2) \sim \mathcal{GP}(\mathbf{0}, k_1(x_1, x'_1) + k_2(x_2, x'_2)) \quad (2.8)$$

Then this is equivalent to the model

$$f_1(x_1) \sim \mathcal{GP}(\mathbf{0}, k_1(x_1, x'_1)) \quad (2.9)$$

$$f_2(x_2) \sim \mathcal{GP}(\mathbf{0}, k_2(x_2, x'_2)) \quad (2.10)$$

$$f(x_1, x_2) = f_1(x_1) + f_2(x_2) \quad (2.11)$$

Figure 2.3 illustrates a decomposition of this form. Note that the product of two kernels does not have an analogous interpretation as the product of two functions.

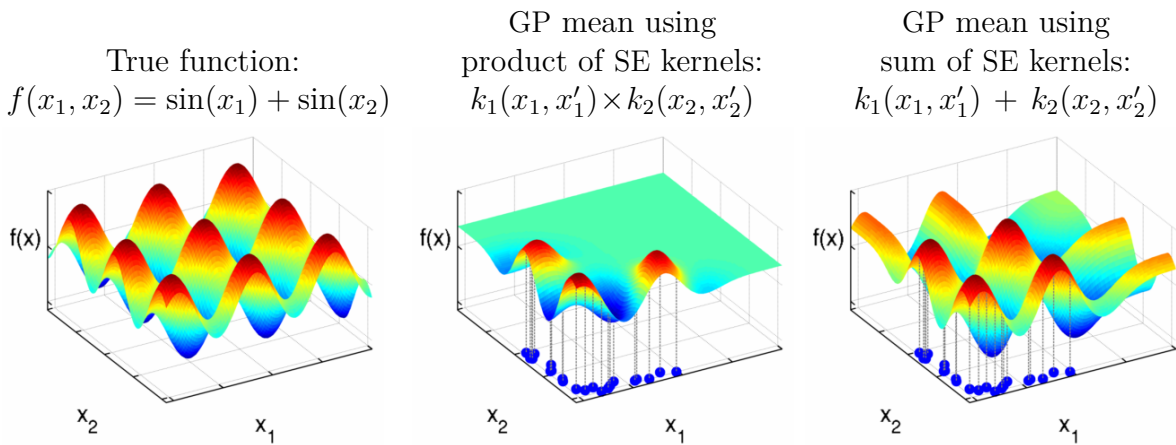


Fig. 2.4 Inference in functions with additive structure. When the function being modeled has additive structure, we can exploit this fact to extrapolate far from the training data. The product kernel allows a different function value for every combination of inputs, and so is uncertain about function values away from the training data.

2.4.2 Long-range Extrapolation through Additivity

Additive structure often allows us to make predictions far from the training data. Figure 2.4 compares the extrapolations made by additive versus non-additive GP models, conditioned on data from a sum of two axis-aligned sine functions, evaluated in a small, L-shaped area. In this example, the additive model is able to correctly predict the height of the function at unseen combinations of inputs. The product-kernel model is more flexible, and so remains uncertain about the function away from the data.

These types of additive models have been well-explored in the statistics literature. For example, generalized additive models (Hastie and Tibshirani, 1990) have seen wide adoption. In high dimensions, we can also consider sums of functions of more than one dimension. Chapter 6 considers this model class in more detail.

2.4.3 Example: An Additive Model of Concrete Strength

To illustrate how additive kernels give rise to interpretable models, we'll build an additive model of the strength of concrete as a function of the amount of 7 different ingredients, plus the age of the concrete (Yeh, 1998).

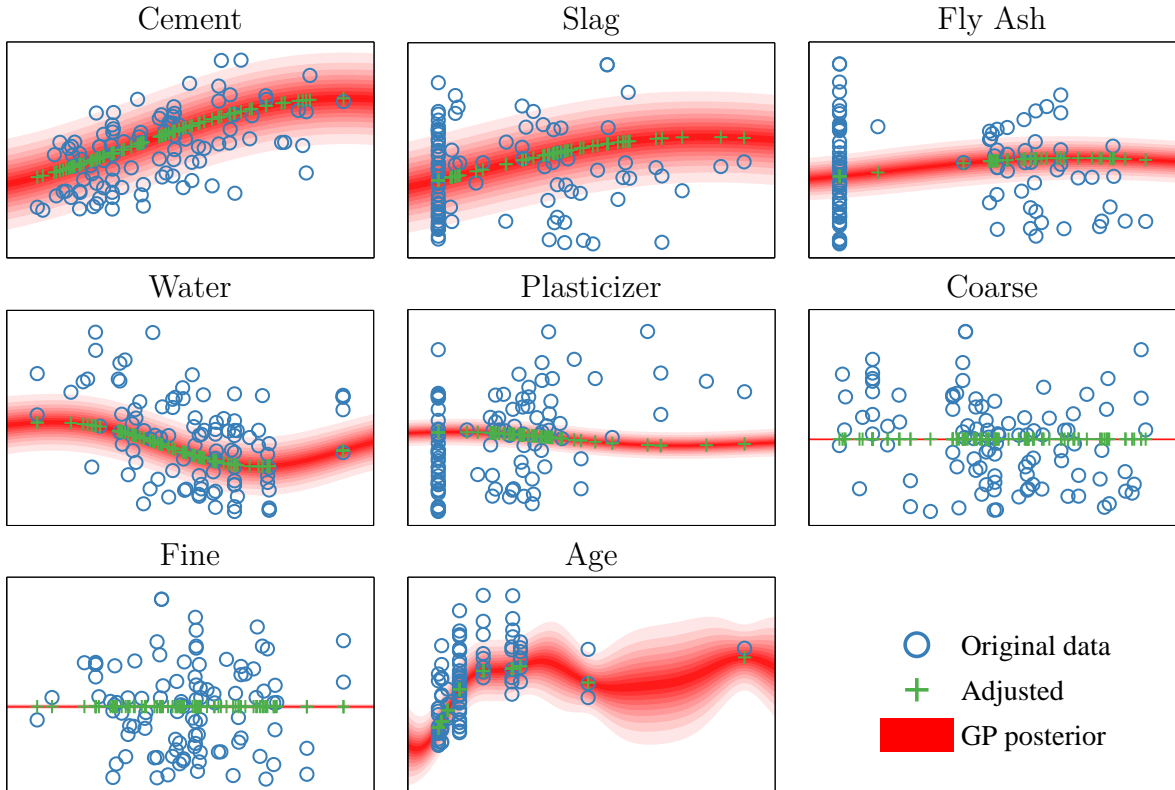


Fig. 2.5 By considering only one-dimensional terms of the additive kernel, we can plot the predictive distribution as a function of each dimension separately. Blue points indicate the original data, green points are data after the average contribution from all other terms has been subtracted. The vertical axis is the same for all plots.

Our simple additive model looks like

$$\begin{aligned} f(\mathbf{x}) = & f_1(\text{cement}) + f_2(\text{slag}) + f_3(\text{fly ash}) + f_4(\text{water}) \\ & + f_5(\text{plasticizer}) + f_6(\text{coarse}) + f_7(\text{fine}) + f_8(\text{age}) + \text{noise} \end{aligned} \quad (2.12)$$

where noise $\stackrel{\text{iid}}{\sim} \mathcal{N}(0, \sigma_n)$. After learning the kernel parameters by maximizing the marginal likelihood of the data, we can visualize the predictive distribution of each component of the model.

Figure 2.5 shows the marginal posterior distribution of each of the 8 components in equation (2.12). We can see that the parameters controlling the variance of two of the components, Coarse and Fine, were set to zero, meaning that the marginal likelihood preferred a parsimonious model which did not depend on these dimensions. This is an example of the automatic sparsity that arises by maximizing marginal likelihood in GP

models, and another example of automatic relevance determination (ARD) (Neal, 1995).

The ability to learn kernel parameters in this way is much more difficult when using non-probabilistic methods such as Support Vector Machines (Cortes and Vapnik, 1995), for which cross-validation is often the best method to select kernel parameters.

2.4.4 Posterior Variance of Additive Components

Here we derive the posterior variance and covariance of all of the additive components of a GP. These formulas allow us to make plots such as figure 2.5.

First, we'll write down the joint prior over the sum of two functions drawn from GP priors. We'll distinguish between $\mathbf{f}(\mathbf{X})$ (the function values at the training locations) and $\mathbf{f}(\mathbf{X}^*)$ (the function values at some set of query locations).

If f_1 and f_2 are *a priori* independent, and $f_1 \sim \text{GP}(\mu_1, k_1)$ and $f_2 \sim \text{GP}(\mu_2, k_2)$, then

$$\begin{bmatrix} f_1(\mathbf{X}) \\ f_1(\mathbf{X}^*) \\ f_2(\mathbf{X}) \\ f_2(\mathbf{X}^*) \\ f_1(\mathbf{X}) + f_2(\mathbf{X}) \\ f_1(\mathbf{X}^*) + f_2(\mathbf{X}^*) \end{bmatrix} \sim \mathcal{N} \left(\begin{bmatrix} \boldsymbol{\mu}_1 \\ \boldsymbol{\mu}_1^* \\ \boldsymbol{\mu}_2 \\ \boldsymbol{\mu}_2^* \\ \boldsymbol{\mu}_1 + \boldsymbol{\mu}_2 \\ \boldsymbol{\mu}_1^* + \boldsymbol{\mu}_2^* \end{bmatrix}, \begin{bmatrix} \mathbf{K}_1 & \mathbf{K}_1^* & 0 & 0 & \mathbf{K}_1 & \mathbf{K}_1^* \\ \mathbf{K}_1^* & \mathbf{K}_1^{**} & 0 & 0 & \mathbf{K}_1^* & \mathbf{K}_1^{**} \\ 0 & 0 & \mathbf{K}_2 & \mathbf{K}_2^* & \mathbf{K}_2 & \mathbf{K}_2^* \\ 0 & 0 & \mathbf{K}_2^* & \mathbf{K}_2^{**} & \mathbf{K}_2^* & \mathbf{K}_2^{**} \\ \mathbf{K}_1 & \mathbf{K}_1^* & \mathbf{K}_2 & \mathbf{K}_2^* & \mathbf{K}_1 + \mathbf{K}_2 & \mathbf{K}_1^* + \mathbf{K}_2^* \\ \mathbf{K}_1^* & \mathbf{K}_1^{**} & \mathbf{K}_2^* & \mathbf{K}_2^{**} & \mathbf{K}_1^* + \mathbf{K}_2^* & \mathbf{K}_1^{**} + \mathbf{K}_2^{**} \end{bmatrix} \right) \quad (2.13)$$

where we represent the Gram matrices, evaluated at all pairs of vectors in bold capitals as $\mathbf{K}_{i,j} = k(\mathbf{x}_i, \mathbf{x}_j)$. So

$$\mathbf{K}_1 = k_1(\mathbf{X}, \mathbf{X}) \quad (2.14)$$

$$\mathbf{K}_1^* = k_1(\mathbf{X}^*, \mathbf{X}) \quad (2.15)$$

$$\mathbf{K}_1^{**} = k_1(\mathbf{X}^*, \mathbf{X}^*) \quad (2.16)$$

By the formula for Gaussian conditionals, (given by equation (A.2)), we get that the conditional distribution of a GP-distributed function conditioned on its sum with another GP-distributed function is given by

$$f_1(\mathbf{X}^*) | f_1(\mathbf{X}) + f_2(\mathbf{X}) \sim \mathcal{N} \left(\boldsymbol{\mu}_1^* + \mathbf{K}_1^{*\top} (\mathbf{K}_1 + \mathbf{K}_2)^{-1} [f_1(\mathbf{X}) + f_2(\mathbf{X}) - \boldsymbol{\mu}_1 - \boldsymbol{\mu}_2] \right. \\ \left. \mathbf{K}_1^{**} - \mathbf{K}_1^{*\top} (\mathbf{K}_1 + \mathbf{K}_2)^{-1} \mathbf{K}_1^* \right) \quad (2.17)$$

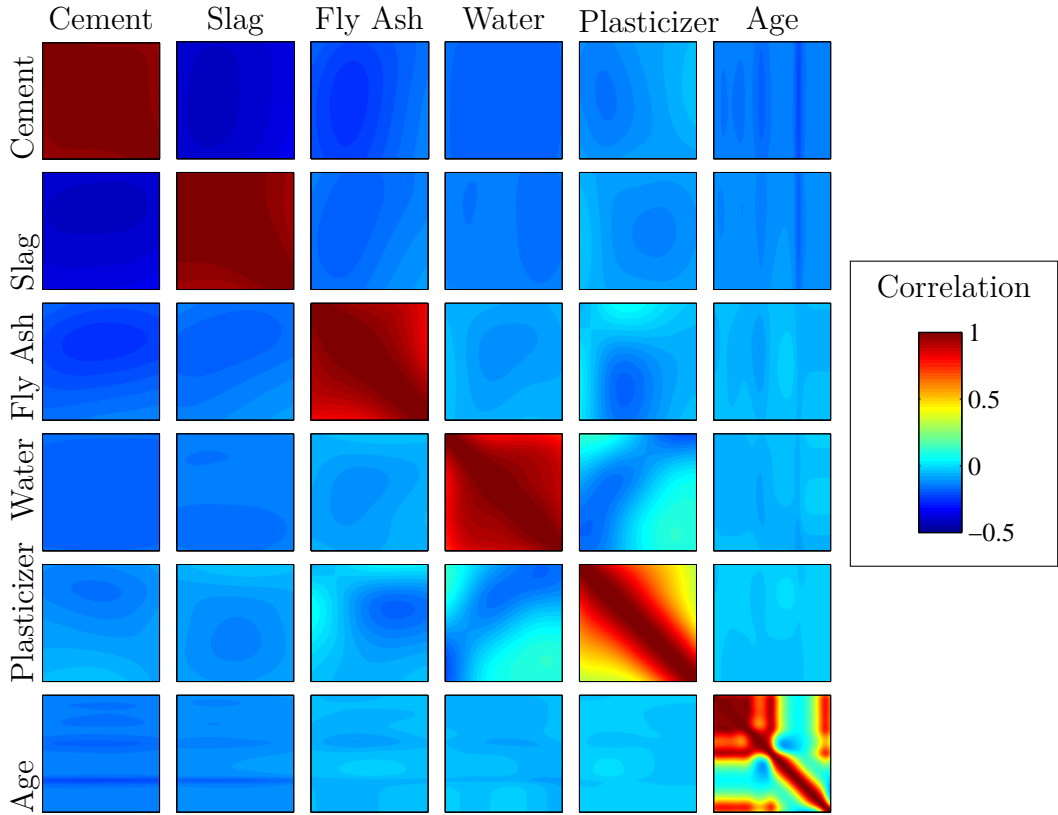


Fig. 2.6 Posterior correlations between the components explaining the concrete dataset. Each plot shows the additive model's posterior correlations between two components, plotted over the domain of the data $\pm 5\%$. Red indicates high correlation, teal indicates no correlation, and blue indicates negative correlation. Plots on the diagonal show posterior correlations within each component.

These formulae express the model's posterior uncertainty about the different components of the signal, integrating over the possible configurations of the other components. If we wish to condition on the sum of more than two functions, the term $\mathbf{K}_1 + \mathbf{K}_2$ can simply be replaced by $\sum_i \mathbf{K}_i$ everywhere.

Posterior Covariance of Additive Components

We can also compute the posterior covariance between any two components, conditioned on their sum: If this quantity is negative, it means that there is ambiguity about which of the two components explains the data at that location.

$$\text{cov} [\mathbf{f}_1(\mathbf{X}^*), \mathbf{f}_2(\mathbf{X}^*) | \mathbf{f}(\mathbf{X})] = -\mathbf{K}_1^{*\top} (\mathbf{K}_1 + \mathbf{K}_2)^{-1} \mathbf{K}_2^* \quad (2.18)$$

Figure 2.6 shows the posterior correlation between all non-zero components of the concrete model. Most of the correlation occurs within components, but there is also negative correlation between the ‘Cement’ and ‘Slag’ variables. This reflects an ambiguity in the model about which one of these functions is high and the other low. Dimensions ‘Coarse’ and ‘Fine’ are not shown, because their variance was zero.

2.5 Changepoints

A simple example of how combining kernels can give rise to more structured priors is given by changepoint kernels. Changepoints kernels can be defined through addition and multiplication with sigmoidal functions:

$$\text{CP}(k_1, k_2)(x, x') = \sigma(x)k_1(x, x')\sigma(x') + (1 - \sigma(x))k_2(x, x')(1 - \sigma(x')) \quad (2.19)$$

which can be written in shorthand as

$$\text{CP}(k_1, k_2) = k_1 \times \boldsymbol{\sigma} + k_2 \times \bar{\boldsymbol{\sigma}} \quad (2.20)$$

where $\boldsymbol{\sigma} = \sigma(x)\sigma(x')$ and $\bar{\boldsymbol{\sigma}} = (1 - \sigma(x))(1 - \sigma(x'))$.

This compound kernel expresses a change from one kernel to another. The parameters of the sigmoid determine where, and how rapidly, this change occurs.

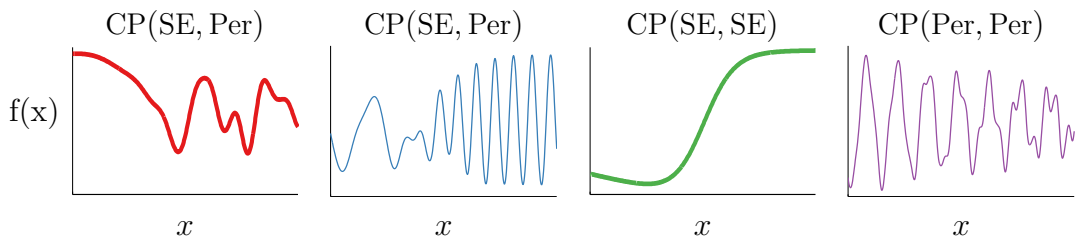


Fig. 2.7 Draws from different priors on using changepoint kernels, constructed by adding and multiplying together base kernels with sigmoidal functions.

We can also express a function whose structure changes within some interval – a *change window* – by replacing $\sigma(x)$ with a product of two sigmoids, one increasing and one decreasing.

2.5.1 Multiplication by a Known Function

More generally, we can model an unknown function that's been multiplied by some fixed, known function $a(x)$, by multiplying the kernel by $a(\mathbf{x})a(\mathbf{x}')$. Formally,

$$f(\mathbf{x}) = a(\mathbf{x})g(\mathbf{x}), \quad g \sim \mathcal{GP}(g | \mathbf{0}, k(\mathbf{x}, \mathbf{x}')) \iff f \sim \mathcal{GP}(f | \mathbf{0}, a(\mathbf{x})k(\mathbf{x}, \mathbf{x}')a(\mathbf{x}')) \quad (2.21)$$

2.6 Feature Representation

By Mercer's theorem (Mercer, 1909), any positive-definite kernel can be represented as the inner product between a fixed set of features, evaluated at x and at x' :

$$k(\mathbf{x}, \mathbf{x}') = \mathbf{h}(\mathbf{x})^\top \mathbf{h}(\mathbf{x}') \quad (2.22)$$

As a simple example, the squared-exponential kernel (SE) on the real line has a representation in terms of infinitely many radial-basis functions of the form $h_i(x) \propto \exp(-\frac{1}{2}\frac{(x-c_i)^2}{2\ell^2})$. More generally, any stationary kernel on the real line can be represented by a set of sines and cosines - a Fourier representation (Bochner, 1959). In general, any particular feature representation of a kernel is not unique, and depends on which space \mathcal{X} is being considered (Minh et al., 2006).

In some cases, \mathcal{X} can even be the infinite-dimensional feature mapping of another kernel. Composing feature maps in this way leads to *deep kernels*, a topic explored in chapter 5.

2.6.1 Relation to Linear Regression

Surprisingly, GP regression is equivalent to Bayesian linear regression on the implicit features $\mathbf{h}(\mathbf{x})$ which give rise to the kernel:

$$f(\mathbf{x}) = \mathbf{w}^\top \mathbf{h}(\mathbf{x}), \quad \mathbf{w} \sim \mathcal{N}(\mathbf{w} | \mathbf{0}, \Sigma) \iff f \sim \mathcal{GP}(f | \mathbf{0}, \mathbf{h}(\mathbf{x})^\top \Sigma \mathbf{h}(\mathbf{x})) \quad (2.23)$$

The link between Gaussian processes, linear regression, and neural networks is explored further in chapter 5.

2.6.2 Feature-space view of Combining Kernels

We can also view kernel addition and multiplication as a combination of the features of the original kernels. For example, if we have two kernels

$$k_a(\mathbf{x}, \mathbf{x}') = \mathbf{a}(\mathbf{x})^\top \mathbf{a}(\mathbf{x}') \quad (2.24)$$

$$k_b(\mathbf{x}, \mathbf{x}') = \mathbf{b}(\mathbf{x})^\top \mathbf{b}(\mathbf{x}') \quad (2.25)$$

and we consider their addition, then

$$k_a(\mathbf{x}, \mathbf{x}') + k_b(\mathbf{x}, \mathbf{x}') = \mathbf{a}(\mathbf{x})^\top \mathbf{b}(\mathbf{x}') + \mathbf{a}(\mathbf{x})^\top \mathbf{b}(\mathbf{x}') \quad (2.26)$$

$$= \begin{bmatrix} \mathbf{a}(\mathbf{x}) \\ \mathbf{b}(\mathbf{x}) \end{bmatrix}^\top \begin{bmatrix} \mathbf{a}(\mathbf{x}') \\ \mathbf{b}(\mathbf{x}') \end{bmatrix} \quad (2.27)$$

meaning that the features of $k_a + k_b$ are the concatenation of the features of each kernel.

We can examine kernel multiplication in a similar way:

$$k_a(\mathbf{x}, \mathbf{x}') \times k_b(\mathbf{x}, \mathbf{x}') = [\mathbf{a}(\mathbf{x})^\top \mathbf{a}(\mathbf{x}')] \times [\mathbf{b}(\mathbf{x})^\top \mathbf{b}(\mathbf{x}')] \quad (2.28)$$

$$= \sum_i a_i(\mathbf{x}) a_i(\mathbf{x}') \times \sum_j b_j(\mathbf{x}) b_j(\mathbf{x}') \quad (2.29)$$

$$= \sum_i \sum_j a_i(\mathbf{x}) a_i(\mathbf{x}') b_j(\mathbf{x}) b_j(\mathbf{x}') \quad (2.30)$$

$$= \sum_{i,j} [a_i(\mathbf{x}) b_j(\mathbf{x})] [a_i(\mathbf{x}') b_j(\mathbf{x}')] \quad (2.31)$$

$$= \text{vec}(\mathbf{a}(\mathbf{x}) \otimes \mathbf{b}(\mathbf{x}'))^\top \text{vec}(\mathbf{a}(\mathbf{x}) \otimes \mathbf{b}(\mathbf{x}')) \quad (2.32)$$

In other words, the features of $k_a \times k_b$ are just the Cartesian product (all possible combinations) of the original two sets of features. For example, the Cartesian product of the features of two one-dimensional SE kernels covers the plane with two-dimensional radial-basis functions of the form

$$h_{ij}(x_1, x_2) \propto \exp\left(-\frac{1}{2} \frac{(x_1 - c_i)^2}{2\ell_1^2}\right) \exp\left(-\frac{1}{2} \frac{(x_2 - c_j)^2}{2\ell_2^2}\right) \quad (2.33)$$

2.7 Expressing Symmetries and Invariants

When modeling functions, encoding known symmetries can improve predictive accuracy. In this section, we'll look at different ways in which we can encode symmetries into a

prior on functions. Many types of symmetry can be enforced through operations on the kernel.

We'll demonstrate the properties of the resulting models by sampling functions from their priors. By using these functions to define warpings from $\mathbb{R}^2 \rightarrow \mathbb{R}^3$, we'll show how to build a nonparametric prior on an open-ended family of topological manifolds, such as cylinders, toruses, and Möbius strips.

Ginsbourger et al. (2012) and Ginsbourger et al. (2013) characterized the set of GP priors on functions which respect any given invariance. They showed that the only way to construct a prior on functions which respect a given invariance is to construct a kernel which respects the same invariance with respect to each of its two inputs.

Formally, given a finite group of operations G to which we wish our function to remain invariant, and $f \sim \mathcal{GP}(0, k(\mathbf{x}, \mathbf{x}'))$, f is invariant under G (up to a modification) if and only if $k(\cdot, \cdot)$ is argument-wise invariant:

$$k(g(\mathbf{x}), g(\mathbf{x}')) = k(\mathbf{x}, \mathbf{x}'), \quad \forall \mathbf{x}, \mathbf{x}' \in \mathcal{X}, \quad \forall g, g' \in G \quad (2.34)$$

As a simple example, consider the symmetry $f(x, y) = f(y, x)$, or the set of functions invariant to swapping their two arguments. The elements of the group G_{swap} describing this symmetry are

$$g_1(f(x, y)) = f(x, y) \quad (\text{identity}) \quad (2.35)$$

$$g_2(f(x, y)) = f(y, x) \quad (\text{swap}) \quad (2.36)$$

It might not be clear how to find a kernel obeying these symmetries.

2.7.1 Three Recipes for Group Invariance

Fortunately, for finite groups, there are a few simple ways to transform any kernel into one which is argument-wise invariant to actions under any finite group:

- 1. Sum over the Orbit.** Ginsbourger et al. (2012) and Kondor (2008) suggest enforcing invariants through a double sum over the orbits of \mathbf{x} and \mathbf{x}' with respect to G :

$$k_{\text{sum}}(\mathbf{x}, \mathbf{x}') = \sum_{g, g' \in G} k(g(\mathbf{x}), g'(\mathbf{x}')) \quad (2.37)$$

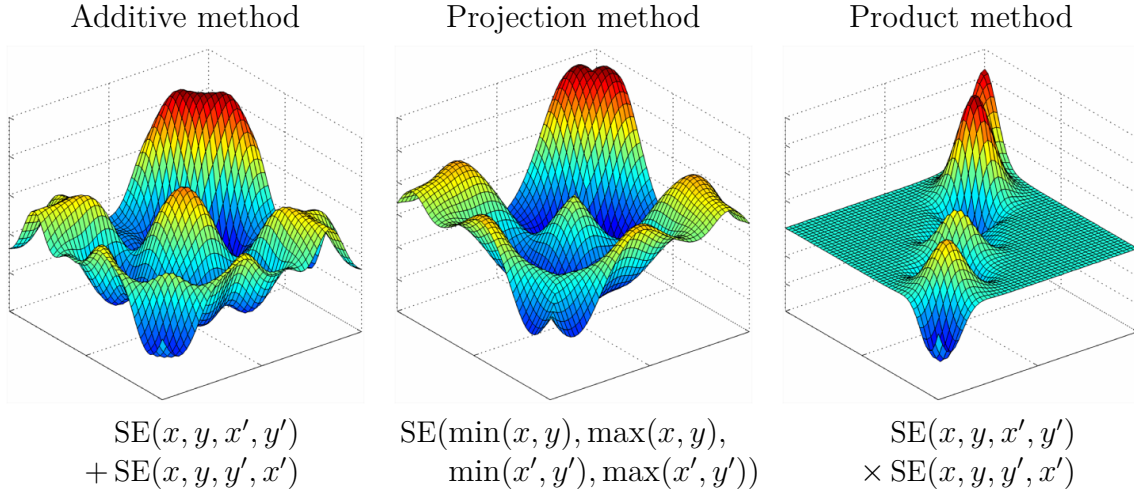


Fig. 2.8 Three methods of introducing symmetry, illustrated through draws from the corresponding priors. All three methods introduce a different type of nonstationarity.

For the group G_{swap} , this operation results in the kernel:

$$k_{\text{switch}}(\mathbf{x}, \mathbf{x}') = \sum_{g, g' \in G_{\text{swap}}} k(g(\mathbf{x}), g'(\mathbf{x}')) \quad (2.38)$$

$$= k(x, y, x', y') + k(x, y, y', x') + k(y, x, x', y') + k(y, x, y', x') \quad (2.39)$$

For stationary kernels, some pairs of elements in this sum will be identical, and can be ignored. Figure 2.8(a) shows a draw from a GP prior with an SE kernel symmetrized in this way. This construction has the property that the marginal variance is doubled near $x = y$, which may or may not be desirable.

- Project onto a Fundamental Domain.** Ginsbourger et al. (2013) also explore the possibility of projecting each datapoint into a fundamental domain of the group, using a mapping A_G :

$$k_{\text{proj}}(\mathbf{x}, \mathbf{x}') = k(A_G(\mathbf{x}), A_G(\mathbf{x}')) \quad (2.40)$$

For the group G_{swap} , a fundamental domain is $\{x, y : x < y\}$, which can be mapped to using $A_{G_{\text{swap}}}(x, y) = [\min(x, y), \max(x, y)]$. Constructing a kernel using this method introduces a non-differentiable “seam” along $x = y$, as shown in figure 2.8(b). The projection method also works for infinite groups, as we shall see below.

3. Multiply over the Orbit. Ryan P. Adams (personal communication) suggests a construction enforcing invariants through products over the orbits:

$$k_{\text{sum}}(\mathbf{x}, \mathbf{x}') = \prod_{g, \in G} \prod_{g' \in G} k(g(\mathbf{x}), g'(\mathbf{x}')) \quad (2.41)$$

This method can sometimes produce GP priors with zero variance in some regions of the space, as in figure 2.8(c).

There are many possible ways to achieve a given symmetry, but we must be careful to do so without compromising other qualities of the model we are constructing. For example, simply setting $k(\mathbf{x}, \mathbf{x}') = 0$ gives rise to a GP prior which obeys *all possible* symmetries, but this is presumably not a model we wish to use.

2.7.2 Periodicity

Periodicity in a one-dimensional function corresponds to the invariance

$$f(x) = f(x + \tau) \quad (2.42)$$

where τ is the period.

The most popular method for building a periodic kernel is due to MacKay (1998), who used the projection method in combination with an SE kernel. A fundamental domain of the symmetry group is a circle, so the kernel

$$\text{Per}(x, x') = \text{SE}\left(\left[\sin(x), \cos(x)\right], \left[\sin(x'), \cos(x')\right]\right) \quad (2.43)$$

achieves the invariance in Equation (2.42). Simple algebra reduces this kernel to the form shown in Table 2.1.

We could also build a periodic kernel with period τ by the mapping $A(x) = \text{mod}(x, \tau)$. However, samples from this prior would be discontinuous at every integer multiple of τ .

2.7.3 Symmetry About Zero

Another simple example of an easily-enforceable symmetry is symmetry about zero:

$$f(x) = f(-x) \quad (2.44)$$

using the sum over orbits method, by the transform

$$k_{\text{reflect}}(x, x') = k(x, x') + k(x, -x') + k(-x, x') + k(-x, -x') \quad (2.45)$$

2.7.4 Translation Invariance in Images

Most models of images are invariant to spatial translations (LeCun and Bengio, 1995). Similarly, most models of sounds are also invariant to translation through time.

This sort of translation invariance is completely distinct from the stationarity of kernels such as SE or Per. A stationary kernel implies that the prior is invariant to translations of the entire training and test set. In contrast, we use translation invariance to refer to a situation where a signal has been discretized, and each pixel (or the audio equivalent) corresponds to a different input dimension. We are interested in creating priors on functions that are invariant to swapping pixels in a manner that corresponds to shifting a in some direction:

$$f\left(\begin{array}{|c|c|c|} \hline & \blacksquare & \\ \hline \blacksquare & & \\ \hline \end{array}\right) = f\left(\begin{array}{|c|c|c|} \hline & & \blacksquare \\ \hline & \blacksquare & \\ \hline \end{array}\right) \quad (2.46)$$

For example, in a one-dimensional image or audio signal, translation of an input vector by i pixels can be defined as

$$\text{shift}(\mathbf{x}, i) = [x_{\text{mod}(i+1, D)}, x_{\text{mod}(i+2, D)}, \dots, x_{\text{mod}(i+D, D)}]^T \quad (2.47)$$

As above, translation invariance in one dimension can be achieved by the transformation

$$k_{\text{invariant}}(\mathbf{x}, \mathbf{x}') = \sum_{i=1}^D \sum_{j=1}^D k(\text{shift}(\mathbf{x}, i), \text{shift}(\mathbf{x}', j)), \quad (2.48)$$

simply defining the covariance between two signals to be the sum of all covariances between all translations of those two signals.

The extension to two dimensions, $\text{shift}(\mathbf{x}, i, j)$ is straightforward, but notationally cumbersome. Kondor (2008) built a more elaborate kernel between images, approximately invariant to both translation and rotation by using the projection method.

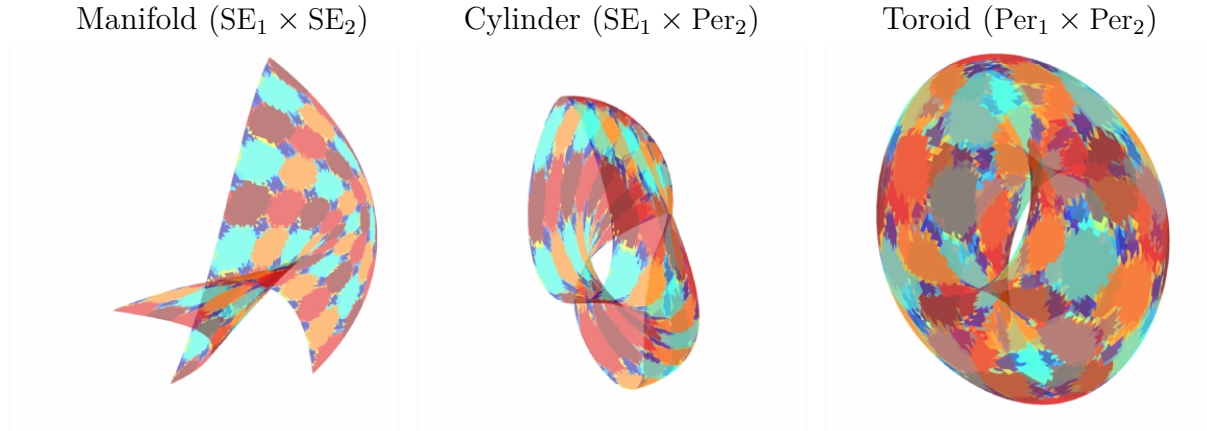


Fig. 2.9 Generating 2D manifolds with different topological structures. By enforcing that the functions mapping from \mathbb{R}^2 to \mathbb{R}^3 obey the appropriate symmetries, the surfaces created have the corresponding topologies, ignoring self-intersections.

2.8 Generating Topological Manifolds

In this section we give a geometric illustration of the symmetries encoded by different compositions of kernels. The work presented in this section is based on a collaboration with David Reshef, Roger Grosse, Josh Tenenbaum, and Zoubin Ghahramani.

Priors on functions exhibiting symmetries can be used to create a prior on topological manifolds, by warping a simply-connected surface into a higher-dimensional space using a mapping expressing symmetries. To build a prior on 2-dimensional manifolds embedded in 3-dimensional space, we simply need a prior on mappings from \mathbb{R}^2 to \mathbb{R}^3 , which we can construct using 3 independent functions $[f_1(\mathbf{x}), f_2(\mathbf{x}), f_3(\mathbf{x})]$, each mapping from \mathbb{R}^2 to \mathbb{R} . GP priors on the mapping functions implicitly give rise to a prior on warped surfaces. Symmetries in $[f_1, f_2, f_3]$ will connect different parts of the manifolds, giving rise to non-trivial topologies on the sampled surfaces. Figure 2.9 shows 2D meshes warped into 3D by functions drawn from GP priors with different kernels, giving rise to a variety of different topologies.

This construction is similar in spirit to the GP latent variable model (GP-LVM) of Lawrence (2005), which learns a latent embedding of the data into a low-dimensional space, using a GP prior on the mapping from the latent space to the observed space.

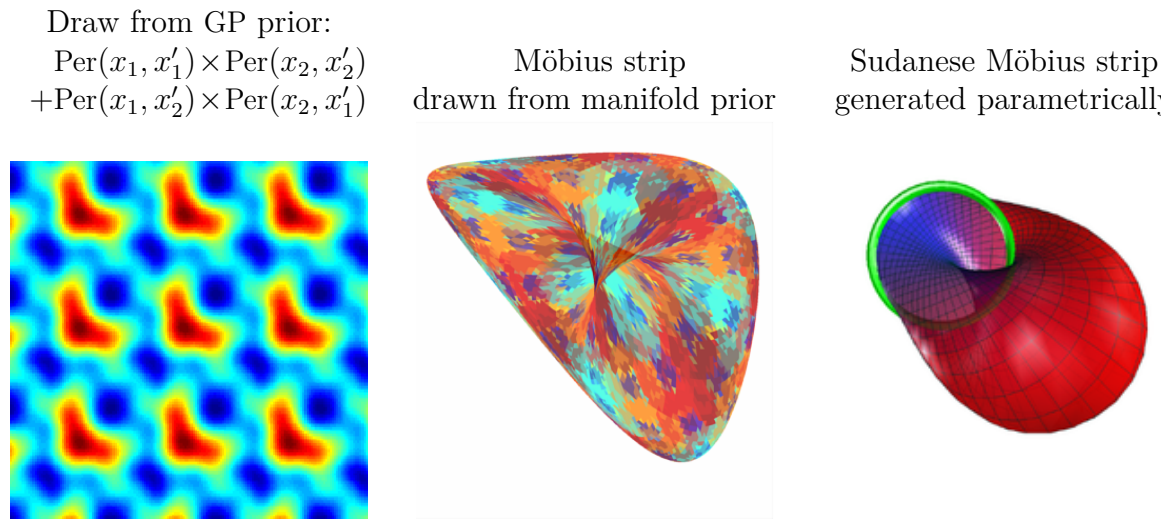


Fig. 2.10 Generating Möbius strips. *Left:* A function drawn from a GP prior obeying the same symmetries as a Möbius strip. *Center:* By enforcing that the functions mapping from \mathbb{R}^2 to \mathbb{R}^3 obey the appropriate symmetries, surfaces sampled from the prior have topology corresponding to a Möbius strip. Surfaces generated this way do not have the familiar shape of a flat surface connected to itself with a half-twist. Instead, they tend to look like *Sudanese Möbius strips* (Lerner and Asimov, 1984), whose edge has a circular shape. *Right:* A Sudanese projection of a Möbius strip. Image adapted from (Commons, 2005).

2.8.1 Möbius Strips

A prior on functions on Möbius strips can be constructed by enforcing the symmetries:

$$f(x, y) = f(x, y + \tau_y) \quad (2.49)$$

$$f(x, y) = f(x + \tau_x, y) \quad (2.50)$$

$$f(x, y) = f(y, x) \quad (2.51)$$

Moving along the diagonal $x = y$ of a function drawn from the corresponding GP prior is equivalent to moving along the edge of a notional Möbius strip which has had the function mapped on to its surface. Figure 2.10(a) shows an example of a function drawn from such a prior.

Figure 2.10(b) shows an example of a 2D mesh mapped to 3D by functions drawn from such a prior. This surface doesn't resemble the typical representation of a Möbius strip, but instead resembles an embedding known as the Sudanese Möbius strip (Lerner and Asimov, 1984), shown in Figure 2.10(c).

2.9 Kernels on Categorical Variables

Categorical variables are variables which can take values only from a discrete, unordered set, such as $\{\text{blue}, \text{green}, \text{red}\}$. A flexible way to construct a kernel over categorical variables is simply to represent that variable through a set of binary variables, using a one-of-k encoding. For example, if x can take one of 4 values, $x \in \{\text{A}, \text{B}, \text{C}, \text{D}\}$, then a one-of-k encoding of x will correspond to 4 binary inputs, and $\text{one-of-k}(\text{C}) = [0, 0, 1, 0]$. Given a one-of-k encoding, we can place any multidimensional kernel on that space, such as the SE-ARD:

$$k_{\text{categorical}}(x, x') = \text{SE-ARD}(\text{one-of-k}(x), \text{one-of-k}(x')) \quad (2.52)$$

Short lengthscales on any particular dimension in the SE-ARD kernel indicate that the function value corresponding to that category is uncorrelated with the others.

A more flexible parameterization suggested by Kevin Swersky (personal communication) allows complete flexibility about which pairs of categories are similar to one another, replacing the SE-ARD kernel with a fully-parameterized kernel, SE-full:

$$\text{SE-full}(\mathbf{x}, \mathbf{x}') = \exp\left(-\frac{1}{2}\mathbf{x}^T \mathbf{L} \mathbf{x}'\right) \quad (2.53)$$

where L is a symmetric matrix, individually parameterizing the covariance between each pair of function values of categories.

2.10 Building a Kernel in Practice

One difficulty in building GP models is choosing, or integrating over, the kernel parameters. If the kernel we construct has relatively few parameters, these parameters can be estimated by maximum marginal likelihood, using gradient-based optimizers. The kernel parameters estimated in the examples above were optimized using the GPML toolbox, available at gaussianprocess.org/gpml/code.

In the next chapter, we'll see how to perform such a search not just over the kernel parameters, but also over the open-ended space of kernel expressions.

Source Code

Source code to produce all figures is available at github.com/duvenaud/pdh-thesis.

Chapter 3

Automatic Model Construction

“It would be very nice to have a formal apparatus that gives us some ‘optimal’ way of recognizing unusual phenomena and inventing new classes of hypotheses that are most likely to contain the true one; but this remains an art for the creative human mind.”

E. T. Jaynes, 1985

In chapter 2, we saw that the choice of kernel determines the type of structure that can be learned by a GP model, and that a wide variety of models could be constructed through simply adding and multiplying a few base kernels together. However, we didn’t answer the difficult question of how which kernel to use for a given problem. Even for experts, choosing the kernel in GP regression remains something of a black art.

In this chapter, we’ll automate the process of building kernels for GP models. To do so, we’ll need to define an open-ended space of kernels. We’ll do this by simply adding and multiplying together simple kernels from a fixed set. We can then simply search over this space to find a kernel which captures as much structure in the data as possible.

Searching over such a large, structured model class has two main benefits. First, this procedure has very good predictive accuracy, since it tries out a large number of different regression models. Second, this procedure can discover interpretable structure in datasets. Because GP posteriors can be decomposed (as in section 2.4.3), we can also examine the resulting structures visually. In chapter 4, we’ll even show how to automatically generate English-language descriptions of the resulting models.

This chapter is based on work done in collaboration with James Robert Lloyd, Roger Grosse, Joshua B. Tenenbaum, and Zoubin Ghahramani. It was published in ([Duvenaud et al., 2013](#)) and ([Lloyd et al., 2014](#)). Myself, James Lloyd and Roger Grosse jointly developed the idea of searching through a grammar-based language of GP models, inspired

by Grosse et al. (2012), and wrote the first versions of the code together. James Lloyd ran most of the experiments.

3.1 Ingredients of an Automatic Statistician

Gelman (2013) asks “How can an artificial intelligence do statistics? ... It needs not just an inference engine, but also a way to construct new models and a way to check models. Currently, those steps are performed by humans, but the AI would have to do it itself.” In this section, we’ll discuss the different parts we think are required to build an artificial intelligence that can do statistics.

1. An open-ended language of models Many learning algorithms consider all models in a class of fixed size. For example, graphical model learning algorithms (Eaton and Murphy, 2007; Friedman and Koller, 2003) search over different connectivity graphs for a given set of nodes. While such methods can be powerful, human statisticians are capable of deriving novel model classes when required. An automatic search through an open-ended class of models can achieve some of this flexibility, growing the complexity of the model as needed, possibly combining existing structures in novel ways.

2. A search through model space An open-ended space of models cannot be searched exhaustively. Just as human researchers iteratively refine their models, search procedures can propose new search directions based on the results of previous model fits. Because any search in an open-ended space must start with relatively simple models before moving on to more complex ones, any search strategy is likely to resemble an iterative model-building procedure.

3. A model comparison procedure A search strategy requires an objective to optimize. In this work, we use approximate marginal likelihood to compare models, penalizing complexity using the Bayesian Information Criterion as a heuristic. More generally, an automatic statistician should be able to question the models it has constructed. Gelman and Shalizi (2012) review the literature on model checking.

4. A model description procedure Part of the value of statistical models comes from helping humans to understand a dataset or a phenomenon. Furthermore, a clear description of the statistical structure found in a dataset helps a user to notice when the

dataset has errors, the wrong question was asked, the model-building procedure failed to capture known structure, a relevant piece of data or constraint is missing, or when a novel statistical structure has been found.

In this chapter, we introduce a system containing all the above ingredients. We call this system the Automatic Bayesian Covariance Discovery (ABCD) system. The next four sections of this chapter describe the mechanisms we use to produce these four ingredients, for this particular example of an artificial intelligence which does statistics.

3.2 A Language of Regression Models

As shown in chapter 2, we can construct a wide variety of kernel structures compositionally by adding and multiplying a small number of base kernels. We can therefore define a language of GP regression models simply by specifying a language of kernels.

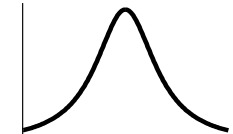
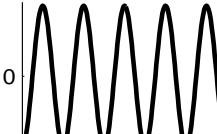
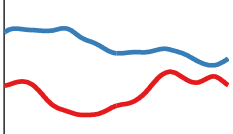
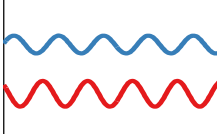
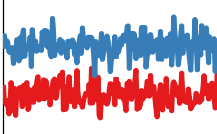
Kernel name:	Rational quadratic (RQ)	Cosine (cos)	White noise (Lin)
$k(x, x') =$	$\left(1 + \frac{(x-x')^2}{2\alpha\ell^2}\right)^{-\alpha}$	$\cos\left(2\pi\frac{(x-x')}{p}\right)$	$\delta(x - x')$
Plot of kernel:			
	$x - x'$ ↓	$x - x'$ ↓	x (with $x' = 1$) ↓
Samples from prior:			
Type of structure:	multiscale variation	sine waves	uncorrelated noise

Table 3.1 New base kernels introduced in this chapter, and the types of structure they encode. More interesting kernels can be constructed by adding and multiplying base kernels together.

To specify an open-ended language of structured kernels, we'll consider the set of all

kernels that can be built by adding and multiplying these base kernels together:

$$k_1 + k_2 = k_1(\mathbf{x}, \mathbf{x}') + k_2(\mathbf{x}, \mathbf{x}')$$
 (3.1)

$$k_1 \times k_2 = k_1(\mathbf{x}, \mathbf{x}') \times k_2(\mathbf{x}, \mathbf{x}')$$
 (3.2)

This language of models is made out of a set of base kernels which capture different properties of functions, and a set of composition rules which combine kernels to yield other valid kernels. In this chapter, we'll use such base kernels as white noise (WN), constant (C), linear (Lin), squared-exponential (SE), rational-quadratic (RQ), sigmoidal (σ) and periodic (Per). We use a generalized form of Per due to [Lloyd \(2013a\)](#) which has $\cos(x - x')$ as a special case. Table 3.1 shows the new kernels introduced in this chapter. For precise definitions of all kernels, see appendix B. Table 3.2 lists common regression models that can be expressed by this language.

Regression model	Kernel	Related work
Linear regression	C + Lin + WN	
Kernel ridge regression	SE + WN	
Linear Semi-parametric	Lin + SE + WN	(e.g. Ruppert et al., 2003)
Multiple kernel learning	\sum SE + WN	(e.g. Bach et al., 2004)
Trend, cyclical, irregular	\sum SE + \sum Per + WN	(Lind et al., 2006)
Fourier decomposition	C + \sum cos + WN	
Sparse spectrum GPs	\sum cos + WN	(Lázaro-Gredilla et al., 2010)
Spectral mixture	\sum SE \times cos + WN	(Wilson and Adams, 2013)
Changepoints	e.g. CP(SE, SE) + WN	(e.g. Garnett et al., 2010)
Heteroscedasticity	e.g. SE + Lin \times WN	
Additive + Flexible	\sum_d SE _d + \prod_d SE _d	(Plate, 1999)

Table 3.2 Common regression models expressible by sums and products of base kernels. $\cos(\cdot, \cdot)$ is a special case of our reparametrised Per(\cdot, \cdot).

3.3 A Model Search Procedure

We explore the space of regression models using a simple greedy search. At each stage, we choose the highest scoring kernel, and propose modifying it by applying an operation to one of its parts, combining or replacing that part with another base kernel. The basic operations we can perform on any part k of a kernel are:

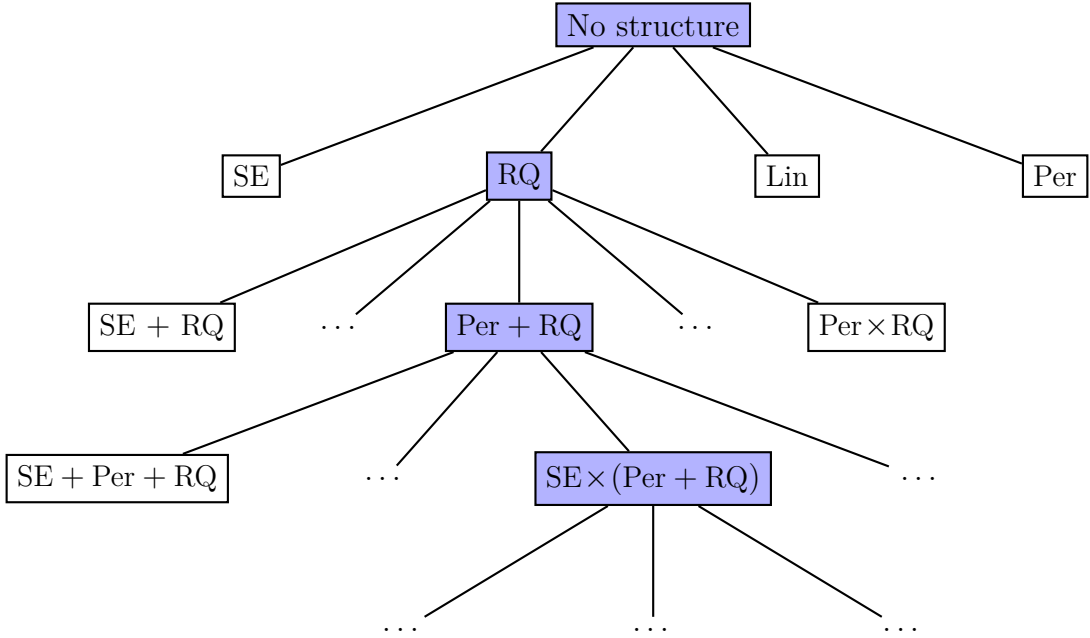


Fig. 3.1 An example of a search tree over kernel expressions. Figure 3.2 shows the corresponding model increasing in sophistication as the kernel expression grows.

$$\begin{aligned}
 \text{Replacement: } & k \rightarrow k' \\
 \text{Addition: } & k \rightarrow k + k' \\
 \text{Multiplication: } & k \rightarrow k \times k'
 \end{aligned}$$

These operators can generate all possible algebraic expressions involving addition and multiplication of base kernels. To see this, observe that if we restricted the addition and multiplication rules to only apply to base kernels, we would obtain a context-free grammar which generates the set of algebraic expressions.

Figure 3.1 shows an example search tree followed by our algorithm. Figure 3.2 shows how the resulting model changes as the search is followed. In practice, we also include extra operators which propose commonly-occurring structures, such as changepoints. A complete list is contained in appendix C.

Our search operators are motivated by strategies that human researchers often use to construct kernels. In particular,

- One can look for structure, such as periodicity, in the residuals of a model, and then extend the model to capture that structure. This corresponds to adding a new kernel to the existing structure.
- One can start with structure, such as linearity, which is assumed to hold glob-

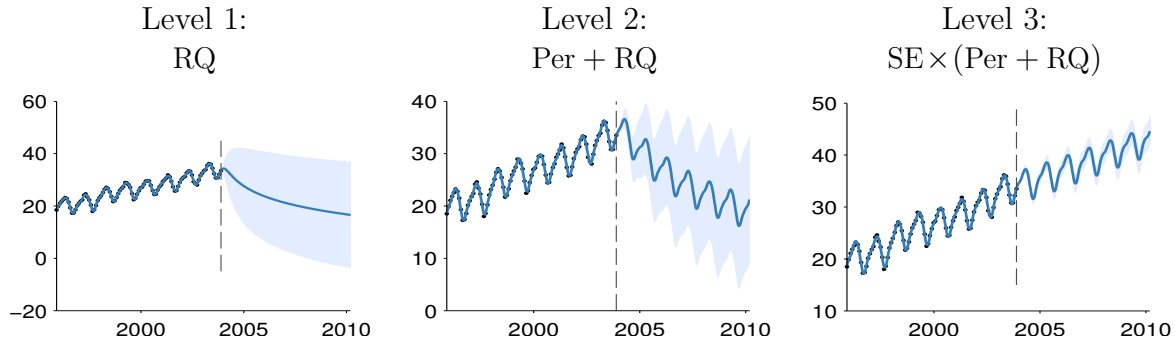


Fig. 3.2 Posterior mean and variance for different depths of kernel search on the Mauna Loa dataset. The dashed line marks the end of the dataset. *Left:* the function is only modeled as a locally smooth function, and the extrapolation is poor. *Middle:* a periodic component is added, and the extrapolation improves. *Right:* at depth 3, the kernel can capture most of the relevant structure, and is able to extrapolate reasonably.

ally, but find that it only holds locally. This corresponds to multiplying a kernel structure by a local kernel, such as SE.

- One can add features incrementally, analogous to algorithms like boosting, back-fitting, or forward selection. This corresponds to adding or multiplying with kernels on dimensions not yet included in the model.

Hyperparameter Initialization

Unfortunately, optimizing the marginal likelihood over parameters is not a convex optimization problem, and the space can have many local optima. For example, in data with periodic structure, integer multiples of the true period (harmonics) are often local optima. We take advantage of our search procedure to provide reasonable initializations: all of the parameters which were part of the previous kernel are initialized to their previous values, while randomly initializing any newly introduced parameters. In the newly proposed kernel, all parameters are then optimized using conjugate gradients. This procedure is not guaranteed to find the global optimum, but it implements the commonly used heuristic of iteratively modeling residuals.

3.4 A Model Comparison Procedure

Choosing a kernel requires a method for comparing models. We choose marginal likelihood as our criterion, since it balances the fit and complexity of a model ([Rasmussen](#)

and Ghahramani, 2001). Conditioned on kernel parameters, the marginal likelihood of a GP can be computed analytically. Given a parametric form of a kernel, we can also choose its parameters using marginal likelihood. However, choosing kernel parameters by maximum likelihood (as opposed to integrating them out) raises the possibility of overfitting. In addition, if we compare two classes of kernels by the maximum likelihood found by optimizing over the kernel parameters, then all else being equal, the kernel class having more free parameters will be chosen. This introduces a bias for more complex models.

We could avoid overfitting by integrating the marginal likelihood over all free parameters, but this integral is difficult to do in general. Instead, we approximate this integral using the Bayesian information criterion (BIC) (Schwarz, 1978):

$$\text{BIC}(M) = \log p(D | M) - \frac{1}{2}|M| \log N \quad (3.3)$$

where $p(D|M)$ is the marginal likelihood of the data (given by equation (1.3)), $|M|$ is the number of kernel parameters, and N is the number of data points. BIC simply penalizes the marginal likelihood in proportion to how many parameters the model has. Because BIC is a function of the number of parameters in a model, we did not count kernel parameters known to not affect the model. For example, when two kernels are multiplied, one of their output variance parameters becomes redundant, and can be ignored.

Other more sophisticated approximations are possible, such as Laplace's approximation. We chose to try BIC first because of its simplicity, and it performed reasonably in our experiments.

3.5 A Model Description Procedure

As discussed in Chapter 2, a GP whose kernel is a sum of kernels can be viewed as a sum of functions drawn from different GPs. We can always express any kernel structure as a sum of products of kernels, by distributing all products of sums. For example,

$$\text{SE} \times (\text{RQ} + \text{Lin}) = \text{SE} \times \text{RQ} + \text{SE} \times \text{Lin} \quad (3.4)$$

This decomposition into additive components provides a method of visualizing the learned model, breaking down the different types of structure discovered in the data. In chapter 4, we extend this model visualization method to include automatically-generated

English text explaining the meaning of each type of structure discovered.

3.6 Structure Discovery in Time Series

To investigate our method’s ability to discover structure, we ran the kernel search on several time-series. In the following examples, the search was run to depth 10, using SE, RQ, Lin, Per and WN as base kernels.

3.6.1 Mauna Loa Atmospheric CO₂

Using our method, we analyzed records of carbon dioxide levels recorded at the Mauna Loa observatory. Since this dataset was analyzed in detail by [Rasmussen and Williams \(2006\)](#), we can compare the kernel chosen by our method to a kernel constructed by human experts.

Figure 3.2 shows the posterior mean and variance on this dataset as the search depth increases. While the data can be smoothly interpolated by a model with only a single base kernel, the extrapolations improve dramatically as the increased search depth allows more structure to be included.

Figure 3.3 shows the final model chosen by our method, together with its decomposition into additive components. The final model exhibits both plausible extrapolation and interpretable components: a long-term trend, annual periodicity, and medium-term deviations. These are the same components chosen in the kernel hand-constructed by [Rasmussen and Williams \(2006, Chapter 5\)](#).

We also plot the residuals modeled by a white noise (WN) component, showing that there is little obvious structure left in the data. More generally, some components capture slowly-changing structure while others capture quickly-varying struture, but there is no hard distinction between “signal” components and “noise” components.

3.6.2 Airline Passenger Counts

Figure 3.4 shows the decomposition produced by applying our method to monthly totals of international airline passengers ([Box et al., 1976](#)). We observe similar components to those in the Mauna Loa dataset: a long term trend, annual periodicity, and medium-term deviations. In addition, the composite kernel captures the near-linearity of the long-term trend, and the linearly growing amplitude of the annual oscillations.

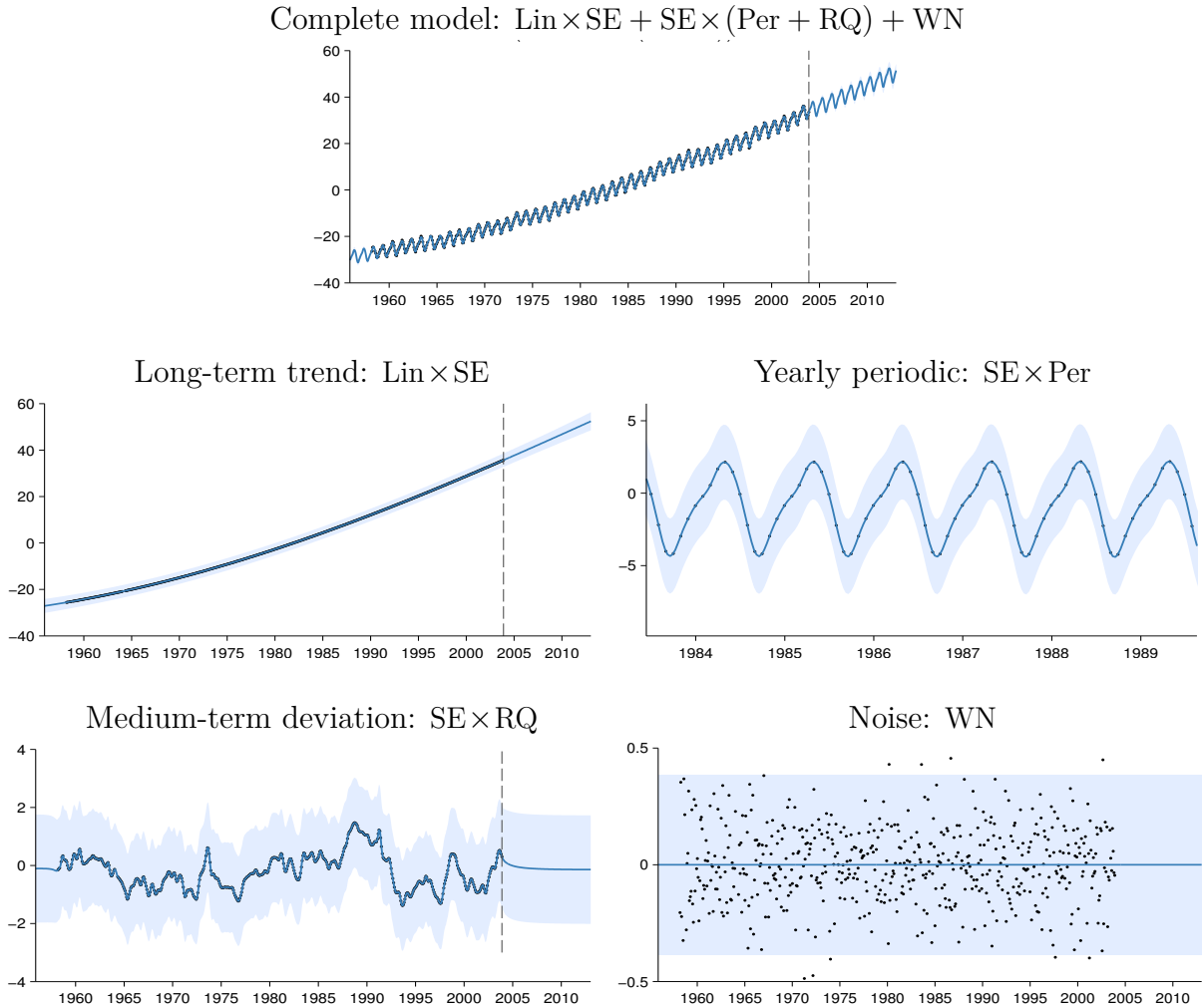


Fig. 3.3 *First row*: The full posterior on the Mauna Loa dataset, after a search of depth 10. *Subsequent rows*: The automatic decomposition of the time series. The decomposition is a sum of long-term, yearly periodic, medium-term components, and residual noise, respectively. The yearly periodic component has been rescaled for clarity.

3.7 Related Work

Building Kernel Functions by Hand

Rasmussen and Williams (2006, Chapter 5) devote 4 pages to manually constructing a composite kernel to model the Mauna Loa dataset. Other examples of papers whose main contribution is to manually construct and fit a composite GP kernel are (Klenske et al., 2013; Lloyd, 2013b; Preotiuc-Pietro and Cohn, 2013).

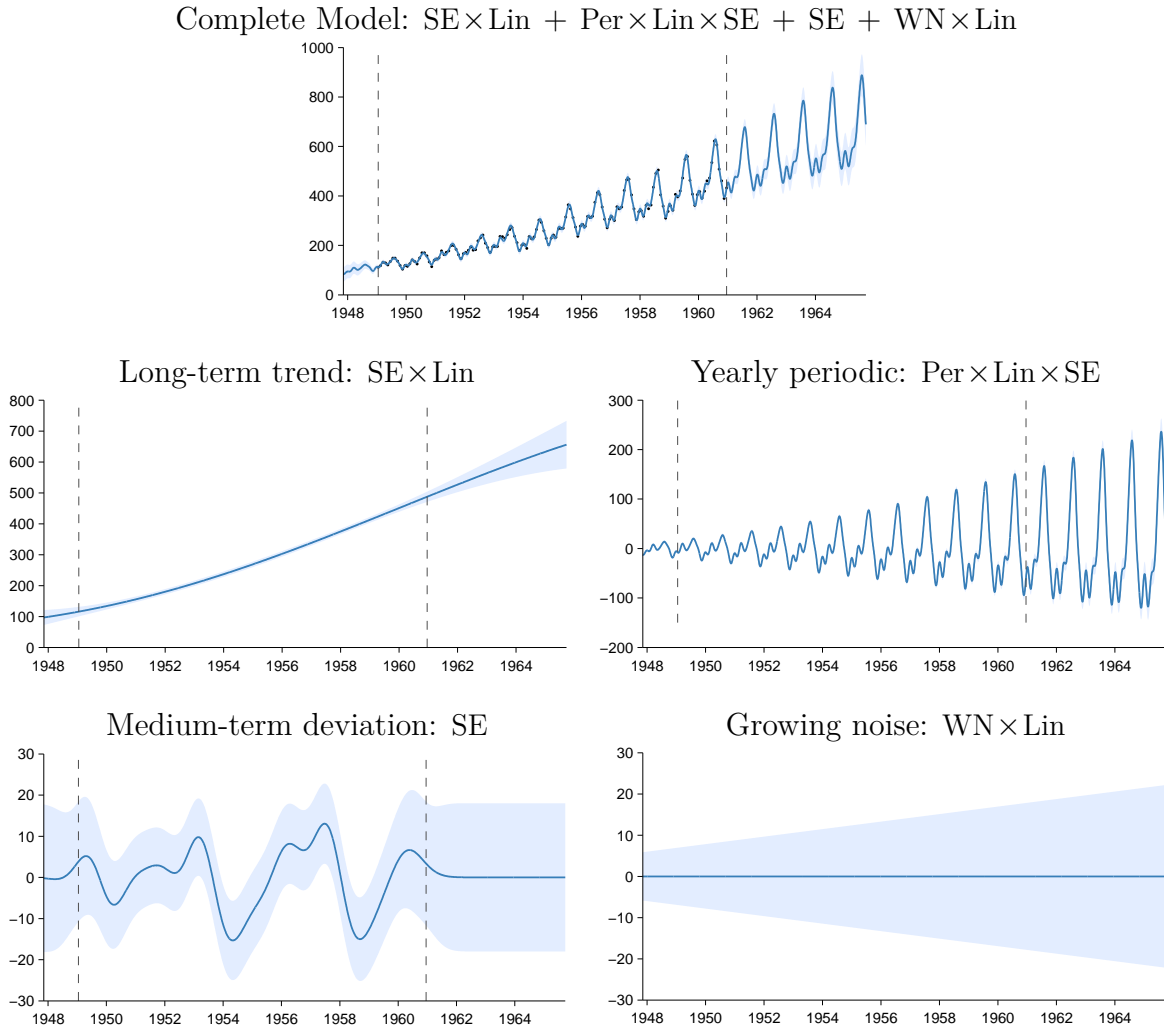


Fig. 3.4 *First row:* The airline dataset and posterior after a search of depth 10. *Subsequent rows:* Additive decomposition of posterior into long-term smooth trend, yearly variation, and short-term deviations. Due to the linear kernel, the marginal variance grows over time, making this a heteroskedastic model.

Nonparametric Regression in High Dimensions

Nonparametric regression methods such as splines, locally-weighted regression, and GP regression are popular because they are capable of learning arbitrary smooth functions of the data. Unfortunately, they suffer from the curse of dimensionality: it is very difficult for these models to generalize well in more than a few dimensions.

Applying nonparametric methods in high-dimensional spaces can require imposing additional structure on the model. One such structure is additivity. Generalized additive

models (GAM) assume the regression function is a transformed sum of functions defined on the individual dimensions: $\mathbb{E}[f(\mathbf{x})] = g^{-1}(\sum_{d=1}^D f_d(x_d))$. These models have a limited compositional form, but one which is interpretable and often generalizes well. In our grammar, we can capture such structure through sums of base kernels along different dimensions, although we have not yet tried incorporating a warping function $g(\cdot)$.

It is possible to add more flexibility to additive models by considering higher-order interactions between different dimensions. In chapter 6, we'll consider GP models whose kernel implicitly sums over all possible products of one-dimensional base kernels. Plate (1999) constructs a special case of this model class, summing an SE kernel along each dimension, with a single SE-ARD kernel (a product of SE over all dimensions). Both of these models can be expressed in our grammar.

A closely related procedure is smoothing-splines ANOVA (Gu, 2002; Wahba, 1990). This model is a linear combinations of splines along each dimension, all pairs of dimensions, and possibly higher-order combinations. Because the number of terms to consider grows exponentially in the order, in practice, only terms of first and second order are usually considered.

Semi-parametric regression (e.g. Ruppert et al., 2003) attempts to combine interpretability with flexibility by building a composite model out of an interpretable, parametric part (such as linear regression) and a ‘catch-all’ nonparametric part (such as a GP with an SE kernel). This model class can be represented through the kernel $\text{SE} + \text{Lin}$.

Kernel Learning

There is a large body of work attempting to construct a rich kernel through a weighted sum of base kernels (e.g. Bach, 2009a; Christoudias et al., 2009). These approaches find the optimal solution in polynomial time, however the component kernels, as well as their parameters, must be specified in advance.

Salakhutdinov and Hinton (2008) use a deep neural network with unsupervised pre-training to learn an embedding $g(\mathbf{x})$ onto which a GP with an SE kernel is placed: $\text{Cov}[f(\mathbf{x}), f(\mathbf{x}')] = k(g(\mathbf{x}), g(\mathbf{x}'))$. This is a flexible approach to kernel learning, but relies upon finding structure in the input density $p(\mathbf{x})$. Instead, we focus on domains where most of the interesting structure is in $f(\mathbf{x})$.

Sparse spectrum GPs (Lázaro-Gredilla et al., 2010) approximate the spectral density of a stationary kernel function using delta functions which corresponds to kernels of the form $\sum \cos$. Similarly, Wilson and Adams (2013) introduce spectral mixture kernels, which approximate the spectral density using a mixture of Gaussians – corresponding

to kernels of the form $\sum SE \times \cos$. Both groups demonstrate, using Bochner’s theorem (Bochner, 1959), that these kernels can approximate any stationary covariance function. Our language of kernels includes both of these kernel classes (see table 3.2).

There is a large body of work attempting to construct rich kernels through a weighted sum of base kernels called multiple kernel learning (MKL) (e.g. Bach et al., 2004). These approaches find the optimal solution in polynomial time, but only if the component kernels and parameters are pre-specified. We compare to a Bayesian variant of MKL in section 3.8, expressed as a restriction of our language of kernels.

Equation Learning

Todorovski and Dzeroski (1997), Washio et al. (1999) and Schmidt and Lipson (2009) learn parametric forms of functions specifying time series, or relations between quantities. In contrast, ABCD learns a parametric form for the covariance, allowing it to model functions which don’t have a simple parametric form but still have high-level structure. An examination of the structure discovered by the automatic equation-learning software Eureqa (Nutonian, 2011) on the airline and Mauna Loa datasets can be found in (Lloyd et al., 2014).

Structure Discovery through Grammars

Kemp and Tenenbaum (2008) learned the structural form of a graph used to model human similarity judgements. Their grammar on graph structures includes planes, trees, and cylinders. Some of their discrete graph structures have continuous analogues in our own space. For example, $SE_1 \times SE_2$ and $SE_1 \times Per_2$ can be seen as mapping the data to a plane and a cylinder, respectively. Section 2.8 examines these structures in more detail.

Diosan et al. (2007) and Bing et al. (2010) learn composite kernels for support vector machines and relevance vector machines, respectively, using genetic search algorithms to optimize cross-validation error. Similarly, Kronberger and Kommenda (2013) search over composite kernels for GPs using genetic programming, optimizing the unpenalized marginal likelihood. These methods explore similar languages of kernels to the one explored in this chapter. It is not clear whether the complex genetic searches used by these methods offer advantages over the straightforward but naïve greedy search used in this chapter. Our search criterion has the advantages of being both differentiable with respect to kernel parameters, and trading off model fit and complexity automatically. This prior work also did not explore the automatic model decomposition, summarization

and description made possible by the use of GP models.

Grosse et al. (2012) performed a greedy search over a compositional model class for unsupervised learning, using a grammar of matrix decomposition models, and a greedy search procedure based on held-out likelihood. This model class contains many existing unsupervised models as special cases, and was able to discover such structure automatically from data. Our framework takes a similar approach, but in a supervised setting.

Similarly, Steinruecken (2014) showed to automatically perform inference in arbitrary compositions of discrete sequence models. More generally, Dechter et al. (2013) and Liang et al. (2010) constructed grammars over programs, and automatically searched the resulting spaces.

3.8 Experiments

3.8.1 Interpretability versus Accuracy

BIC trades off model fit and complexity by penalizing the number of parameters in a kernel expression. This can result in ABCD favoring kernel expressions with nested products of sums, producing descriptions involving many additive components when expressions are expanded. While these models typically have good predictive performance, the large number of components can make them less interpretable. We experimented with not allowing parentheses during the search, discouraging nested expressions. We call this procedure ABCD-interpretability, in contrast to the unrestricted version of the search, ABCD-accuracy.

3.8.2 Predictive Accuracy on Time Series

We evaluate the performance of the algorithms listed below on 13 real time-series from various domains from the time series data library (Hyndman, Accessed July 2013).

Algorithms

We compare ABCD to equation learning using Eureqa (Nutonian, 2011), as well as six other regression algorithms: linear regression, GP regression with a single SE kernel (squared exponential), a Bayesian variant of multiple kernel learning (MKL) (e.g. Bach et al., 2004), changepoint modeling (e.g. Fox and Dunson, 2013; Garnett et al.,

2010; Saatçi et al., 2010), spectral mixture kernels (Wilson and Adams, 2013) (spectral kernels), and trend-cyclical-irregular models (e.g. Lind et al., 2006).

We set Eureqa’s search objective to the default mean-absolute-error. All algorithms besides Eureqa can be expressed as restrictions of our modeling language (see table 3.2), so we perform inference using the same search and objective function, with appropriate restrictions to the language. For MKL, trend-cyclical-irregular, and spectral kernels, the greedy search procedure of ABCD corresponds to a forward-selection algorithm. For squared-exponential and linear regression, the procedure corresponds to standard marginal likelihood optimization.

We restricted to regression algorithms for comparability; we did not include models which regress on previous values of times series, such as auto-regressive or moving-average models (e.g. Box et al., 2013). Constructing a language of autoregressive time-series models would be an interesting area for future research.

Extrapolation Experiments

To test extrapolation, we trained all algorithms on the first 90% of the data, predicted the remaining 10% and then computed the root mean squared error (RMSE). The RMSEs are then standardised by dividing by the smallest RMSE for each data set, so the best performance on each data set will have a value of 1.

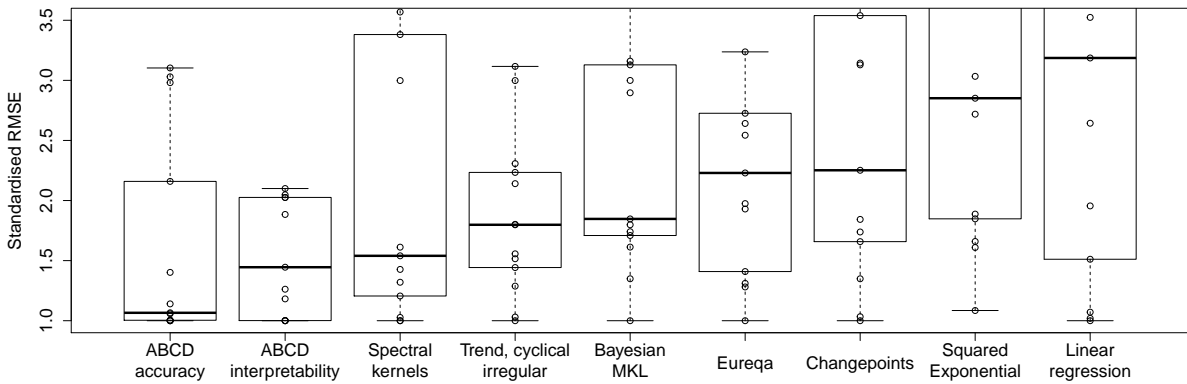


Fig. 3.5 Box plot (showing median and quartiles) of standardised extrapolation RMSE (best performance = 1) on 13 time-series. The methods are ordered by median.

Figure 3.5 shows the standardised RMSEs across algorithms. ABCD-accuracy outperforms ABCD-interpretability. Both algorithms have lower quartiles than all other

methods.

Overall, the model construction methods with greater capacity perform better: ABCD outperforms trend-cyclical-irregular, which outperforms Bayesian MKL, which outperforms squared-exponential. Despite searching over a rich model class, Eureqa performs relatively poorly, since very few datasets are parsimoniously explained by a parametric equation.

Not shown on the plot are large outliers for spectral kernels, Eureqa, squared exponential and linear regression with normalized RMSEs of 11, 493, 22 and 29 respectively.

3.8.3 High-dimensional Prediction

ABCD can also be applied to multidimensional regression problems without modification. An experimental comparison with other methods can be found in section 6.5, where it outperforms a wide variety of multidimensional regression methods.

3.8.4 Structure Recovery on Synthetic Data

The structure found in the examples above may seem reasonable, but we may wonder to what extent ABCD is consistent - that is, when do we recover all the structure in any given dataset? It is difficult to tell from predictive accuracy alone if the search procedure is finding the correct structure, especially in multiple dimensions. To address this question, we tested our method's ability to recover known structure on a set of synthetic datasets.

For several composite kernel expressions, we constructed synthetic data by first sampling 300 points uniformly at random, then sampling function values at those points from a GP prior. We then added i.i.d. Gaussian noise to the functions at various signal-to-noise ratios (SNR).

Table 3.3 shows the results. For the highest SNR, the method finds all relevant structure except in one case. The reported additional linear structure in the last row is explainable by the fact that functions sampled from SE kernels with long length-scales occasionally have near-linear trends. As the noise increases, our method generally backs off to simpler structures, rather than over-fitting.

Source Code

Source code to perform all experiments is available at github.com/jamesrobertlloyd/gpss-research/. All GP parameter optimisation was performed by automated calls to

Table 3.3 Kernels chosen by our method on synthetic data generated using known kernel structures. D denotes the dimension of the functions being modeled. SNR indicates the signal-to-noise ratio. Dashes (-) indicate no structure was found. Each kernel implicitly has a WN kernel included.

True Kernel	D	SNR = 10	SNR = 1	SNR = 0.1
SE + RQ	1	SE	SE × Per	SE
Lin × Per	1	Lin × Per	Lin × Per	SE
SE ₁ + RQ ₂	2	SE ₁ + SE ₂	Lin ₁ + SE ₂	Lin ₁
SE ₁ + SE ₂ × Per ₁ + SE ₃	3	SE ₁ + SE ₂ × Per ₁ + SE ₃	SE ₂ × Per ₁ + SE ₃	-
SE ₁ × SE ₂	4	SE ₁ × SE ₂	Lin ₁ × SE ₂	Lin ₂
SE ₁ × SE ₂ + SE ₂ × SE ₃	4	SE ₁ × SE ₂ + SE ₂ × SE ₃	SE ₁ + SE ₂ × SE ₃	SE ₁
(SE ₁ + SE ₂) × (SE ₃ + SE ₄)	4	(SE ₁ + SE ₂) × ...	(SE ₁ + SE ₂) × ...	-
		(SE ₃ × Lin ₃ × Lin ₁ + SE ₄)	SE ₃ × SE ₄	

the GPML toolbox, available at www.gaussianprocess.org/gpml/code/.

3.9 Discussion

Towards the goal of automating statistical modeling, we developed a system which constructs an appropriate model from an open-ended language, and automatically generates plots decomposing the different types of structure present in the model.

We achieved this by introducing a space kernels defined compositionally as sums and products of a small number of base kernels. The set of models in this space includes many standard regression models. We proposed a search procedure for this space of kernels, and argued that this search process parallels the process of scientific discovery, and of model-building by statisticians.

We found that the learned structures are often capable of accurate extrapolation in complex time-series datasets, and are competitive with widely used kernel classes and kernel combination methods on a variety of prediction tasks. The learned kernels often yield decompositions of a signal into diverse and interpretable components, enabling model-checking by humans. We hope that this procedure has the potential to make powerful statistical model-building techniques accessible to non-experts.

In the next chapter, we'll see how the model components found by this procedure can be automatically described in terms of English-language text.

Chapter 4

Automatic Model Description

The previous chapter showed how to automatically build structured models through a language of kernels, how to decompose the resulting models into the different types of structure present, and how to visually illustrate the type of structure captured by each component.

Most of the structure present in each component was determined by that component's kernel. Even across different datasets, the meaning of the individual parts of those kernels is relatively consistent. For example, `Per` usually indicates some sort of repeating structure, and `SE` usually indicates smooth change over time. This chapter shows how to take advantage of this modularity to develop a method for automatically describing the structure represented by components of structured GP models through text. The main idea is to treat every component of a product kernel as an adjective, or as a short phrase which modifies the description of a kernel.

Combining model search, plots, and text, we present a system which automatically generates reports which highlight interpretable features discovered in a variety of data sets. An example of a complete automatically-generated report can be found in chapter D.

The work appearing in this chapter was written in collaboration with James Robert Lloyd, Roger Grosse, Joshua B. Tenenbaum, Zoubin Ghahramani, and was published in (Lloyd et al., 2014). The procedure translating kernels into adjectives grew out of discussions between James and myself. James Lloyd wrote the code to automatically generate reports, and ran all of the experiments.

4.1 Generating Descriptions of Kernels

There are two main features of our language of GP models that allow description to be performed automatically. First, the sometimes complicated kernel expressions found by the model search can always be simplified into a sum of products. As discussed in chapter 2, a sum of kernels corresponds to a sum of functions, so each product can be described separately. Second, each kernel in a product modifies the resulting model in a consistent way. Therefore, to generate a description of a product of kernels, we can describe one kernel using a noun with all others described using adjectives.

For example, we can describe the product of kernels Per \times SE by representing Per by a noun (“a periodic function”) modified by a phrase representing the effect of the SE kernel (“whose shape varies smoothly over time”). To simplify the system, we restrict the base kernels to C, Lin, WN, SE, Per, and σ (allowing changepoints and change-windows).

4.1.1 Simplification Rules

In order to be able to use the same adjectives to for each type of kernel in different circumstances, we must convert each kernel expression into a standard, simplified form.

We do this by first distributing all products of sums into a sum of products. Then, we apply several simplifications to the kernel expression:

- Products of two or more SE kernels can be equivalently represented by a single SE with different parameters.
- Multiplying the white-noise kernel WN by any stationary kernel (C, WN, SE, or Per) gives another WN kernel.
- Multiplying any kernel by C only changes the parameters of the original kernel, and so can be factored out of any product in which it appears.

After applying these rules, any kernel can be written as a sum of terms of the form:

$$K \prod_m \text{Lin}^{(m)} \prod_n \boldsymbol{\sigma}^{(n)}, \quad (4.1)$$

where K is one of $\{\text{WN}, \text{C}, \text{SE}, \prod_k \text{Per}^{(k)}\}$ or $\{\text{SE} \prod_k \text{Per}^{(k)}\}$, where $\prod_i k^{(i)}$ denotes a product of kernels, each with different parameters. We use superscripts to distinguish between different instances of the same kernel appearing in a product: $\text{SE}^{(1)}$ can have different kernel parameters than $\text{SE}^{(2)}$.

4.1.2 Describing Each Kernel in a Product

Loosely speaking, each kernel in a product modifies the resulting GP model in a consistent way. This allows us to describe the contribution of each kernel in a product as an adjective, or more generally as a post-modifier of a noun. We now describe how each of the kernels in our grammar modifies a GP model.

- **Multiplication by SE** removes long range correlations from a model since, $\text{SE}(x, x')$ decreases monotonically to 0 as $|x - x'|$ increases. This will convert any global correlation structure into local correlation only.
- **Multiplication by Lin** is equivalent to multiplying the function being modeled by a linear function. If $f(x) \sim \text{GP}(0, k)$, then $xf(x) \sim \text{GP}(0, \text{Lin} \times k)$. This causes the standard deviation of the model to vary linearly without affecting the correlation.
- **Multiplication by σ** is equivalent to multiplying the function being modeled by a sigmoid, which means that the function goes to zero before or after some point.
- **Multiplication by Per** modifies the correlation structure in the same way as multiplying the function by an independent periodic function. This follows from the fact that if $f_1(x) \sim \text{GP}(0, k_1)$ and $f_2(x) \sim \text{GP}(0, k_2)$ then

$$\text{Cov}[f_1(x)f_2(x), f_1(x')f_2(x')] = k_1(x, x')k_2(x, x'). \quad (4.2)$$

Put more plainly, a GP whose covariance is a product of kernels has the same covariance (but not necessarily the same higher moments) as a product of two functions, each drawn from the corresponding GP prior. This identity holds for any two kernels, and can be used to generate a cumbersome “worst-case” description in cases where a more meaningful description of the effect of a kernel is not obvious.

Table 4.1 gives the corresponding description of the effect of adding each type of kernel to a product, written as a post-modifier. Table 4.2 gives the corresponding description of each kernel before it has been multiplied by any other, written as a noun phrase.

4.1.3 Combining Descriptions into Noun Phrases

In order to build a noun phrase describing a product of kernels, we can choose one kernel to act as a head noun, which is then modified by appending descriptions of the other

Kernel	Postmodifier phrase
SE	whose shape changes smoothly
Per	modulated by a periodic function
Lin	with linearly varying amplitude
$\prod_k \text{Lin}^{(k)}$	with polynomially varying amplitude
$\prod_k \sigma^{(k)}$	which applies until / from [changepoint]

Table 4.1 Descriptions of the effect of each kernel, written as a post-modifier.

Kernel	Noun phrase
WN	uncorrelated noise
C	constant
SE	smooth function
Per	periodic function
Lin	linear function
$\prod_k \text{Lin}^{(k)}$	polynomial

Table 4.2 Noun phrase descriptions of each type of kernel

kernels in the product.

As an example, a kernel of the form $\text{Per} \times \text{Lin} \times \sigma$ could be described as a

$\underbrace{\text{Per}}_{\text{periodic function}} \quad \times \quad \underbrace{\text{Lin}}_{\text{with linearly varying amplitude}} \quad \times \quad \underbrace{\sigma}_{\text{which applies until 1700.}}$

where Per was chosen to be the head noun. The head noun is chosen according to the following ordering:

$$\text{Per}, \text{WN}, \text{SE}, \text{C}, \prod_m \text{Lin}^{(m)}, \prod_n \sigma^{(n)} \quad (4.3)$$

Combining tables 4.1 and 4.2 and equation (4.3) provides a general method to produce descriptions of kernels.

In practice, we also incorporate a number of other rules which help to make the descriptions shorter, easier to parse, or clearer:

- We add extra adjectives depending on kernel parameters. For example, an SE with a relatively short lengthscale might be described as “a rapidly-varying smooth function”.
- Descriptions can include kernel parameters. For example, we might write that a

function is “repeating with a period of 7 days”.

- Descriptions can include extra information about the model not contained in the kernel. For example, based on the slope of the posterior mean, we might “a linearly increasing function”.
- Some kernels can be described through pre-modifiers. For example, we might write “an approximately periodic function” as opposed to “a periodic function whose shape changes smoothly”.

Ordering additive components

The reports generated by ABCD attempt to present the most interesting or important features of a data set first. As a heuristic, we order components by always adding next the component which most reduces the 10-fold cross-validated mean absolute error.

4.1.4 Worked Example

Suppose we start with a kernel of the form

$$\text{SE} \times (\text{WN} \times \text{Lin} + \text{CP}(\text{C}, \text{Per})). \quad (4.4)$$

This is converted to a sum of products:

$$\text{SE} \times \text{WN} \times \text{Lin} + \text{SE} \times \text{C} \times \sigma + \text{SE} \times \text{Per} \times \bar{\sigma}. \quad (4.5)$$

which is simplified to

$$\text{WN} \times \text{Lin} + \text{SE} \times \sigma + \text{SE} \times \text{Per} \times \bar{\sigma}. \quad (4.6)$$

To describe the first component, the head noun description for WN, “uncorrelated noise”, is concatenated with a modifier for Lin, “with linearly increasing standard deviation”. The second component is described as “A smooth function with a lengthscale of [lengthscale] [units]”, corresponding to the SE, “which applies until [changepoint]”, which corresponds to the σ . Finally, the third component is described as “An approximately periodic function with a period of [period] [units] which applies from [changepoint]”.

4.2 Example Descriptions

In this section, we demonstrate the ability of our procedure to write intelligible descriptions of the structure present in two time series. The model descriptions were generated based off of models produced by the automatic search method presented in chapter 3.

4.2.1 Summarizing 400 Years of Solar Activity

First, we show excerpts from the report automatically generated on annual solar irradiation data from 1610 to 2011. This dataset is shown in figure 4.1.

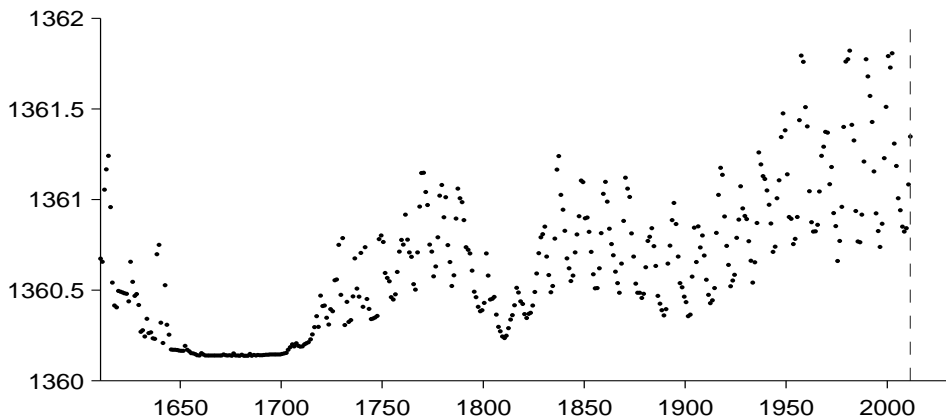


Fig. 4.1 Solar irradiance data.

This time series has two pertinent features: a roughly 11-year cycle of solar activity, and a period lasting from 1645 to 1715 with much smaller variance than the rest of the dataset. This flat region corresponds to the Maunder minimum, a period in which sunspots were extremely rare (Lean et al., 1995). The Maunder minimum is an example of the type of structure which can be captured by changewindows. ABCD clearly identifies these two features, as discussed below.

Figure 4.2 show plots and natural-language summaries of the top four components discovered by ABCD. From these short summaries, we can see that the system has identified the Maunder minimum (second component) and 11-year solar cycle (fourth component). These components are visualized and described in figures 4.3 and 4.5, respectively. The third component, visualized in figure 4.4, captures long-term trends.

The complete report generated on this dataset can be found in chapter D.

The structure search algorithm has identified eight additive components in the data. The first 4 additive components explain 92.3% of the variation in the data as shown by the coefficient of determination (R^2) values in table 1. The first 6 additive components explain 99.7% of the variation in the data. After the first 5 components the cross validated mean absolute error (MAE) does not decrease by more than 0.1%. This suggests that subsequent terms are modelling very short term trends, uncorrelated noise or are artefacts of the model or search procedure. Short summaries of the additive components are as follows:

- A constant.
- A constant. This function applies from 1643 until 1716.
- A smooth function. This function applies until 1643 and from 1716 onwards.
- An approximately periodic function with a period of 10.8 years. This function applies until 1643 and from 1716 onwards.

Fig. 4.2 Automatically generated descriptions of the components discovered by ABCD on the solar irradiance data set. The dataset has been decomposed into diverse structures with simple descriptions.

This component is constant. This component applies from 1643 until 1716.

This component explains 37.4% of the residual variance; this increases the total variance explained from 0.0% to 37.4%. The addition of this component reduces the cross validated MAE by 31.97% from 0.33 to 0.23.

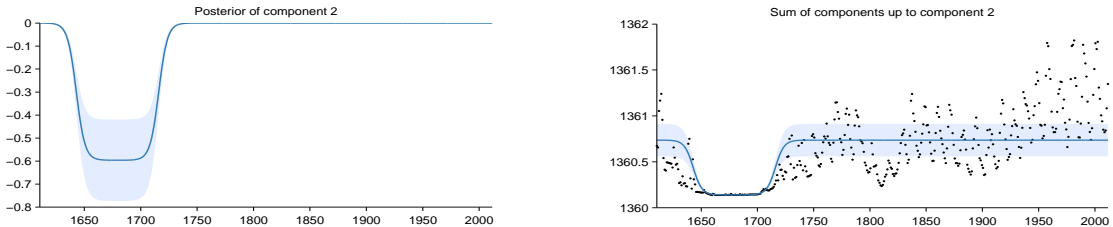


Figure 4: Pointwise posterior of component 2 (left) and the posterior of the cumulative sum of components with data (right)

Fig. 4.3 One of the learned components corresponds to the Maunder minimum.

4.2.2 Describing Varying Noise Levels in Air Traffic Data

Next, we present excerpts of the description generated by our procedure on international airline passenger data. The model being described is the same as that shown in figure 3.4.

High-level descriptions of the four components discovered are shown in figure 4.6. The second component, shown in figure 4.7, is accurately described as approximately (SE) periodic (Per) with linearly growing amplitude (Lin). By multiplying a white noise

This component is a smooth function with a typical lengthscale of 23.1 years. This component applies until 1643 and from 1716 onwards.

This component explains 56.6% of the residual variance; this increases the total variance explained from 37.4% to 72.8%. The addition of this component reduces the cross validated MAE by 21.08% from 0.23 to 0.18.

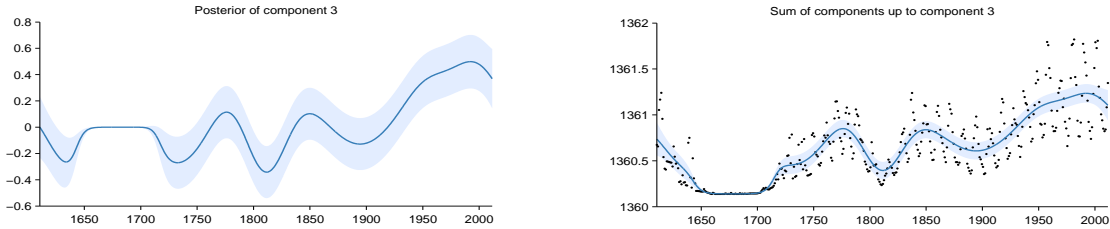


Figure 6: Pointwise posterior of component 3 (left) and the posterior of the cumulative sum of components with data (right)

Fig. 4.4 Characterizing the medium-term smoothness of solar activity levels. By allowing other components to explain the periodicity, noise, and the Maunder minimum, ABCD can isolate the part of the signal best explained by a slowly-varying trend.

This component is approximately periodic with a period of 10.8 years. Across periods the shape of this function varies smoothly with a typical lengthscale of 36.9 years. The shape of this function within each period is very smooth and resembles a sinusoid. This component applies until 1643 and from 1716 onwards.

This component explains 71.5% of the residual variance; this increases the total variance explained from 72.8% to 92.3%. The addition of this component reduces the cross validated MAE by 16.82% from 0.18 to 0.15.

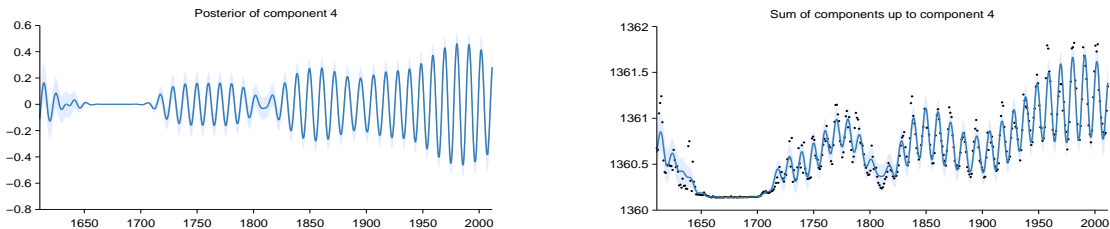


Figure 8: Pointwise posterior of component 4 (left) and the posterior of the cumulative sum of components with data (right)

Fig. 4.5 Extract from an automatically-generated report describing the model components discovered by automatic model search. This part of the report isolates and describes the approximately 11-year sunspot cycle, also noting its disappearance during the 16th century, a time known as the Maunder minimum (Lean et al., 1995).

The structure search algorithm has identified four additive components in the data. The first 2 additive components explain 98.5% of the variation in the data as shown by the coefficient of determination (R^2) values in table 1. The first 3 additive components explain 99.8% of the variation in the data. After the first 3 components the cross validated mean absolute error (MAE) does not decrease by more than 0.1%. This suggests that subsequent terms are modelling very short term trends, uncorrelated noise or are artefacts of the model or search procedure. Short summaries of the additive components are as follows:

- A linearly increasing function.
- An approximately periodic function with a period of 1.0 years and with linearly increasing amplitude.
- A smooth function.
- Uncorrelated noise with linearly increasing standard deviation.

#	R^2 (%)	ΔR^2 (%)	Residual R^2 (%)	Cross validated MAE	Reduction in MAE (%)
-	-	-	-	280.30	-
1	85.4	85.4	85.4	34.03	87.9
2	98.5	13.2	89.9	12.44	63.4
3	99.8	1.3	85.1	9.10	26.8
4	100.0	0.2	100.0	9.10	0.0

Fig. 4.6 Short descriptions and summary statistics for the four components of the airline model.

kernel by a linear kernel, the model is able to express heteroscedasticity (covariance which changes over time). This component is described in figure 4.8.

The complete report generated on this dataset can be found in the supplementary material of (Lloyd et al., 2014). Other example reports describing a wide variety of time-series can be found at mlg.eng.cam.ac.uk/Lloyd/abcdoutput/

4.3 Related Work

To the best of our knowledge, our procedure is the first example of automatic description of nonparametric statistical models. However, systems with natural language output have been built in the areas of video interpretation (Barbu et al., 2012) and automated theorem proving (Ganesalingam and Gowers, 2013).

Source Code

Source code to perform all experiments is available at github.com/jamesrobertlloyd/gpss-research.

2.2 Component 2 : An approximately periodic function with a period of 1.0 years and with linearly increasing amplitude

This component is approximately periodic with a period of 1.0 years and varying amplitude. Across periods the shape of this function varies very smoothly. The amplitude of the function increases linearly. The shape of this function within each period has a typical lengthscale of 6.0 weeks.

This component explains 89.9% of the residual variance; this increases the total variance explained from 85.4% to 98.5%. The addition of this component reduces the cross validated MAE by 63.45% from 34.03 to 12.44.

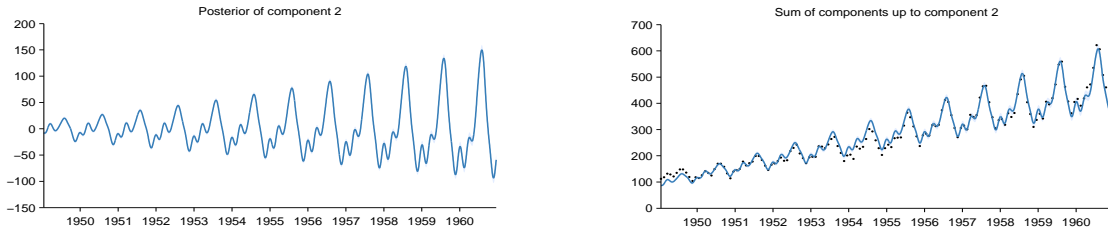


Figure 4: Pointwise posterior of component 2 (left) and the posterior of the cumulative sum of components with data (right)

Fig. 4.7 Capturing non-stationary periodicity in the airline data

2.4 Component 4 : Uncorrelated noise with linearly increasing standard deviation

This component models uncorrelated noise. The standard deviation of the noise increases linearly.

This component explains 100.0% of the residual variance; this increases the total variance explained from 99.8% to 100.0%. The addition of this component reduces the cross validated MAE by 0.00% from 9.10 to 9.10. This component explains residual variance but does not improve MAE which suggests that this component describes very short term patterns, uncorrelated noise or is an artefact of the model or search procedure.

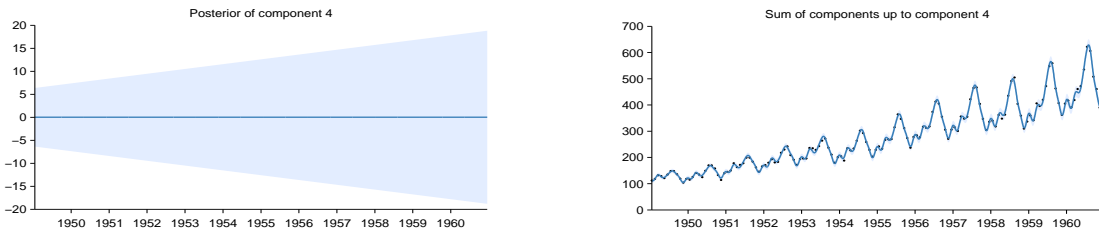


Figure 8: Pointwise posterior of component 4 (left) and the posterior of the cumulative sum of components with data (right)

Fig. 4.8 Modeling heteroscedasticity in the airline dataset.

4.4 Conclusion

Towards the goal of automating statistical modeling we have presented a system which, given a structured GP model, automatically generates detailed reports that describe patterns in the data captured by the model. Combined with the automatic model-search of chapter 3, we demonstrate a procedure which can discover and describe a variety of patterns on several time series.

Chapter 5

Deep Gaussian Processes

“I asked myself: On any given day, would I rather be wrestling with a sampler, or proving theorems?”

Peter Orbanz, personal communication

Choosing appropriate architectures and regularization strategies of deep networks is important for good predictive performance. In this chapter, we propose to study this problem by viewing deep nets as priors on functions. By viewing neural networks this way, we can analyze their properties without reference to any particular dataset, loss function, or training method. Instead, we can ask what sorts of information-processing structures these priors give rise to, and check whether those structures are the same sort which we expect to find in useful models.

As a starting point, we’ll relate neural networks to Gaussian processes, and examine a class of infinitely-wide, deep neural networks called *deep Gaussian processes*. Deep GPs are an attractive model class to study for several reasons. [Damianou and Lawrence \(2013\)](#) showed that the probabilistic nature of deep GPs guards against overfitting, and allows us to use the marginal likelihood to automatically tune the model architecture without the need for cross-validation. [Hensman et al. \(2014\)](#) showed that stochastic variational inference is possible in deep GPs. Together, these results suggest that deep GPs are a promising alternative to neural nets. For the analysis in this chapter, deep GPs are attractive because they abstract away some of the details of finite neural networks.

Our analysis will show that in standard architectures, the representational capacity of standard deep networks tends to decrease as the number of layers increases, retaining only a single degree of freedom in the limit. We’ll propose an alternate network architecture – one which connects the input to each layer – which does not suffer from this

pathology. We'll also examine *deep kernels*, obtained by composing infinitely-many fixed feature transforms.

The ideas contained in this chapter were developed through discussions with Oren Rippel, Ryan Adams and Zoubin Ghahramani, and appear in (Duvenaud et al., 2014).

5.1 Relating Neural Networks to Deep Gaussian Processes

Deep GPs are simply priors on compositions of vector-valued functions, where each function in each layer is drawn independently from a GP prior:

$$\begin{aligned} \mathbf{f}^{(1:L)}(\mathbf{x}) &= \mathbf{f}^{(L)}(\mathbf{f}^{(L-1)}(\dots \mathbf{f}^{(2)}(\mathbf{f}^{(1)}(\mathbf{x})) \dots)) \\ \text{with each } \mathbf{f}_d^{(\ell)} &\stackrel{\text{ind}}{\sim} \text{GP}\left(0, k_d^\ell(\mathbf{x}, \mathbf{x}')\right) \end{aligned} \quad (5.1)$$

A multilayer neural network also implements a composition of vector-valued functions, one per layer. In this section, we'll show the precise relationship between Gaussian processes and neural nets, then show two equivalent ways of constructing neural networks which give rise to deep GPs.

5.1.1 Single-layer Models

First, we'll relate neural networks with one hidden layer to Gaussian processes, using the standard neural network architecture known as the multi-layer perceptron (MLP). In the typical definition of an MLP, the hidden units of the first layer are defined as:

$$\mathbf{h}^{(1)}(\mathbf{x}) = \sigma(\mathbf{b}^{(1)} + \mathbf{W}^{(1)}\mathbf{x}) \quad (5.2)$$

where \mathbf{h} are the hidden unit activations, \mathbf{b} is a bias vector, \mathbf{W} is a weight matrix and σ is a one-dimensional nonlinear function applied element-wise. The output vector $f(\mathbf{x})$ is simply a weighted sum of these hidden unit activations:

$$f(\mathbf{x}) = \mathbf{V}^{(1)}\sigma(\mathbf{b}^{(1)} + \mathbf{W}^{(1)}\mathbf{x}) = \mathbf{V}^{(1)}\mathbf{h}^{(1)}(\mathbf{x}) \quad (5.3)$$

where $\mathbf{V}^{(1)}$ is another weight matrix.

Neal (1995) showed that GPs can be viewed as a prior on neural networks with infinitely many hidden units and unknown weights. More precisely, for any model of the

form

$$f(\mathbf{x}) = \frac{1}{K} \boldsymbol{\alpha}^\top \mathbf{h}(\mathbf{x}) = \frac{1}{K} \sum_{i=1}^K \alpha_i h_i(\mathbf{x}), \quad (5.4)$$

with fixed features $[h_1(\mathbf{x}), \dots, h_K(\mathbf{x})]^\top = \mathbf{h}(\mathbf{x})$ and i.i.d. α 's with zero mean and finite variance σ^2 , the central limit theorem implies that as the number of features K grows, any two function values $f(\mathbf{x}), f(\mathbf{x}')$ have a joint distribution approaching a Gaussian:

$$\lim_{K \rightarrow \infty} p\left(\begin{bmatrix} f(\mathbf{x}) \\ f(\mathbf{x}') \end{bmatrix}\right) = \mathcal{N}\left(\begin{bmatrix} 0 \\ 0 \end{bmatrix}, \frac{\sigma^2}{K} \begin{bmatrix} \sum_{i=1}^K h_i(\mathbf{x})h_i(\mathbf{x}) & \sum_{i=1}^K h_i(\mathbf{x})h_i(\mathbf{x}') \\ \sum_{i=1}^K h_i(\mathbf{x}')h_i(\mathbf{x}) & \sum_{i=1}^K h_i(\mathbf{x}')h_i(\mathbf{x}') \end{bmatrix}\right) \quad (5.5)$$

A joint Gaussian distribution between any set of function values is the definition of a Gaussian process.

The result is surprisingly general: it puts no constraints on the features (other than having uniformly bounded activation), nor does it require that the feature weights $\boldsymbol{\alpha}$ be Gaussian distributed.

We can also work backwards to derive a one-layer MLP from any GP. Mercer's theorem implies that any positive-definite kernel function corresponds to an inner product of features: $k(\mathbf{x}, \mathbf{x}') = \mathbf{h}(\mathbf{x})^\top \mathbf{h}(\mathbf{x}')$. Thus in the one-hidden-layer case, the correspondence between MLPs and GPs is simple: the features $\mathbf{h}(\mathbf{x})$ of the kernel correspond to the hidden units of the MLP.

5.1.2 Multiple Hidden Layers

In an MLP with multiple hidden layers, activation of the ℓ th layer units are given by

$$\mathbf{h}^{(\ell)}(\mathbf{x}) = \sigma(\mathbf{b}^{(\ell)} + \mathbf{W}^{(\ell)} \mathbf{h}^{(\ell-1)}(\mathbf{x})). \quad (5.6)$$

This architecture is shown on the right of figure 5.1. For example, if we extend the model given by equation (5.3) to have two layers of feature mappings, the resulting model would become

$$f(\mathbf{x}) = \frac{1}{K} \boldsymbol{\alpha}^\top \mathbf{h}^{(2)}(\mathbf{h}^{(1)}(\mathbf{x})). \quad (5.7)$$

If the features $\mathbf{h}^{(1)}(\mathbf{x})$ and $\mathbf{h}^{(2)}(\mathbf{x})$ are considered fixed with only the last-layer weights

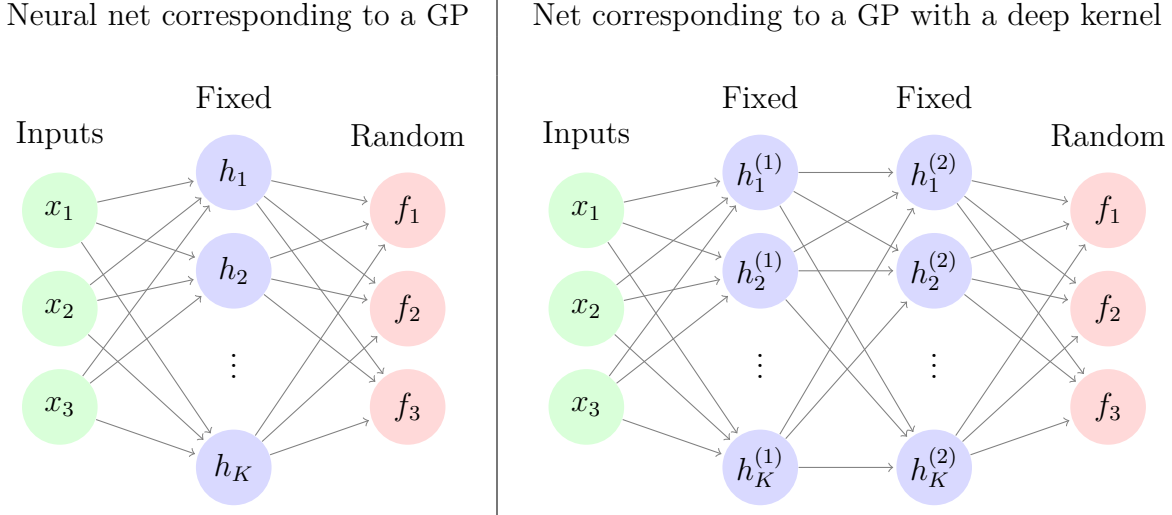


Fig. 5.1 *Left*: GPs can be understood as a one-hidden-layer MLP with infinitely many fixed hidden units having unknown weights. *Right*: Multiple layers of fixed hidden units gives rise to a GP with a deep kernel, but not a deep GP.

α unknown, this model corresponds to a (non-deep) GP with a “deep kernel”, given by

$$k(\mathbf{x}, \mathbf{x}') = (\mathbf{h}^{(2)}(\mathbf{h}^{(1)}(\mathbf{x})))^\top \mathbf{h}^{(2)}(\mathbf{h}^{(1)}(\mathbf{x}')) \quad (5.8)$$

GPs with deep kernels, explored in section 5.5, imply a fixed representation as opposed to a prior over representations. Thus, unless we richly parameterize these kernels, their capacity to learn an appropriate representation is limited in comparison to more flexible models such as deep neural networks, or deep GPs.

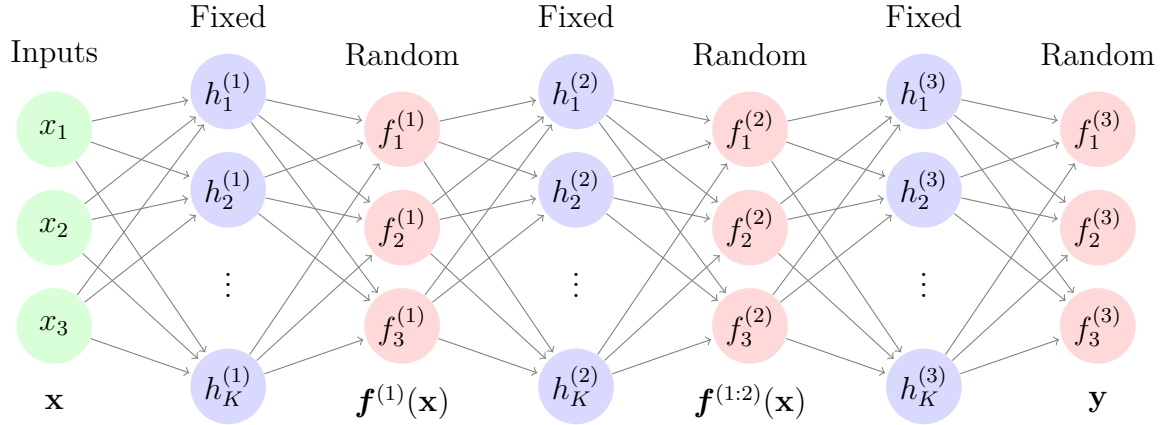
5.1.3 Two Network Architectures Equivalent to Deep GPs

There are two equivalent neural net architectures which correspond to deep GPs: one with fixed non-linearities, and another with GP-distributed nonlinearities.

To construct a neural network with fixed nonlinearities that corresponds to a deep GP, one can start with the infinitely-wide deep GP shown in figure 5.1(right), and introduce a finite set of nodes in between each infinitely-wide set of fixed basis functions. This architecture is shown in the top of figure 5.2. The $D^{(\ell)}$ outputs $\mathbf{f}^{(\ell)}(\mathbf{x})$ in between each layer are weighted sums (with random weights) of the fixed hidden units of the layer below, and the next layer’s hidden units depend only on these $D^{(\ell)}$ outputs.

This alternating-layer architecture has an interpretation as a series of linear information bottlenecks. To see this, we can simply substitute equation (5.3) into equation (5.6)

A neural net with fixed activation functions corresponding to a 3-layer deep GP



A net with nonparametric activation functions corresponding to a 3-layer deep GP

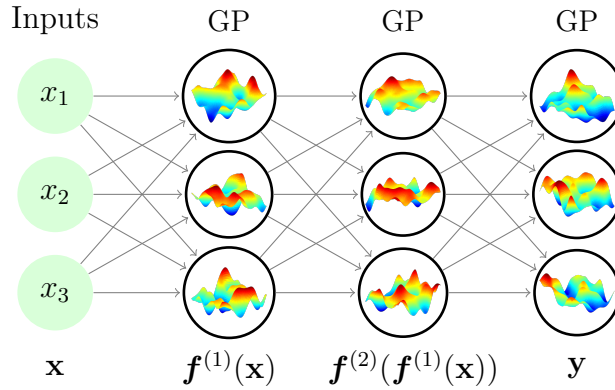


Fig. 5.2 Two equivalent views of deep GPs as neural networks. *Top:* A neural network whose every second layer is a weighted sum of an infinite number of fixed hidden units, where the weights are initially unknown. *Bottom:* A neural network with a finite number of hidden units, each with a different unknown non-parametric activation function.

to get

$$\mathbf{h}^{(\ell)}(\mathbf{x}) = \sigma \left(\mathbf{b}^{(\ell)} + \mathbf{W}^{(\ell)} \mathbf{V}^{(\ell-1)} \mathbf{h}^{(\ell-1)}(\mathbf{x}) \right). \quad (5.9)$$

Thus, ignoring the intermediate outputs $\mathbf{f}^{(\ell)}(\mathbf{x})$, a deep GP is an infinitely-wide, deep MLP with each pair of layers connected by random, rank- D_ℓ matrices $\mathbf{W}^{(\ell)} \mathbf{V}^{(\ell-1)}$.

The second, more direct way to construct a network architecture corresponding to a deep GP is to integrate out all $\mathbf{V}^{(\ell)}$, and view deep GPs as a neural network with a

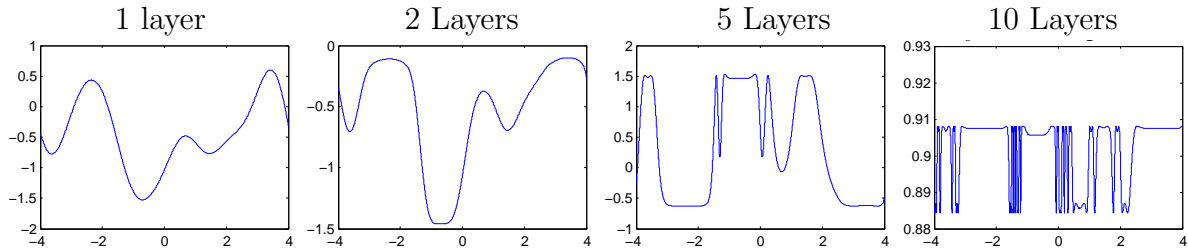


Fig. 5.3 One-dimensional draws from a deep gp prior. After a few layers, the functions begin to be either nearly flat, or highly varying, everywhere. This is a consequence of the distribution on derivatives becoming heavy-tailed.

finite number of nonparametric, GP-distributed basis functions at each layer, in which $f^{(1:\ell)}(\mathbf{x})$ represent the output of the hidden nodes at the ℓ^{th} layer. This second view lets us compare deep GP models to standard neural net architectures more directly. Figure 5.1(bottom) shows this architecture.

5.2 Characterizing Deep Gaussian Processes

In this section, we develop several theoretical results that explore the behavior of deep GPs as a function of their depth. This will allow us in section 5.3 to formally identify a pathology that emerges in very deep networks.

Specifically, we will show that the size of the derivative of a one-dimensional deep GP becomes log-normal distributed as the network becomes deeper. We'll also show that the Jacobian of a multivariate deep GP is a product of independent Gaussian matrices with independent entries.

5.2.1 One-dimensional Asymptotics

In this section, we derive the limiting distribution of the derivative of an arbitrarily deep, one-dimensional GP with a squared-exp kernel:

$$\text{SE}(x, x') = \sigma^2 \exp\left(\frac{-(x-x')^2}{2w^2}\right). \quad (5.10)$$

The parameter σ^2 controls the variance of functions drawn from the prior, and the lengthscale parameter w controls the smoothness. The derivative of a GP with a squared-exp kernel is point-wise distributed as $\mathcal{N}(0, \sigma^2/w^2)$. Intuitively, a draw from a GP is likely to have large derivatives if the kernel has high variance and small lengthscales.

By the chain rule, the derivative of a one-dimensional deep GP is simply a product of the derivatives of each layer, which are drawn independently. The distribution of the absolute value of this derivative is a product of half-normals, each with mean $\sqrt{2\sigma^2/\pi w^2}$. If we choose kernel parameters so that $\sigma^2/w^2 = \pi/2$, then the expected magnitude of the derivative remains constant regardless of the depth.

The log of the magnitude of the derivatives has moments

$$\begin{aligned} m_{\log} &= \mathbb{E} \left[\log \left| \frac{\partial f(x)}{\partial x} \right| \right] = 2 \log \left(\frac{\sigma}{w} \right) - \log 2 - \gamma \\ v_{\log} &= \mathbb{V} \left[\log \left| \frac{\partial f(x)}{\partial x} \right| \right] = \frac{\pi^2}{4} + \frac{\log^2 2}{2} - \gamma^2 - \gamma \log 4 + 2 \log \left(\frac{\sigma}{w} \right) \left[\gamma + \log 2 - \log \left(\frac{\sigma}{w} \right) \right] \end{aligned} \quad (5.11)$$

where $\gamma \approx 0.5772$ is Euler's constant. Since the second moment is finite, by the central limit theorem, the limiting distribution of the size of the gradient approaches log-normal as L grows:

$$\log \left| \frac{\partial f^{(1:L)}(x)}{\partial x} \right| = \sum_{\ell=1}^L \log \left| \frac{\partial f^{(\ell)}(x)}{\partial x} \right| \xrightarrow{L \rightarrow \infty} \mathcal{N}(Lm_{\log}, L^2v_{\log}) \quad (5.12)$$

Even if the expected magnitude of the derivative remains constant, the variance of the log-normal distribution grows without bound as the depth increases.

Because the log-normal distribution is heavy-tailed and its domain is bounded below by zero, the derivative will become very small almost everywhere, with rare but very large jumps. Figure 5.3 shows this behavior in a draw from a 1D deep GP prior, at varying depths. This figure also shows that once the derivative in one region of the input space becomes very large or very small, it is likely to remain that way in subsequent layers.

5.2.2 Distribution of the Jacobian

Next, we characterize the distribution on Jacobians of multivariate functions drawn from a deep GP prior.

Lemma 5.2.1. *The partial derivatives of a function mapping $\mathbb{R}^D \rightarrow \mathbb{R}$ drawn from a GP prior with a product kernel are independently Gaussian distributed.*

Proof. Because differentiation is a linear operator, the derivatives of a function drawn from a GP prior are also jointly Gaussian distributed. The covariance between partial

derivatives with respect to input dimensions d_1 and d_2 of vector \mathbf{x} are given by Solak et al. (2003):

$$\text{cov} \left(\frac{\partial f(\mathbf{x})}{\partial x_{d_1}}, \frac{\partial f(\mathbf{x})}{\partial x_{d_2}} \right) = \frac{\partial^2 k(\mathbf{x}, \mathbf{x}')}{\partial x_{d_1} \partial x'_{d_2}} \Big|_{\mathbf{x}=\mathbf{x}'} \quad (5.13)$$

If our kernel is a product over individual dimensions $k(\mathbf{x}, \mathbf{x}') = \prod_d^D k_d(x_d, x'_d)$, then the off-diagonal entries are zero, implying that all elements are independent. \square

For example, in the case of the multivariate squared-exp kernel, the covariance between derivatives has the form:

$$\begin{aligned} f(\mathbf{x}) &\sim \text{GP} \left(0, \sigma^2 \prod_{d=1}^D \exp \left(-\frac{1}{2} \frac{(x_d - x'_d)^2}{w_d^2} \right) \right) \\ \implies \text{cov} \left(\frac{\partial f(\mathbf{x})}{\partial x_{d_1}}, \frac{\partial f(\mathbf{x})}{\partial x_{d_2}} \right) &= \begin{cases} \frac{\sigma^2}{w_{d_1}^2} & \text{if } d_1 = d_2 \\ 0 & \text{if } d_1 \neq d_2 \end{cases} \end{aligned} \quad (5.14)$$

Lemma 5.2.2. *The Jacobian of a set of D functions $\mathbb{R}^D \rightarrow \mathbb{R}$ drawn from independent GP priors, each having product kernel is a $D \times D$ matrix of independent Gaussian R.V.'s*

Proof. The Jacobian of the vector-valued function $\mathbf{f}(\mathbf{x})$ is a matrix J with elements $J_{ij} = \frac{\partial f_i(\mathbf{x})}{\partial x_j}$. Because the GPs on each output dimension $f_d(\mathbf{x})$ are independent, it follows that each row of J is independent. Lemma 5.2.1 shows that the elements of each row are independent Gaussian. Thus all entries in the Jacobian of a GP-distributed transform are independent Gaussian R.V.'s. \square

Theorem 5.2.3. *The Jacobian of a deep GP with a product kernel is a product of independent Gaussian matrices, with each entry in each matrix being drawn independently.*

Proof. When composing L different functions, we'll denote the *immediate* Jacobian of the function mapping from layer $\ell - 1$ to layer ℓ as $J^\ell(\mathbf{x})$, and the Jacobian of the entire composition of L functions by $J^{1:L}(\mathbf{x})$. By the multivariate chain rule, the Jacobian of a composition of functions is simply the product of the immediate Jacobian matrices of each function. Thus the Jacobian of the composed (deep) function $\mathbf{f}^{(L)}(\mathbf{f}^{(L-1)}(\dots \mathbf{f}^{(3)}(\mathbf{f}^{(2)}(\mathbf{f}^{(1)}(\mathbf{x}))) \dots))$ is

$$J^{1:L}(\mathbf{x}) = J^L J^{(L-1)} \dots J^3 J^2 J^1. \quad (5.15)$$

By lemma 5.2.2, each $J_{i,j}^\ell \stackrel{\text{ind}}{\sim} \mathcal{N}$, so the complete Jacobian is a product of independent Gaussian matrices, with each entry of each matrix drawn independently. \square

Theorem 5.2.3 allows us to analyze the representational properties of a deep Gaussian process by examining the properties of products of independent Gaussian matrices.

5.3 Formalizing a Pathology

Rifai et al. (2011a) argue that good representations of data manifolds are invariant in directions orthogonal to the manifold. Conversely, a good representation must also change in directions tangent to the data manifold, in order to preserve relevant information. Figure 5.4 visualizes this idea.

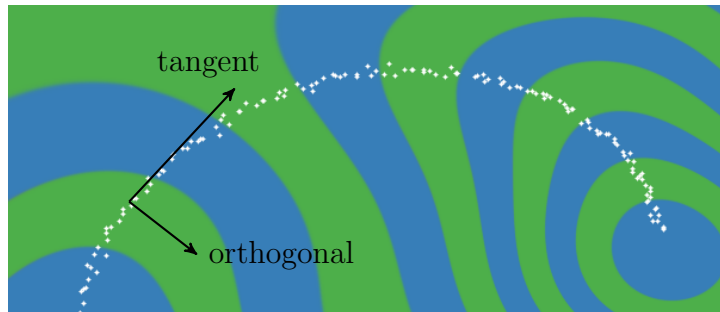


Fig. 5.4 Representing a 1-D data manifold. Colors correspond to the computed representation as a function of the input space. The representation (blue & green) varies in directions tangent to the data manifold (white), preserving information for later layers. The representation changes little in directions orthogonal to the manifold, making it robust to noise in those directions.

As in (Rifai et al., 2011b), we characterize the representational properties of a function by the singular value spectrum of the Jacobian. The number of relatively large singular values of the Jacobian roughly correspond to the number of directions in which the representation varies. Rifai et al. (2011b) analyzed the Jacobian at location of the training points, but because the priors we are examining are stationary, the distribution of the Jacobian is identical everywhere. Figure 5.5 shows the singular value spectrum for 5-dimensional deep GPs of different depths. As the net gets deeper, the largest singular value dominates, implying there is usually only one effective degree of freedom in representation being computed.

Figure 5.6 demonstrates a related pathology that arises when composing functions to produce a deep density model. The density in the observed space eventually be-

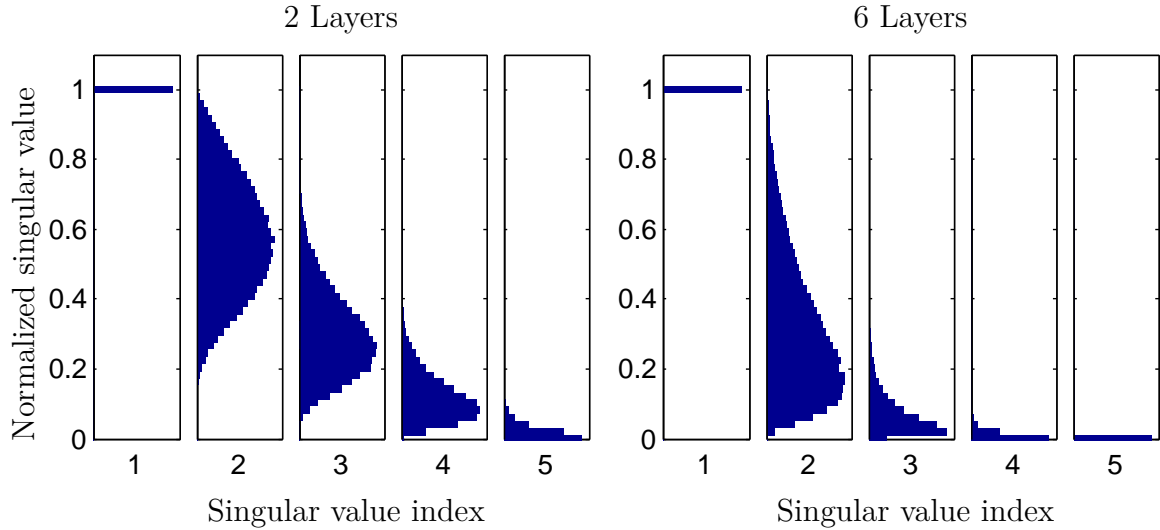


Fig. 5.5 The distribution of normalized singular values of the Jacobian of a function drawn from a 5-dimensional deep GP prior 25 layers deep (*Left*) and 50 layers deep (*Right*). As nets get deeper, the largest singular value tends to become much larger than the others. This implies that with high probability, these functions vary little in all directions but one, making them unsuitable for computing representations of manifolds of more than one dimension.

comes locally concentrated onto one-dimensional manifolds, or *filaments*, again implying that such models are unsuitable to model manifolds whose underlying dimensionality is greater than one.

To visualize this pathology in another way, figure 5.7 illustrates a color-coding of the representation computed by a deep GP, evaluated at each point in the input space. After 10 layers, we can see that locally, there is usually only one direction that one can move in \mathbf{x} -space in order to change the value of the computed representation. This means that such representations are likely to be unsuitable for decision tasks that depend on more than one property of the input.

To what extent are these pathologies present in the types of neural networks commonly used in practice? In simulations, we found that for deep functions with a fixed latent dimension D , the singular value spectrum remained relatively flat for hundreds of layers as long as $D > 100$. Thus, these pathologies are unlikely to severely effect the relatively shallow, wide networks most commonly used in practice.

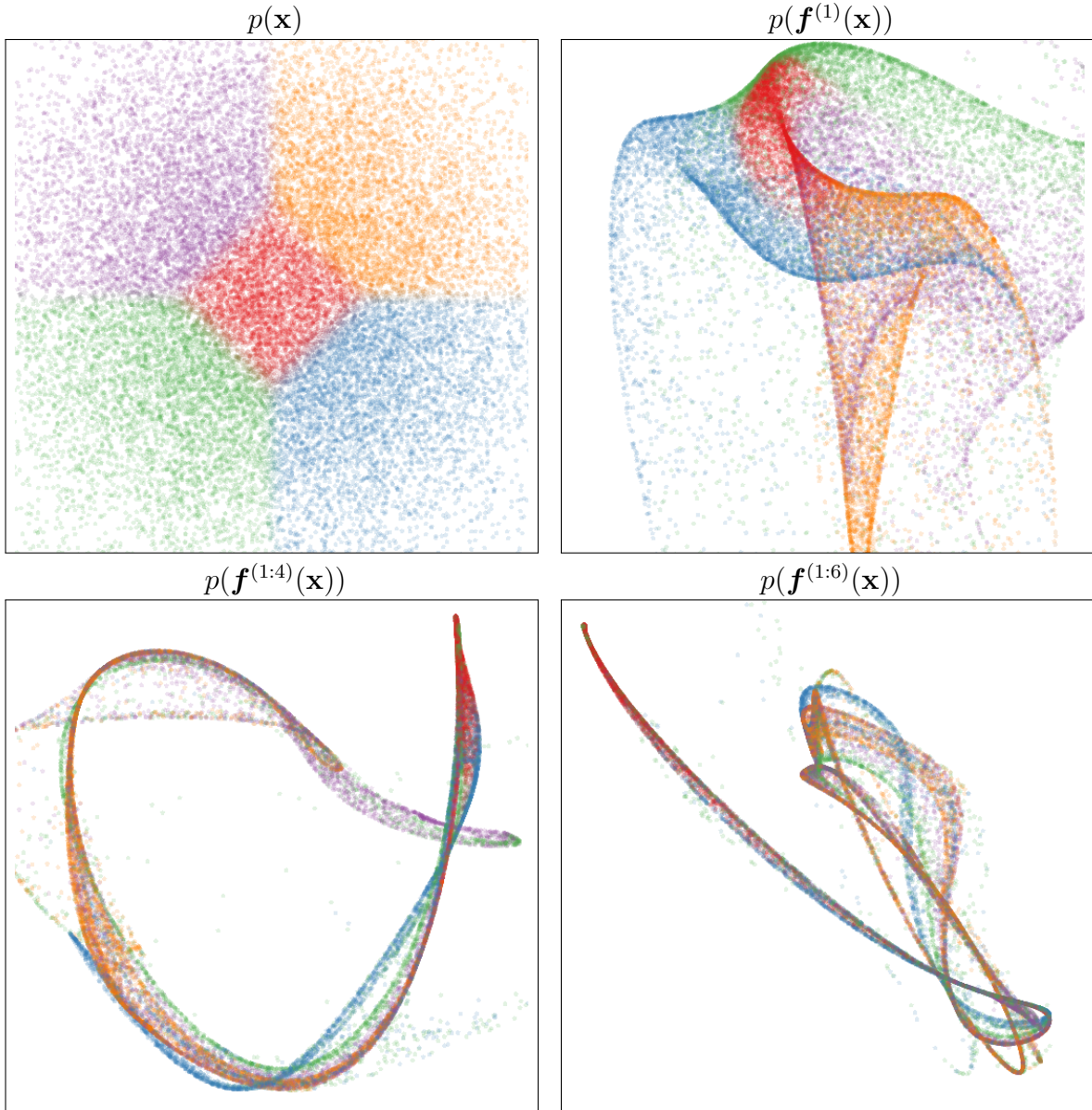


Fig. 5.6 Points warped by a function drawn from a deep GP prior. *Top left:* Points drawn from a 2-dimensional Gaussian distribution, color-coded by their location. *Subsequent panels:* Those same points, successively warped by functions drawn from a GP prior. As the number of layers increases, the density concentrates along one-dimensional filaments.

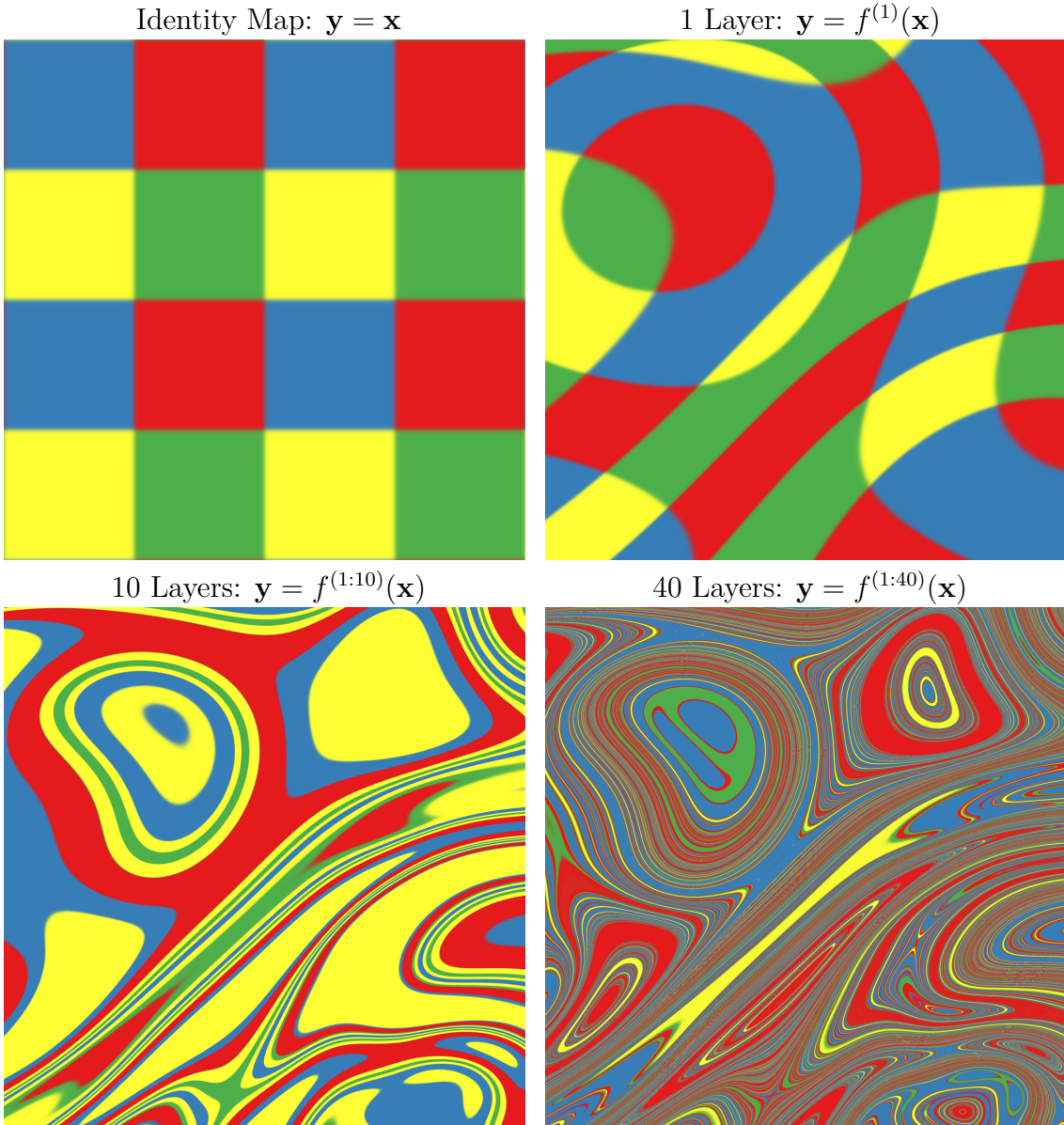


Fig. 5.7 A visualization of the feature map implied by a draw from a deep GP. Colors correspond to the location $\mathbf{y} = \mathbf{f}(\mathbf{x})$ that each point is mapped to after being warped by a deep GP. The number of directions in which the color changes rapidly corresponds to the number of large singular values in the Jacobian. Just as the densities in figure 5.6 became locally one-dimensional, there is usually only one direction that one can move \mathbf{x} in locally to change \mathbf{y} . This means that \mathbf{f} is unlikely to be a suitable representation for decision tasks that depend on more than one aspect of \mathbf{x} .

5.4 Fixing the Pathology

Following Neal (1995), we can fix the pathologies exhibited in figures figure 5.6 and 5.7 by simply making each layer depend not only on the output of the previous layer, but also on the original input \mathbf{x} . We refer to these models as *input-connected* networks, and denote deep functions having this architecture with the subscript C , as in $f_C(\mathbf{x})$. Figure 5.8 shows a graphical representation of the two connectivity architectures. Similar connections between non-adjacent layers can also be found in the primate visual cortex (Maunsell and van Essen, 1983). Formally, this functional dependence can be written as

$$f_C^{(1:L)}(\mathbf{x}) = \mathbf{f}^{(L)} \left(f_C^{(1:L-1)}(\mathbf{x}), \mathbf{x} \right), \quad \forall L \quad (5.16)$$

Visualizations of the resulting prior on functions are shown in figures 5.9, 5.10 and 5.12.

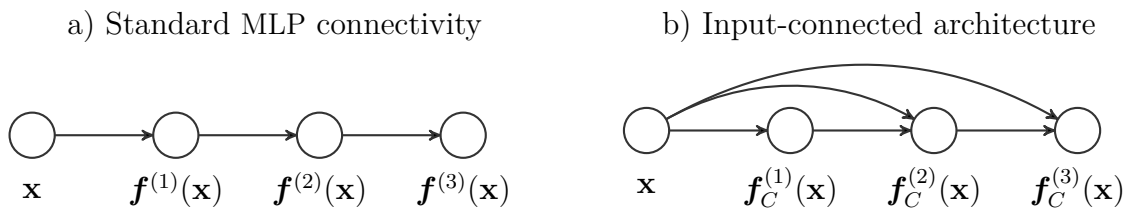


Fig. 5.8 Two different architectures for deep neural networks. *Left:* The standard architecture connects each layer's outputs to the next layer's inputs. *Right:* The input-connected architecture also connects the original input \mathbf{x} to each layer.

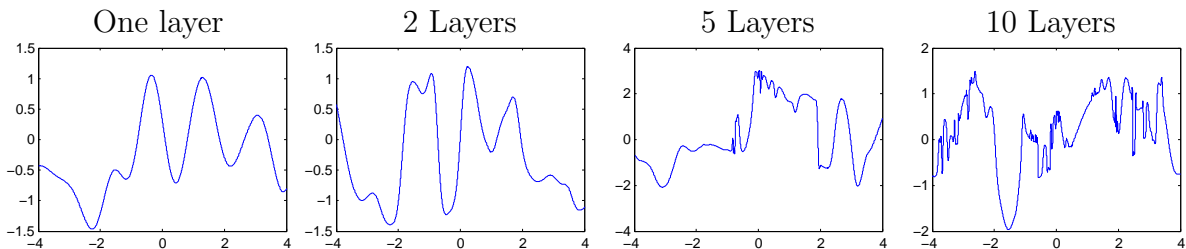


Fig. 5.9 Draws from a 1D deep GP prior with each layer connected to the input. Even after many layers, the functions remain smooth in some regions, while varying rapidly in other regions. Compare to standard-connectivity deep GP draws shown in figure 5.3.

The Jacobian of an input-connected deep function is defined by the recurrence

$$J_C^{1:L}(\mathbf{x}) = J^L \begin{bmatrix} J_C^{1:L-1} \\ I_D \end{bmatrix}. \quad (5.17)$$

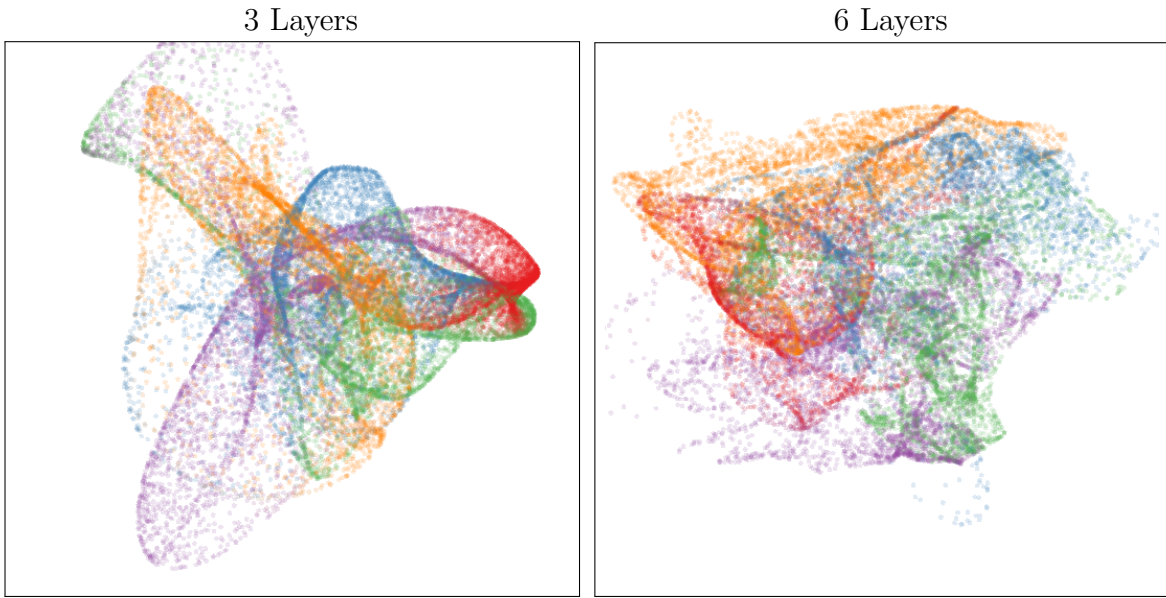


Fig. 5.10 Points warped by a draw from a deep GP, with each layer connected to the input \mathbf{x} . As depth increases, the density becomes more complex without concentrating everywhere along one-dimensional filaments.

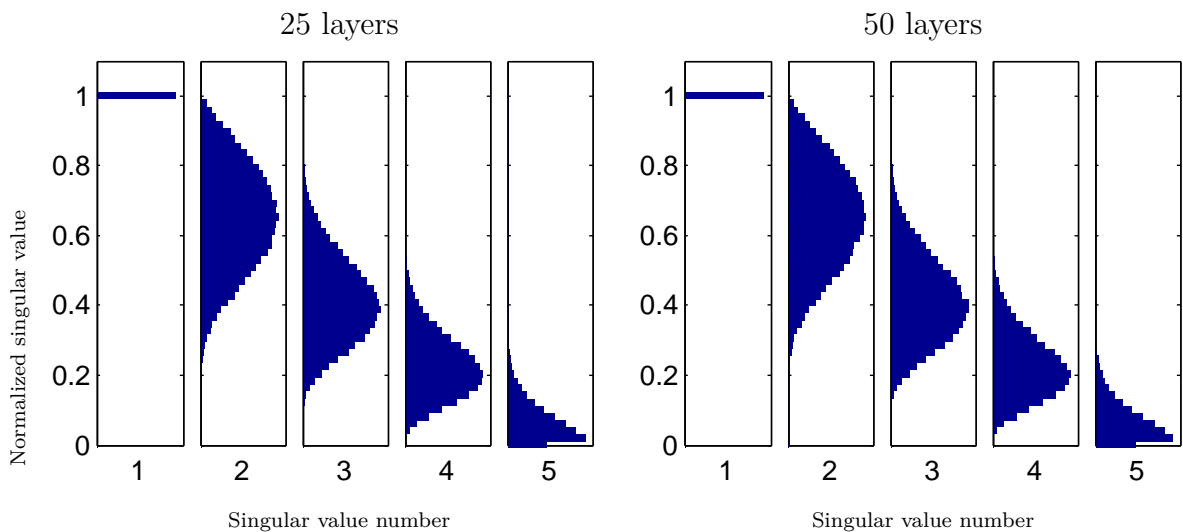


Fig. 5.11 The distribution of singular values drawn from 5-dimensional input-connected deep GP priors, 25 and 50 layers deep. The singular values remain roughly the same scale as one another.

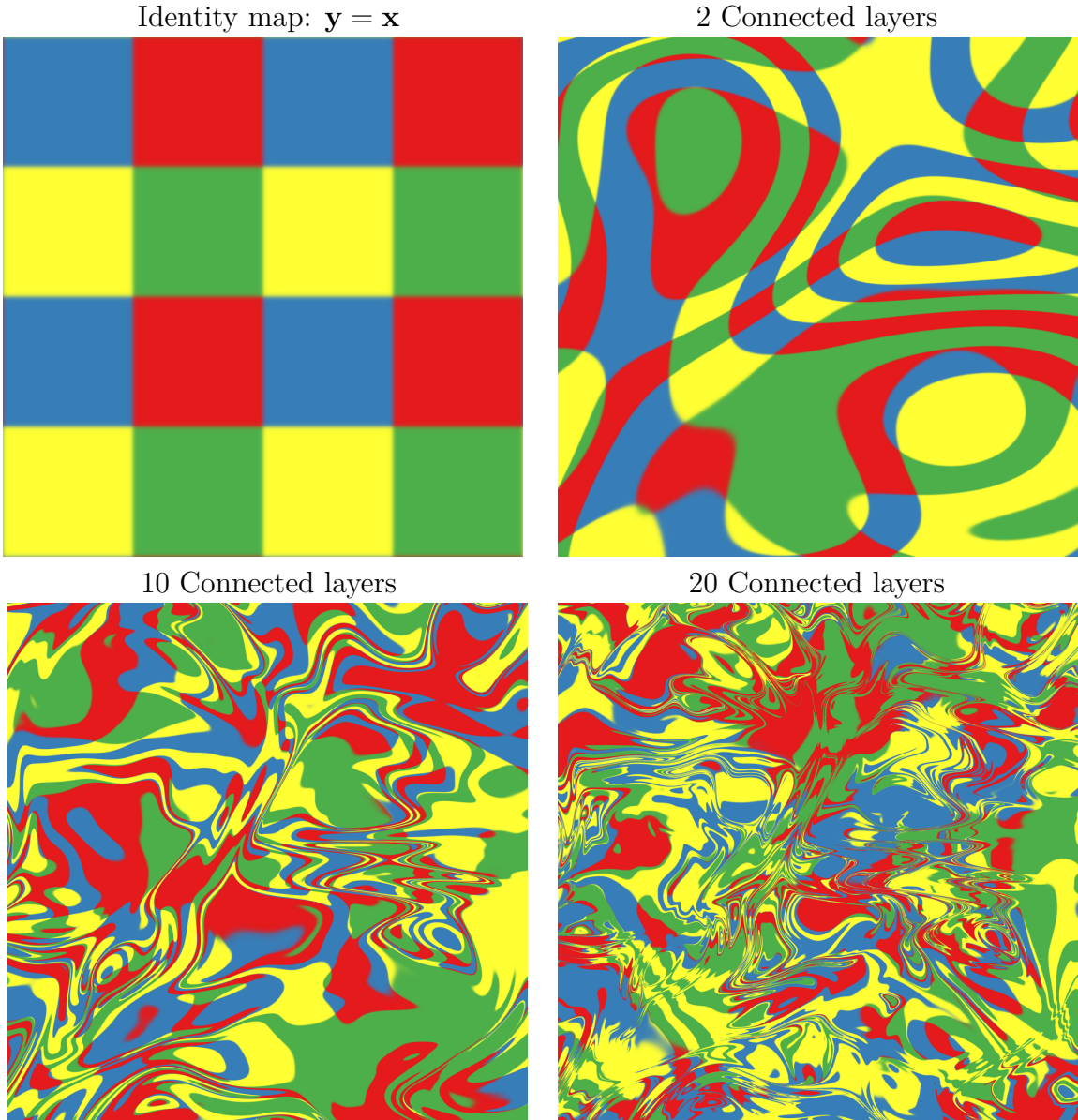


Fig. 5.12 Feature mapping of a deep GP with each layer connected to the input \mathbf{x} . Compare to the mappings shown in figure 5.7. Just as the densities in figure 5.10 remained locally two-dimensional even after many warpings, in the mapping shown here there are sometimes two directions that one can move locally in \mathbf{x} to in order to change the values of $f(\mathbf{x})$. This means that the input-connected prior puts mass on a greater variety of types of representations, some of which depend on all aspects of the input.

which, in the case of a deep GP, is still a product of independent Gaussian matrices. Figure 5.11 shows that with this architecture, even 50-layer deep GPs have well-behaved singular value spectra.

The pathology examined in this section is an example of the sort of analysis made possible by a well-defined prior on functions.

5.5 Deep Kernels

Bengio et al. (2006) showed that kernel machines have limited generalization ability when they use “local” kernels, such as the squared-exp. However, as we saw in chapters 2 and 3, structured kernels can be constructed through addition and multiplication which allow non-local extrapolation.

We can also build non-local kernels by composing fixed feature maps. To return to an example given in section 2.7, periodic kernels can be viewed as a 2-layer-deep kernel, in which the first layer maps $x \rightarrow [\sin(x), \cos(x)]$, and the second layer maps through basis functions corresponding to the SE kernel.

Can we construct other useful kernels by composing fixed feature maps several times, creating deep kernels? Cho (2012) constructed kernels of this form, repeatedly applying multiple layers of feature mappings. In principle, we can compose the feature mapping of any two kernels to get a new one:

$$k_1(\mathbf{x}, \mathbf{x}') = \mathbf{h}_1(\mathbf{x})^\top \mathbf{h}_1(\mathbf{x}') \quad (5.18)$$

$$k_2(\mathbf{x}, \mathbf{x}') = \mathbf{h}_2(\mathbf{x})^\top \mathbf{h}_2(\mathbf{x}') \quad (5.19)$$

$$(k_2 \circ k_1)(\mathbf{x}, \mathbf{x}') = k_2(\mathbf{h}_1(\mathbf{x}), \mathbf{h}_1(\mathbf{x}')) \quad (5.20)$$

$$= [\mathbf{h}_2(\mathbf{h}_1(\mathbf{x}))]^\top \mathbf{h}_2(\mathbf{h}_1(\mathbf{x}')) \quad (5.21)$$

However, this composition might not always have a closed form.

Fortunately, composing the squared-exp kernel with any implicit mapping $\mathbf{h}(\mathbf{x})$ has

a simple closed form:

$$\begin{aligned}
(\text{SE} \circ k)(\mathbf{x}, \mathbf{x}') &= k_{SE}(\mathbf{h}(\mathbf{x}), \mathbf{h}(\mathbf{x}')) = \\
&= \exp\left(-\frac{1}{2}\|\mathbf{h}(\mathbf{x}) - \mathbf{h}(\mathbf{x}')\|_2^2\right) \\
&= \exp\left(-\frac{1}{2}\left[\mathbf{h}(\mathbf{x})^\top \mathbf{h}(\mathbf{x}) - 2\mathbf{h}(\mathbf{x})^\top \mathbf{h}(\mathbf{x}') + \mathbf{h}(\mathbf{x}')^\top \mathbf{h}(\mathbf{x}')\right]\right) \\
&= \exp\left(-\frac{1}{2}[k(\mathbf{x}, \mathbf{x}) - 2k(\mathbf{x}, \mathbf{x}') + k(\mathbf{x}', \mathbf{x}')]\right)
\end{aligned} \tag{5.22}$$

which lets us express the composed kernel, $\text{SE} \circ k$, exactly in terms of evaluations of k .

5.5.1 Infinitely Deep Kernels

What happens when we repeat this composition of feature maps many times, starting with the squared-exp kernel? If the output variance is set to 1, then in the infinite limit, this operation converges to $(\text{SE} \circ \text{SE} \circ \text{SE} \circ \dots \text{SE})(\mathbf{x}, \mathbf{x}') = 1$ for all pairs of inputs, which corresponds to a prior on constant functions $f(\mathbf{x}) = c$.

As before, we can overcome this degeneracy by connecting the inputs \mathbf{x} to each layer. To do so, we simply augment the feature vector at each layer, $\mathbf{h}^{(\ell)}(\mathbf{x})$, with the input vector \mathbf{x} :

$$\begin{aligned}
k^{(\ell+1)}(\mathbf{x}, \mathbf{x}') &= \exp\left(-\frac{1}{2}\left\|\begin{bmatrix} \mathbf{h}^{(\ell)}(\mathbf{x}) \\ \mathbf{x} \end{bmatrix} - \begin{bmatrix} \mathbf{h}^{(\ell)}(\mathbf{x}') \\ \mathbf{x}' \end{bmatrix}\right\|_2^2\right) \\
&= \exp\left(-\frac{1}{2}\left[k^{(\ell)}(\mathbf{x}, \mathbf{x}) - 2k^{(\ell)}(\mathbf{x}, \mathbf{x}') + k^{(\ell)}(\mathbf{x}', \mathbf{x}') - \|\mathbf{x} - \mathbf{x}'\|_2^2\right]\right)
\end{aligned} \tag{5.23}$$

Starting with the squared-exp kernel, this repeated mapping satisfies

$$k^{(\infty)}(\mathbf{x}, \mathbf{x}') - \log(k^{(\infty)}(\mathbf{x}, \mathbf{x}')) = 1 + \frac{1}{2}\|\mathbf{x} - \mathbf{x}'\|_2^2 \tag{5.24}$$

The solution to this recurrence has no closed form, but has a similar shape to the Ornstein-Uhlenbeck covariance $\text{OU}(x, x') = \exp(-|x - x'|)$ but with lighter tails. Samples from a GP prior with this kernel are not differentiable, and are locally fractal. Figure 5.13 shows this kernel at different depths, as well as samples from the resulting GP prior.

We can also consider two other connectivity architectures: one in which each layer is connected to the output layer, and another in which every layer is connected to all

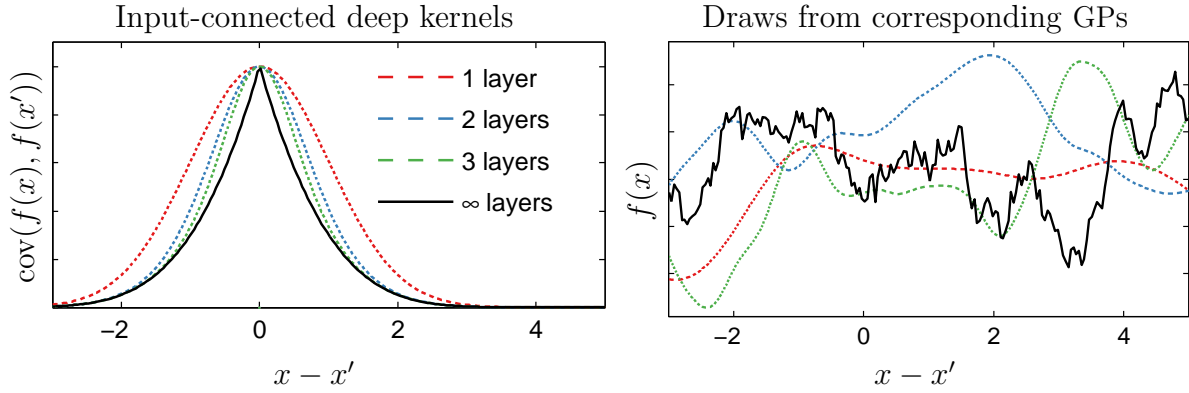


Fig. 5.13 *Left*: Input-connected deep kernels of different depths. By connecting the inputs \mathbf{x} to each layer, the kernel can still depend on its input even after arbitrarily many layers of computation. *Right*: Draws from GPs with deep input-connected kernels.

subsequent layers. It is easy to show that in the limit of infinite depth, both these architectures converge to $k(\mathbf{x}, \mathbf{x}') = \delta(\mathbf{x}, \mathbf{x}')$, a white noise kernel.

5.5.2 When are Deep Kernels Useful Models?

Kernels correspond to fixed feature maps, and so kernel learning is an example of implicit representation learning. As we saw in chapters 2 and 3, kernels can capture rich structure, and can enable many types of generalization. The relatively uninteresting properties of the kernels derived in this section simply reflect the fact that an arbitrary computation, even if it is “deep”, is not likely to give rise to a useful representation, unless combined with learning. To put it another way, any fixed representation is unlikely to be useful unless it has been chosen specifically for the problem at hand.

5.6 Related Work

Deep Gaussian Processes

Neal (1995) discussed the properties of arbitrarily deep random networks, including those that would give rise to deep GPs. However, deep GPs were first clearly defined and developed by Lawrence and Moore (2007), as a model of hierarchical generative relationships. Deep GPs were first referred to as such by Damianou and Lawrence (2013), who developed a variational inference scheme and analyzed the effect of automatic relevance determination in that model.

Nonparametric Neural Networks

Adams et al. (2010) proposed a prior on arbitrarily deep Bayesian networks. Their architecture has connections only between adjacent layers, and may also be expected to have similar pathologies to those of deep GPs as the number of layers increases.

Deep Density Networks (Rippel and Adams, 2013) were constructed with invertibility in mind, with penalty terms encouraging the preservation of information about lower layers. This is another promising approach to fixing the pathology discussed above.

Wilson et al. (2012) introduced GP Regression Networks (GPRN), which define a matrix product of GPs, rather than a composition. The form of a GPRN is

$$\mathbf{y}(\mathbf{x}) = \mathbf{W}(\mathbf{x})\mathbf{f}(\mathbf{x}) \quad \text{with each } f_d, W_{d,j} \stackrel{\text{iid}}{\sim} \mathcal{GP}(\mathbf{0}, \text{SE} + \text{WN}). \quad (5.25)$$

We can easily define a “deep” GPRN:

$$\mathbf{y}(\mathbf{x}) = \mathbf{W}^{(3)}(\mathbf{x})\mathbf{W}^{(2)}(\mathbf{x})\mathbf{W}^{(1)}(\mathbf{x})\mathbf{f}(\mathbf{x}) \quad (5.26)$$

which repeatedly adds and multiplies functions drawn from GPs, in contrast to deep GPs which repeatedly compose functions. This prior on functions might be amenable to a similar analysis to that of section 5.2.

Recurrent Networks

Bengio et al. (1994) and Pascanu et al. (2012) analyze a related problem with gradient-based learning in recurrent nets, the “exploding-gradients” problem. Specifically, they note that in recurrent neural networks, the size of the training gradient can grow or shrink exponentially as it is back-propagated, making gradient-based training difficult.

Deep Kernels

Hermans and Schrauwen (2012) construct deep kernels in a time-series setting, constructing kernels corresponding to infinite-width *recurrent* neural networks. They also propose concatenating the implicit feature vectors from previous time-steps with the current inputs, resulting in an architecture analogous to the input-connected architecture proposed by Neal (1995).

Analyses of Deep Learning

Montavon et al. (2010) perform a layer-wise analysis of deep networks, and note that the performance of MLPs degrades as the number of layers with random weights increases. The importance of network architectures relative to learning has been examined by Saxe et al. (2011). Later, Saxe et al. (2013) looked at the dynamics of learning in deep linear models, as a tractable approximation to deep neural networks.

5.7 Conclusions

In this chapter, we showed that well-defined priors allow us to explicitly examine the assumptions being made about functions we may wish to learn. As an example of the sort of analysis made possible this way, we attempted to gain insight into the properties of deep neural networks by characterizing the sorts of functions likely to be obtained under different choices of priors on compositions of functions.

First, we identified deep Gaussian processes as an easy-to-analyze model corresponding to multi-layer perceptrons with nonparametric activation functions. We then showed that representations based on repeated composition of independent functions exhibit a pathology where the representations becomes invariant to all directions of variation but one. Finally, we showed that this problem could be alleviated by connecting the input to each layer. We also examined properties of deep kernels, corresponding to arbitrarily many compositions of fixed features.

Much recent work on deep networks has focused on weight initialization (Martens, 2010), regularization (Lee et al., 2007) and network architecture (Gens and Domingos, 2013). However, the interactions between these different design decisions can be complex and difficult to characterize. If we can identify classes of priors that give our models desirable properties, these in turn may suggest regularization, initialization, and architecture choices that also provide such properties.

Source Code

Source code to produce all figures is available at github.com/duvenaud/deep-limits/.

Chapter 6

Modeling Additive Interactions

In chapter 2, we saw how additive structure in a GP prior enabled long-range extrapolation in multivariate problems. In general, models of the form

$$g(y) = f(x_1) + f(x_2) + \cdots + f(x_D) \quad (6.1)$$

are widely used in machine learning and statistics, because they are relatively easy to fit and interpret. Examples include logistic regression, linear regression, Generalized Linear Models (Nelder and Wedderburn, 1972) and Generalized Additive Models (GAM) (Hastie and Tibshirani, 1990).

At the other end of the spectrum are models which allow the response to depend on all input variables simultaneously, having the form

$$y = f(x_1, x_2, \dots, x_D) \quad (6.2)$$

An example would be a GP with an SE-ARD kernel. Such models are much more flexible than those having the form (6.1), but this flexibility makes it difficult to generalize to new combinations of input variables.

In between these extremes, we can consider function classes depending on pairs or triplets of inputs, such as

$$g(y) = f(x_1, x_2) + f(x_2, x_3) + f(x_1, x_3) \quad (6.3)$$

In this chapter, we'll consider a GP model consisting of a sum of functions of all possible combinations of input variables. We'll call this model class *Additive Gaussian processes*. This model can be expressed by specifying a kernel which is a sum of all

possible products of one-dimensional kernels.

There are 2^D combinations of D kernels, so a naïve computation of such a kernel would be intractable. Furthermore, if each term has different kernel parameters, fitting or integrating over so many parameters would pose severe difficulty. To get around this problem, we introduce an expressive but tractable parameterization of the kernel function which also allows efficient evaluation of all interaction terms. Empirically, this kernel results in good predictive power in regression tasks, as well as increased interpretability.

In chapter 3, we showed how to learn the structure of a kernel by building it up piece-by-piece. This chapter presents an alternative approach, where we start with many different types of structure in the kernel from the beginning, and adjust the kernel parameters to discard whichever types *aren't* present in the current dataset. The advantage of this approach is that we don't need to run an expensive, mixed discrete-continuous optimization problem in order to build a structured model. Implementation is also much simpler.

The work in this chapter was done in collaboration with Hannes Nickisch and Carl Rasmussen, who derived and coded up the initial model. My role in the project was to examine the properties of the resulting model, clarify the connections to existing methods, to create all figures and run all experiments. This work was published in (Duvenaud et al., 2011).

6.1 Additive Kernels

We now give a precise definition of additive kernels. We first assign each dimension $i \in \{1 \dots D\}$ a one-dimensional *base kernel* $k_i(x_i, x'_i)$. We then define the first order, second order and n th order additive kernel as:

$$k_{add_1}(\mathbf{x}, \mathbf{x}') = \sigma_1^2 \sum_{i=1}^D k_i(x_i, x'_i) \quad (6.4)$$

$$k_{add_2}(\mathbf{x}, \mathbf{x}') = \sigma_2^2 \sum_{i=1}^D \sum_{j=i+1}^D k_i(x_i, x'_i) k_j(x_j, x'_j) \quad (6.5)$$

$$k_{add_n}(\mathbf{x}, \mathbf{x}') = \sigma_n^2 \sum_{1 \leq i_1 < i_2 < \dots < i_n \leq D} \left[\prod_{d=1}^n k_{i_d}(x_{i_d}, x'_{i_d}) \right] \quad (6.6)$$

$$k_{add_D}(\mathbf{x}, \mathbf{x}') = \sigma_n^2 \sum_{1 \leq i_1 < i_2 < \dots < i_D \leq D} \left[\prod_{d=1}^D k_{i_d}(x_{i_d}, x'_{i_d}) \right] = \sigma_D^2 \prod_{d=1}^D k_d(x_d, x'_d) \quad (6.7)$$

where D is the dimension of our input space, and σ_n^2 is the variance assigned to all n th order interactions. The n th covariance function is a sum of $\binom{D}{n}$ terms. In particular, the D th order additive covariance function has $\binom{D}{D} = 1$ term, a product of each dimension's covariance function:

$$k_{add_D}(\mathbf{x}, \mathbf{x}') = \sigma_D^2 \prod_{d=1}^D k_d(x_d, x'_d) \quad (6.8)$$

In the case where each base kernel is a one-dimensional squared-exponential kernel, the D th-order term corresponds to the multivariate squared-exponential kernel:

$$k_{add_D}(\mathbf{x}, \mathbf{x}') = \sigma_D^2 \prod_{d=1}^D k_d(x_d, x'_d) = \sigma_D^2 \prod_{d=1}^D \exp\left(-\frac{(x_d - x'_d)^2}{2l_d^2}\right) = \sigma_D^2 \exp\left(-\sum_{d=1}^D \frac{(x_d - x'_d)^2}{2l_d^2}\right) \quad (6.9)$$

also commonly known as the Gaussian kernel. The full additive kernel is a sum of the additive kernels of all orders.

6.1.1 Parameterization

The only design choice necessary in specifying an additive kernel is the selection of a one-dimensional base kernel for each input dimension. Any parameters (such as length-scales) of the base kernels can be learned as usual by maximizing the marginal likelihood of the training data.

In addition to the parameters of each dimension-wise kernel, additive kernels are equipped with a set of D parameters $\sigma_1^2 \dots \sigma_D^2$ controlling how much variance we assign to each order of interaction. These “order variance” parameters have a useful interpretation: the d th order variance hyperparameter controls how much of the target function’s variance comes from interactions of the d th order. Table 6.1 shows examples of the variance contributed by the different orders of interaction, learned on real datasets.

On different datasets, the dominant order of interaction estimated by the additive model varies widely. An additive GP with all of its variance coming from the 1st order is equivalent to a sum of one-dimensional functions; an additive GP with all its variance coming from the D th order is equivalent to a SE-GP.

Because the variance parameters can specify which degrees of interaction are important, the additive GP can capture many different types of structure. If the function we are modeling is decomposable into a sum of low-dimensional functions, our model can

Table 6.1 Percentage of variance contributed by each order of the additive model, on different datasets. The maximum order of interaction is set to 10, or smaller if the input dimension less than 10.

Dataset	Order of interaction									
	1st	2nd	3rd	4th	5th	6th	7th	8th	9th	10th
pima	0.1	0.1	0.1	0.3	1.5	96.4	1.4	0.0		
liver	0.0	0.2	99.7	0.1	0.0	0.0				
heart	77.6	0.0	0.0	0.0	0.1	0.1	0.1	0.1	0.1	22.0
concrete	70.6	13.3	13.8	2.3	0.0	0.0	0.0	0.0		
pumadyn-8nh	0.0	0.1	0.1	0.1	0.1	0.1	0.1	99.5		
servo	58.7	27.4	0.0	13.9						
housing	0.1	0.6	80.6	1.4	1.8	0.8	0.7	0.8	0.6	12.7

discover this fact and exploit it. Discovering such structure allows long-range extrapolation, as we saw in section 2.4.2. If low-dimensional additive structure is not present, the kernel parameters can specify a suitably flexible model, with interactions between as many variables as necessary.

6.1.2 Efficient Evaluation of Additive Kernels

An additive kernel over D inputs with interactions up to order n has $O(2^n)$ terms. Naïvely summing over these terms quickly becomes intractable. In this section, we show how one can evaluate the sum over all terms in $O(D^2)$.

To efficiently compute the additive kernel, we exploit the fact that the n th order additive kernel corresponds to the n th *elementary symmetric polynomial* (Macdonald, 1998) of the base kernels, which we denote e_n . For example: if \mathbf{x} has 4 input dimensions ($D = 4$), and if we use the shorthand notation $k_d = k_d(x_d, x'_d)$, then

$$k_{\text{add}_0}(\mathbf{x}, \mathbf{x}') = e_0(k_1, k_2, k_3, k_4) = 1 \quad (6.10)$$

$$k_{\text{add}_1}(\mathbf{x}, \mathbf{x}') = e_1(k_1, k_2, k_3, k_4) = k_1 + k_2 + k_3 + k_4 \quad (6.11)$$

$$k_{\text{add}_2}(\mathbf{x}, \mathbf{x}') = e_2(k_1, k_2, k_3, k_4) = k_1 k_2 + k_1 k_3 + k_1 k_4 + k_2 k_3 + k_2 k_4 + k_3 k_4 \quad (6.12)$$

$$k_{\text{add}_3}(\mathbf{x}, \mathbf{x}') = e_3(k_1, k_2, k_3, k_4) = k_1 k_2 k_3 + k_1 k_2 k_4 + k_1 k_3 k_4 + k_2 k_3 k_4 \quad (6.13)$$

$$k_{\text{add}_4}(\mathbf{x}, \mathbf{x}') = e_4(k_1, k_2, k_3, k_4) = k_1 k_2 k_3 k_4 \quad (6.14)$$

The Newton-Girard formulae give an efficient recursive form for computing these poly-

nomials:

$$k_{\text{add}_n}(\mathbf{x}, \mathbf{x}') = e_n(k_1, \dots, k_D) = \frac{1}{n} \sum_{a=1}^n (-1)^{(a-1)} e_{n-a}(k_1, \dots, k_D) \sum_{i=1}^D k_i^a \quad (6.15)$$

The Newton-Girard formulae have time complexity $\mathcal{O}(D^2)$, while computing a sum over an exponential number of terms. Note that the same sum can be computed in time

Conveniently, we can use the same trick to efficiently compute all of the necessary derivatives of the additive kernel with respect to the base kernels. We merely need to remove the kernel of interest from each term of the polynomials:

$$\frac{\partial k_{\text{add}_n}}{\partial k_j} = e_{n-1}(k_1, \dots, k_{j-1}, k_{j+1}, \dots, k_D) \quad (6.16)$$

This trick allows us to optimize the base kernel parameters with respect to the marginal likelihood.

6.1.3 Computational Cost

The computational cost of evaluating the Gram matrix of a product kernel (such as the SE kernel) is $\mathcal{O}(N^2D)$, while the cost of evaluating the Gram matrix of the additive kernel is $\mathcal{O}(N^2DR)$, where R is the maximum degree of interaction allowed (up to D). In higher dimensions, this can be a significant cost, even relative to the fixed $\mathcal{O}(N^3)$ cost of inverting the Gram matrix. However, as our experiments show, typically only the first few orders of interaction are important for modeling a given function; hence if one is computationally limited, one can simply limit the maximum degree of interaction without losing much accuracy.

6.2 Non-local Interactions

By far the most popular kernels for regression and classification tasks on continuous data are the SE kernel, and the Matérn kernels. These kernels depend only on the scaled Euclidean distance between two points, both having the form:

$$k(\mathbf{x}, \mathbf{x}') = g\left(\sum_{d=1}^D \left(\frac{x_d - x'_d}{l_d} \right)^2 \right) \quad (6.17)$$

Bengio et al. (2006) argue that models based on squared-exponential kernels are particularly susceptible to the *curse of dimensionality*. They emphasize that the locality of the kernels means that these models cannot capture non-local structure. They argue that many functions that we care about have such structure. Methods based solely on local kernels will require training examples at all combinations of relevant inputs.

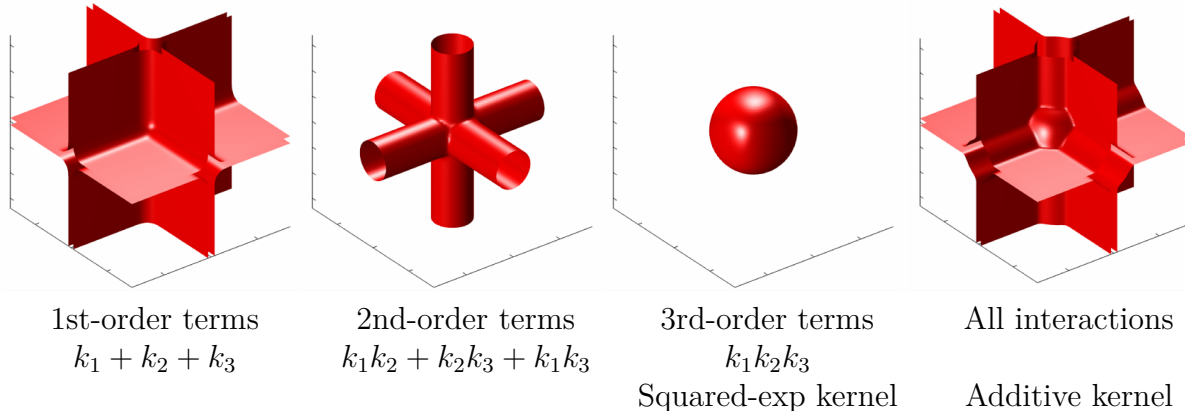


Fig. 6.1 Isocontours of additive kernels in 3 dimensions. The third-order kernel only considers nearby points relevant, while the lower-order kernels allow the output to depend on distant points, as long as they share one or more input value.

Additive kernels have a much more complex structure, and allow extrapolation based on distant parts of the input space, without spreading the mass of the kernel over the whole space. For example, additive kernels of the second order allow strong non-local interactions between any points which are similar in any two input dimensions. Figure 6.1 provides a geometric comparison between squared-exponential kernels and additive kernels in 3 dimensions.

In chapter 2, section 2.4.1 gives an example of how additive kernels extrapolate differently than local kernels.

6.3 Dropout in Gaussian Processes

Dropout is a method for regularizing neural networks (Hinton et al., 2012; Srivastava, 2013). Training with dropout entails randomly and independently “dropping” (setting to zero) some proportion p of features or inputs, in order to improve the robustness of the resulting network by reducing co-dependence between neurons. To maintain similar overall activation levels, weights are multiplied by $1/p$ at test time. Alternatively, feature

activations are multiplied by $1/p$ during training. At test time, the set of models defined by all possible ways of dropping-out neurons is averaged over, usually in an approximate way.

Baldi and Sadowski (2013) and Wang and Manning (2013) analyzed dropout in terms of the effective prior induced by this procedure in several models, such as linear and logistic regression. In this section, we examine the priors on functions that result from performing dropout in the one-hidden-layer neural network implicitly defined by a GP.

Recall that GPs can be derived as an infinitely-wide one-layer neural network, with fixed activation functions $\mathbf{h}(\mathbf{x})$, and independent random weights $\boldsymbol{\alpha}$ with finite variance σ_α^2 :

$$f(\mathbf{x}) = \frac{1}{K} \boldsymbol{\alpha}^\top \mathbf{h}(\mathbf{x}) = \frac{1}{K} \sum_{i=1}^K \alpha_i h_i(\mathbf{x}) \quad (6.18)$$

$$\implies f(\mathbf{x}) \xrightarrow{K \rightarrow \infty} \mathcal{GP}\left(\mathbb{E} [\boldsymbol{\alpha}^\top \mathbf{h}(\mathbf{x})], \sigma_\alpha^2 \mathbf{h}(\mathbf{x})^\top \mathbf{h}(\mathbf{x}')\right) \quad (6.19)$$

Mercer's theorem implies that we can write any GP prior equivalently in this way. Now that we've expressed a GP as a neural network, we can examine the prior we get from performing dropout in this network.

6.3.1 Dropout on Hidden Units

First, we'll examine the prior we get from independently dropping features from $\mathbf{h}(\mathbf{x})$ by setting some of the weights $\boldsymbol{\alpha}$ to zero with probability p . For simplicity, we'll assume that $\mathbb{E} [\boldsymbol{\alpha}] = \mathbf{0}$. If the weights initially have finite variance σ_α^2 before dropout, then after dropout they'll have variance

$$r_i \stackrel{\text{iid}}{\sim} \text{Ber}(p) \quad \mathbb{V}[r_i \alpha_i] = p \sigma_\alpha^2. \quad (6.20)$$

Because equation (6.19) is a result of the central limit theorem, it does not depend on the form of the distribution on $\boldsymbol{\alpha}$, only its mean and variance. Thus, dropping out features of an infinitely-wide MLP does not change the model at all, except to rescale the output variance, since no individual feature can have more than infinitesimal contribution to the network output. Indeed, multiplying all weights by $p^{-1/2}$, the initial variance is restored:

$$\mathbb{V}\left[\frac{1}{p^{1/2}} r_i \alpha_i\right] = \frac{p}{p} \sigma_\alpha^2 = \sigma_\alpha^2. \quad (6.21)$$

In which case dropout on the hidden units has no effect at all.

6.3.2 Dropout on Inputs

In a GP with kernel $k(\mathbf{x}, \mathbf{x}') = \prod_{d=1}^D k_d(x_d, x'_d)$, exact averaging over all possible ways of dropping out inputs with probability $1/2$ results in a mixture of GPs, each depending on only a subset of the inputs:

$$p(f(\mathbf{x})) = \frac{1}{2^D} \sum_{\mathbf{r} \in \{0,1\}^D} \text{GP} \left(f(\mathbf{x}) \mid 0, \prod_{d=1}^D k_d(x_d, x'_d)^{r_d} \right) \quad (6.22)$$

We present two results ways to gain intuition about this model.

First, if the kernel on each dimension has the form $k_d(x_d, x'_d) = g\left(\frac{x_d - x'_d}{w_d}\right)$, as does the SE kernel, then any input dimension can be dropped out by setting its lengthscale w_d to ∞ . Thus, dropout on the inputs of a GP corresponds to a spike-and-slab prior on lengthscales, with each dimension independently having $w_d = \infty$ with probability $1/2$.

Another way to understand the resulting prior is to note that the dropout mixture (6.22) has the same covariance as

$$f(\mathbf{x}) \sim \text{GP} \left(0, \frac{1}{2^{-2D}} \sum_{\mathbf{r} \in \{0,1\}^D} \prod_{d=1}^D k_d(x_d, x'_d)^{r_d} \right) \quad (6.23)$$

Therefore, dropout on the inputs to a GP can be approximated by the all-subsets additive kernel. This suggests an interpretation of additive kernels as an approximation to a mixture of models, each of which depends on only a subset of the input variables.

6.4 Related Work

Since additive models are a relatively natural and easy-to-analyze model class, the literature on similar model classes is extensive. We try to give a broad overview in this section.

Additive GPs

Since the non-local structure capturable by additive kernels is necessarily axis-aligned, we can naturally consider that an initial transformation of the input space might allow us to recover non-axis aligned additivity in functions. This avenue was explored by [Gilboa](#)

et al. (2013), who developed a linearly-transformed first-order additive GP model, called projection-pursuit GP regression. They further showed that inference in this model was possible in $\mathcal{O}(N)$ time.

Durrande et al. (2011) also examined the properties of additive GPs, and proposed a layer-wise optimization strategy for kernel hyperparameters in these models.

Plate (1999) constructed an additive GP using only the first-order and D th-order terms. This model is motivated by the desire to trade off the interpretability of first-order models with the flexibility of full-order models. Our experiments show that often, the intermediate degrees of interaction contribute most of the variance.

A related functional ANOVA GP model (Kaufman and Sain, 2010) decomposes the *mean* function into a weighted sum of GPs. However, the effect of a particular degree of interaction cannot be quantified by that approach. Also, computationally, the Gibbs sampling approach used in (Kaufman and Sain, 2010) is disadvantageous.

Christoudias et al. (2009) previously showed how mixtures of kernels can be learnt by gradient descent in the Gaussian process framework. They call this *Bayesian localized multiple kernel learning*. However, their approach learns a mixture over a small, fixed set of kernels, while our method learns a mixture over all possible products of those kernels.

Hierarchical Kernel Learning

A similar model class was recently explored by Bach (2009b) called Hierarchical Kernel Learning (HKL). HKL uses a regularized optimization framework to learn a weighted sum over an exponential number of kernels which can be computed in polynomial time. This method chooses among *hull* of kernels, defined as a subset of all terms such that if $\prod_{j \in J} k_j(\mathbf{x}, \mathbf{x}')$ is included in the subset, then so are all terms $\prod_{j \in J/i} k_j(\mathbf{x}, \mathbf{x}')$, for all $i \in J$. HKL computes the sum over all orders in $\mathcal{O}(D)$ time by the formula:

$$k_a(\mathbf{x}, \mathbf{x}') = v^2 \prod_{d=1}^D (1 + \alpha k_d(x_d, x'_d)) \quad (6.24)$$

which forces the weight of all n th order terms to be weighted by α^n .

Figure 6.2 contrasts the HKL model class with the additive GP model. Neither method is strictly more flexible than the other. The main difficulty with the approach of Bach (2009b) is that the kernel parameters are hard to set, other than by cross-validation.

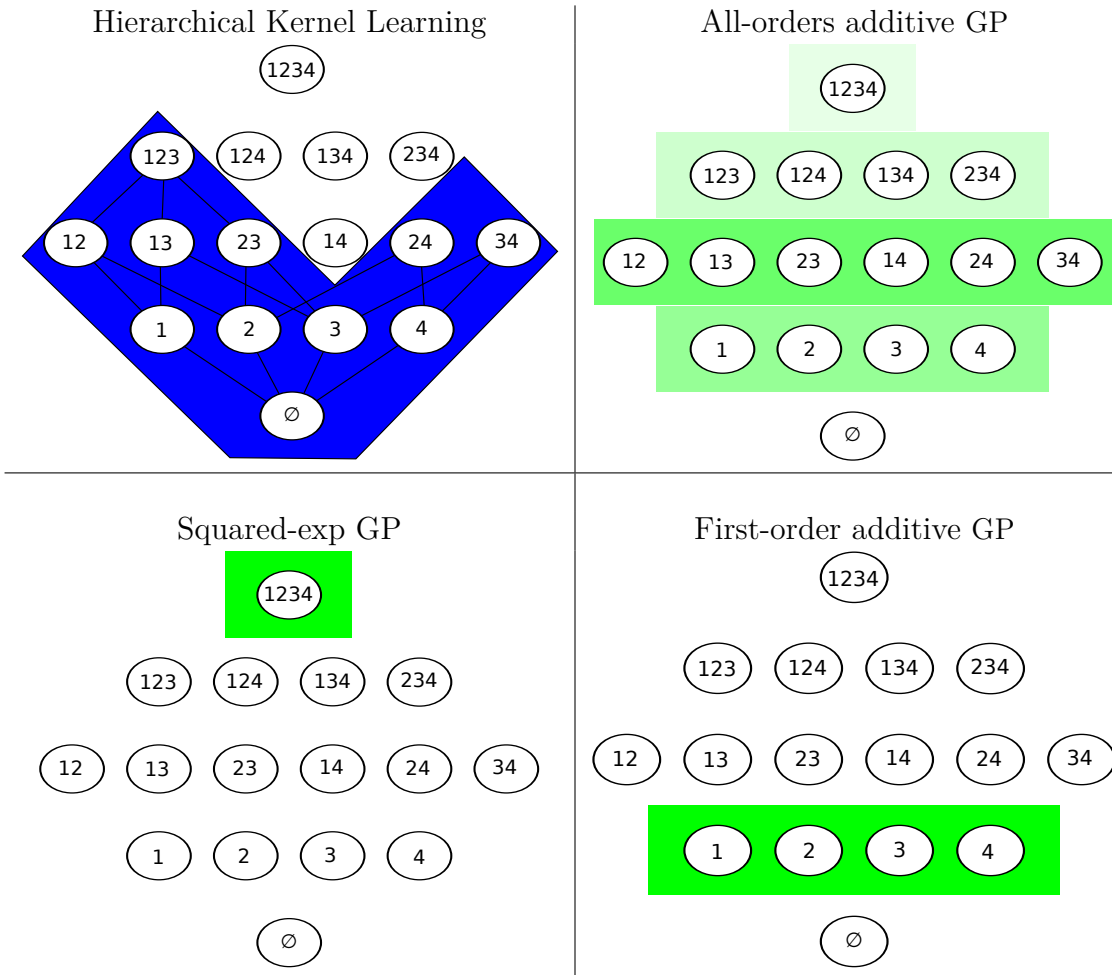


Fig. 6.2 A comparison of different additive model classes. Nodes represent different interaction terms, ranging from first-order to fourth-order interactions. Coloured boxes represent the weightings of different terms. *Top left:* HKL can select a hull of interaction terms, but must use a pre-determined weighting over those terms. *Top right:* the additive GP model can weight each order of interaction separately. *Bottom row:* Neither HKL nor the additive model dominate one another in terms of flexibility, however the SE-GP and first-order additive GP models are special cases of the all-orders additive GP.

Support Vector Machines

Vapnik (1998) introduced the support vector ANOVA decomposition, which has the same form as our additive kernel. They recommend approximating the sum over all D orders with only one term “of appropriate order”, presumably because of the difficulty of setting the parameters of an SVM. Stitson et al. (1999) performed experiments which favourably compared the predictive accuracy of the support vector ANOVA decomposition against polynomial and spline kernels. They too allowed only one order to be active, and set

parameters by cross-validation.

Other Related Models

A closely related procedure from [Wahba \(1990\)](#) is smoothing-splines ANOVA (SS-ANOVA). An SS-ANOVA model is a weighted sum of splines along each dimension, plus a sum of splines over all pairs of dimensions, all triplets, etc, with each individual interaction term having a separate weighting parameter. Because the number of terms to consider grows exponentially in the order, in practice, only terms of first and second order are usually considered.

This more general model class, in which each interaction term is estimated separately, is known in the physical sciences as High Dimensional Model Representation (HDMR). [Rabitz and Aliş \(1999\)](#) review some properties and applications of this model class.

The main benefits of the model setup and parameterization proposed in this chapter are the ability to include all D orders of interaction with differing weights, and the ability to learn kernel parameters individually per input dimension, allowing automatic relevance determination to operate.

6.5 Experiments

Parameterization

A D -dimensional SE-ARD kernel has D lengthscale parameters and the output variance. An first-order additive SE model has $2 \times D$ parameters. A fully-parametrized model including all orders of interaction, with a separate output variance for each scale will have $3 \times D$ parameters. Because each additional parameter increases the tendency to overfit, we recommend allowing only one kernel parameter per input dimension. In our experiments, we parametrized each one-dimensional kernel with only the lengthscale, fixing the output variance to be 1.

Methods

We compare six different methods. In the results tables below, GP Additive refers to a GP using the additive kernel with squared-exp base kernels. For speed, we limited the maximum order of interaction in the additive kernels to 10. GP-1st denotes an additive GP model with only first-order interactions - a sum of one-dimensional kernels. GP Squared-Exp is a GP model with a squared-exponential ARD kernel. HKL was run

using the all-subsets kernel, which corresponds to the same set of kernels as considered by the additive GP with a squared-exp base kernel.

For all GP models, we fit kernel parameters by the standard method of maximizing training-set marginal likelihood, using L-BFGS (Nocedal, 1980) for 500 iterations, allowing five random restarts. In addition to learning kernel parameters, we fit a constant mean function to the data. In the classification experiments, approximate GP inference was done using Expectation Propagation (Minka, 2001).

For the regression experiments, we also compared against the structure search method from chapter 3, run up to depth 10, using the SE and RQ base kernel families.

6.5.1 Datasets

We compared these methods on a diverse set of regression and classification datasets from the UCI repository (Bache and Lichman, 2013). Their size and dimension are given in tables 6.2 and 6.3:

Table 6.2 Regression Dataset Statistics

Method	bach	concrete	pumadyn	servo	housing
Dimension	8	8	8	4	13
Number of datapoints	200	500	512	167	506

Table 6.3 Classification Dataset Statistics

Method	breast	pima	sonar	ionosphere	liver	heart
Dimension	9	8	60	32	6	13
Number of datapoints	449	768	208	351	345	297

Bach Synthetic Dataset

In addition to standard UCI repository datasets, we generated a synthetic dataset following the same recipe as Bach (2009b). This dataset was designed to demonstrate the advantages of HKL over GP-SE. It is generated by passing correlated Gaussian-

distributed inputs x_1, x_2, \dots, x_8 through the quadratic function

$$f(\mathbf{x}) = \sum_{i=1}^4 \sum_{j=i+1}^4 x_i x_j + \epsilon \quad \epsilon \sim \mathcal{N}(0, \sigma_\epsilon) \quad (6.25)$$

This dataset is well-modeled by an additive kernel which includes all two-way interactions over the first 4 variables, but does not depend on the extra 4 irrelevant inputs.

If the dataset is large enough, HKL can construct a hull around only the 16 cross-terms optimal for predicting the output. GP-SE, in contrast, can learn to ignore the noisy copy variables, but cannot learn to ignore the higher-order interactions between dimensions. However, a GP with an additive kernel can learn both to ignore irrelevant variables, and to ignore missing orders of interaction. With enough data, the marginal likelihood will favour hyperparameters specifying such a model.

6.5.2 Results

Tables 6.4 to 6.7 show mean performance across 10 train-test splits. Because HKL does not specify a noise model, it could not be included in the likelihood comparisons.

Table 6.4 Regression Mean Squared Error

Method	bach	concrete	pumadyn-8nh	servo	housing
Linear Regression	1.031	0.404	0.641	0.523	0.289
GP-1st	1.259	0.149	0.598	0.281	0.161
HKL	0.199	0.147	0.346	0.199	0.151
GP Squared-exp	0.045	0.157	0.317	0.126	0.092
GP Additive	0.045	0.089	0.316	0.110	0.102
Structure Search	0.044	0.087	0.315	0.102	0.082

The model with best performance on each dataset is in bold, along with all other models that were not significantly different under a paired t -test. The additive and structure search methods usually outperformed the other methods, especially on regression problems. The structure search outperforms the additive GP, but at the cost of a slow search over kernels.

The additive GP performed best on datasets well-explained by low orders of interaction, and approximately as well as the SE-GP model on datasets which were well explained by high orders of interaction (see table 6.1). Because the additive GP is a su-

Table 6.5 Regression Negative Log Likelihood

Method	bach	concrete	pumadyn-8nh	servo	housing
Linear Regression	2.430	1.403	1.881	1.678	1.052
GP-1st	1.708	0.467	1.195	0.800	0.457
GP Squared-exp	-0.131	0.398	0.843	0.429	0.207
GP Additive	-0.131	0.114	0.841	0.309	0.194
Structure Search	-0.141	0.065	0.840	0.265	0.059

Table 6.6 Classification percent error

Method	breast	pima	sonar	ionosphere	liver	heart
Logistic Regression	7.611	24.392	26.786	16.810	45.060	16.082
GP-1st	5.189	22.419	15.786	8.524	29.842	16.839
HKL	5.377	24.261	21.000	9.119	27.270	18.975
GP Squared-exp	4.734	23.722	16.357	6.833	31.237	20.642
GP Additive	5.566	23.076	15.714	7.976	30.060	18.496

Table 6.7 Classification negative log-likelihood

Method	breast	pima	sonar	ionosphere	liver	heart
Logistic Regression	0.247	0.560	4.609	0.878	0.864	0.575
GP-1st	0.163	0.461	0.377	0.312	0.569	0.393
GP Squared-exp	0.146	0.478	0.425	0.236	0.601	0.480
GP Additive	0.150	0.466	0.409	0.295	0.588	0.415

subset of both the GP-1st model and the SE-GP model, instances where the additive GP performs slightly worse are presumably due to over-fitting, or due to the hyperparameter optimization becoming stuck in a local maximum. Performance could be expected to benefit from approximately integrating over the kernel parameters.

The performance of HKL is consistent with the results in (Bach, 2009b), performing competitively but slightly worse than SE-GP.

6.5.3 Source Code

Additive Gaussian processes are particularly appealing in practice because their use requires only the specification of the base kernel; all other aspects of GP inference remain the same. Note that we are also free to choose a different covariance function along each dimension.

All of the experiments in this chapter were performed using the standard GPML toolbox, available at <http://www.gaussianprocess.org/gpml/code/>. Code to perform all experiments is available at <http://github.com/duvenaud/additive-gps>

6.6 Conclusion

In this chapter, we presented a parameterization of higher-order additive GPs allowing for tractable inference. Our experiments indicate that, to varying degrees, additive structure is present in real datasets. When it is present, modeling this structure allows our model to perform better than standard GP models. In the case where no such structure exists, the higher-order interaction terms present in the kernel can recover arbitrarily flexible models, as well.

The additive GP also affords extra interpretability: the variance parameters on each order of interaction indicate which sorts of structure are present in the data.

Chapter 7

Warped Mixture Models

“What, exactly, is a cluster?”

- Bernhard Schölkopf, personal communication

A mixture of Gaussians fit to a single curved or heavy-tailed cluster will report that the data contains many clusters. To produce more appropriate clusterings, we introduce a model which warps a latent mixture of Gaussians to produce nonparametric cluster shapes. The possibly low-dimensional latent mixture model allows us to summarize the properties of the high-dimensional clusters (or density manifolds) describing the data. The number of manifolds, as well as the shape and dimension of each manifold is automatically inferred. We derive a simple inference scheme for this model which analytically integrates out both the mixture parameters and the warping function. We show that our model is effective for density estimation, performs better than infinite Gaussian mixture models at recovering the true number of clusters, and produces interpretable summaries of high-dimensional datasets.

Probabilistic mixture models are often used for clustering. However, if the mixture components are parametric (e.g. Gaussian), then the clustering obtained can be heavily dependent on how well each actual cluster can be modeled by a Gaussian. For example, a heavy tailed or curved cluster may need many components to model it. Thus, although mixture models are widely used for probabilistic clustering, their assumptions are generally inappropriate if the primary goal is to discover clusters in data. Dirichlet process mixture models can alleviate the problem of an unknown number of clusters, but this does not address the problem that real clusters may not be well matched by any parametric density.

In this paper, we propose a nonparametric Bayesian model that can find non-linearly separable clusters with complex shapes. The proposed model assumes that each observa-

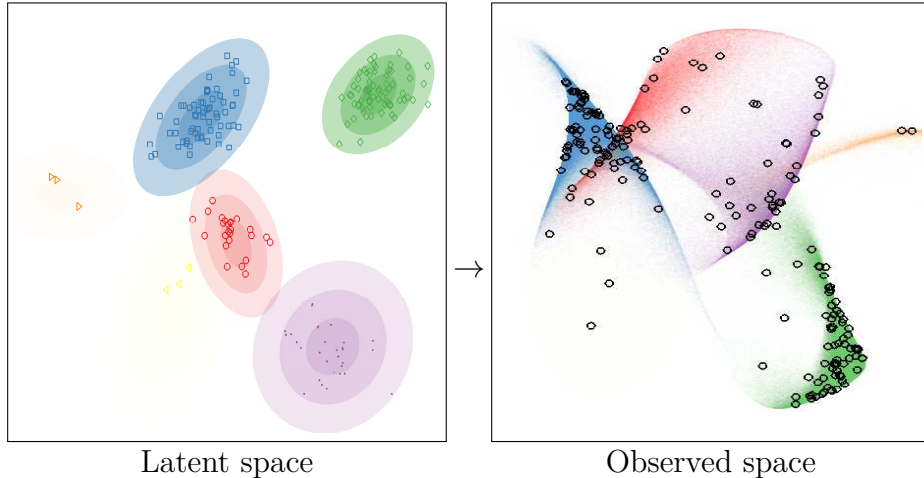


Fig. 7.1 A sample from the iWMM prior. *Left:* In the latent space, a mixture distribution is sampled from a Dirichlet process mixture of Gaussians. *Right:* The latent mixture is smoothly warped to produce non-Gaussian manifolds in the observed space.

tion has coordinates in a latent space, and is generated by warping the latent coordinates via a nonlinear function from the latent space to the observed space. By this warping, complex shapes in the observed space can be modeled by simpler shapes in the latent space. In the latent space, we assume an infinite Gaussian mixture model (Rasmussen, 2000), which allows us to automatically infer the number of clusters. For the prior on the nonlinear mapping function, we use Gaussian processes (Rasmussen and Williams, 2006), which enable us to flexibly infer the nonlinear warping function from the data. We call the proposed model the *infinite warped mixture model* (iWMM). Figure 7.1 shows a set of manifolds and datapoints sampled from the prior defined by this model.

To our knowledge this is the first probabilistic generative model for clustering with flexible nonparametric component densities. Since the proposed model is generative, it can be used for density estimation as well as clustering. It can also be extended to handle missing data, integrate with other probabilistic models, and use other families of distributions for the latent components.

We derive an inference procedure for the iWMM based on Markov chain Monte Carlo (MCMC). In particular, we sample the cluster assignments using Gibbs sampling, sample the latent coordinates using Hamiltonian Monte Carlo, and analytically integrate out both the mixture parameters (weights, means and covariance matrices), and the nonlinear warping function.

The work comprising the bulk of this chapter was done in collaboration with Tomoharu Iwata and Zoubin Ghahramani, and appeared in (Iwata et al., 2013). Specifically,

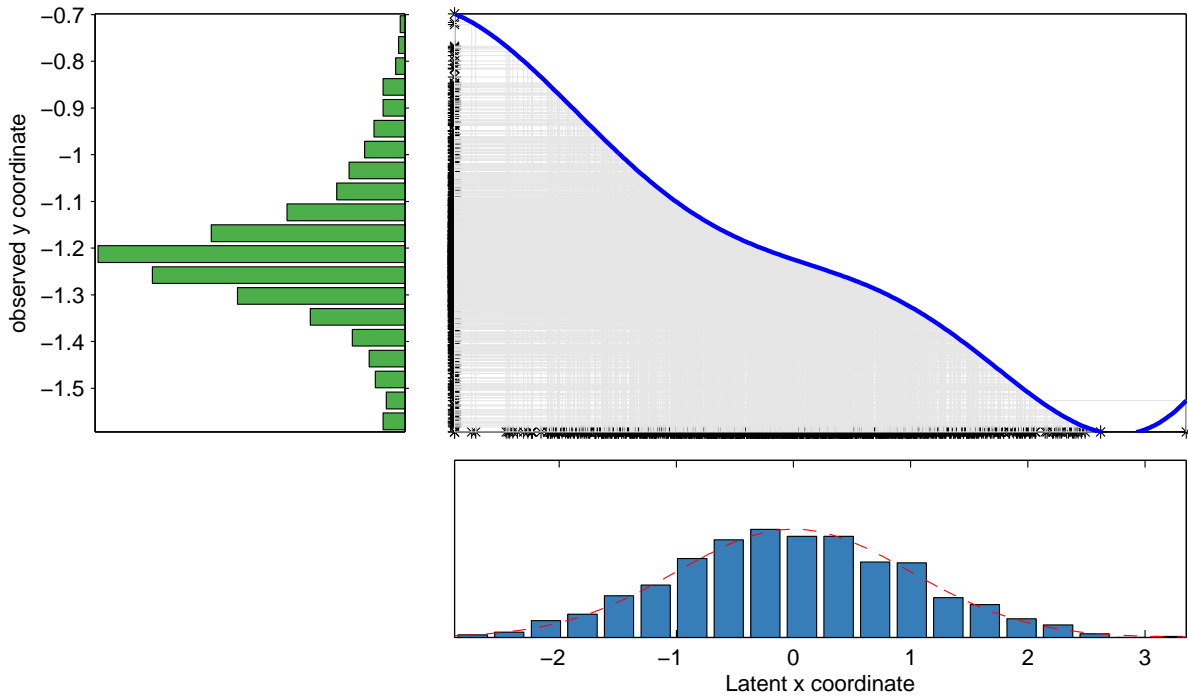


Fig. 7.2 A visual representation of the Gaussian process latent variable model. Bottom: density and samples from a 1D Gaussian, specifying the distribution $p(\mathbf{X})$ in the latent space. Top Right: A function drawn from a GP prior. Left: A nonparametric density defined by warping the latent density through the function drawn from a GP prior.

the main idea was borne out of a conversation between Tomo and myself, and together we wrote almost all of the code together as well as the paper. Tomo ran most of the experiments. Zoubin Ghahramani provided guidance and many helpful suggestions throughout the project.

7.1 The Gaussian Process Latent Variable Model

Besides being useful for modeling functions, a simple extension allows GPs to be useful for general density modeling, at the cost of non-analytic inference. The GP-LVM can also be thought of as a method for modeling the covariance between rows of Y , using a number of parameters which grows only linearly with N .

In this section, we give a brief introduction to the GP-LVM, which can be viewed as a special case of the iWMM. The GP-LVM is a probabilistic model of nonlinear manifolds. While not typically thought of as a density model, the GP-LVM does in fact define a posterior density over observations (Nickisch and Rasmussen, 2010). It does this by

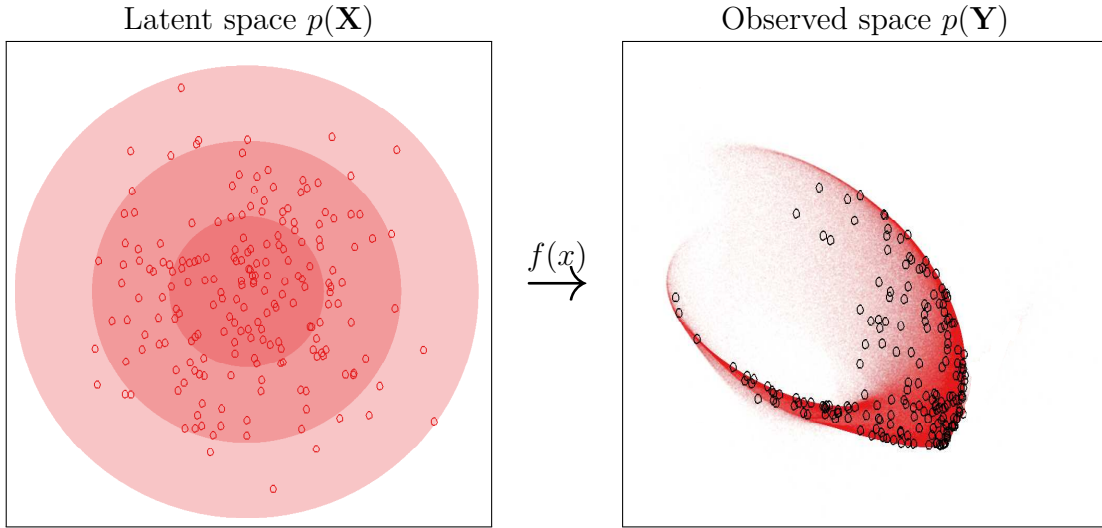


Fig. 7.3 A visual representation of the Gaussian process latent variable model. Left: Isocontours and samples from a 2D Gaussian, specifying the distribution $p(\mathbf{X})$ in the latent space. Right: Density and samples from a nonparametric density defined by warping the latent density through a function drawn from a GP prior.

smoothly warping a single, isotropic Gaussian density in the latent space into a more complicated distribution in the observed space.

Suppose that we have a set of observations $\mathbf{Y} = (\mathbf{y}_1, \dots, \mathbf{y}_N)^\top$, where $\mathbf{y}_n \in \mathbb{R}^D$, and they are associated with a set of latent coordinates $\mathbf{X} = (\mathbf{x}_1, \dots, \mathbf{x}_N)^\top$, where $\mathbf{x}_n \in \mathbb{R}^Q$. The GP-LVM assumes that observations are generated by mapping the latent coordinates through a set of smooth functions, over which Gaussian process priors are placed. Under the GP-LVM, the probability of observations given the latent coordinates, integrating out the mapping functions, is

$$p(\mathbf{Y}|\mathbf{X}, \boldsymbol{\theta}) = (2\pi)^{-\frac{DN}{2}} |\mathbf{K}|^{-\frac{D}{2}} \exp\left(-\frac{1}{2}\text{tr}(\mathbf{Y}^\top \mathbf{K}^{-1} \mathbf{Y})\right), \quad (7.1)$$

where \mathbf{K} is the $N \times N$ covariance matrix defined by the kernel function $k(\mathbf{x}_n, \mathbf{x}_m)$, and $\boldsymbol{\theta}$ is the kernel hyperparameter vector. In this paper, we use an RBF kernel with an additive noise term:

$$k(\mathbf{x}_n, \mathbf{x}_m) = \alpha \exp\left(-\frac{1}{2\ell^2}(\mathbf{x}_n - \mathbf{x}_m)^\top(\mathbf{x}_n - \mathbf{x}_m)\right) + \delta_{nm}\beta^{-1}. \quad (7.2)$$

This likelihood is simply the product of D independent Gaussian process likelihoods, one for each output dimension.

Typically, the GP-LVM is used for dimensionality reduction or visualization, and the latent coordinates are determined by maximizing the posterior probability of the latent coordinates, while integrating out the warping function. In that setting, the Gaussian prior density on \mathbf{x} is essentially a regularizer which keeps the latent coordinates from spreading arbitrarily far apart. In contrast, we instead integrate out the latent coordinates as well as the warping function, and place a more flexible parameterization on $p(\mathbf{x})$ than a single isotropic Gaussian.

Just as the GP-LVM can be viewed as a manifold learning algorithm, the iWMM can be viewed as learning a set of manifolds, one for each cluster.

7.2 The Infinite Warped Mixture Model

In this section, we define in detail the infinite warped mixture model (iWMM). In the same way as the GP-LVM, the iWMM assumes a set of latent coordinates and a smooth, nonlinear mapping from the latent space to the observed space. In addition, the iWMM assumes that the latent coordinates are generated from a Dirichlet process mixture model. In particular, we use the following infinite Gaussian mixture model,

$$p(\mathbf{x}|\{\lambda_c, \boldsymbol{\mu}_c, \mathbf{R}_c\}) = \sum_{c=1}^{\infty} \lambda_c \mathcal{N}(\mathbf{x}|\boldsymbol{\mu}_c, \mathbf{R}_c^{-1}), \quad (7.3)$$

where λ_c , $\boldsymbol{\mu}_c$ and \mathbf{R}_c is the mixture weight, mean, and precision matrix of the c^{th} mixture component. We place Gaussian-Wishart priors on the Gaussian parameters $\{\boldsymbol{\mu}_c, \mathbf{R}_c\}$,

$$p(\boldsymbol{\mu}_c, \mathbf{R}_c) = \mathcal{N}(\boldsymbol{\mu}_c|\mathbf{u}, (r\mathbf{R}_c)^{-1}) \mathcal{W}(\mathbf{R}_c|\mathbf{S}^{-1}, \nu), \quad (7.4)$$

where \mathbf{u} is the mean of $\boldsymbol{\mu}_c$, r is the relative precision of $\boldsymbol{\mu}_c$, \mathbf{S}^{-1} is the scale matrix for \mathbf{R}_c , and ν is the number of degrees of freedom for \mathbf{R}_c . The Wishart distribution is defined as follows:

$$\mathcal{W}(\mathbf{R}|\mathbf{S}^{-1}, \nu) = \frac{1}{G} |\mathbf{R}|^{\frac{\nu-Q-1}{2}} \exp\left(-\frac{1}{2} \text{tr}(\mathbf{S}\mathbf{R})\right), \quad (7.5)$$

where G is the normalizing constant. Because we use conjugate Gaussian-Wishart priors for the parameters of the Gaussian mixture components, we can analytically integrate out those parameters, given the assignments of points to components. Let z_n be the latent assignment of the n^{th} point. The probability of latent coordinates \mathbf{X} given latent assignments $\mathbf{Z} = (z_1, z_2, \dots, z_N)$ is obtained by integrating out the Gaussian parameters

$\{\boldsymbol{\mu}_c, \mathbf{R}_c\}$ as follows:

$$p(\mathbf{X}|\mathbf{Z}, \mathbf{S}, \nu, r) = \prod_{c=1}^{\infty} \pi^{-\frac{N_c Q}{2}} \frac{r^{Q/2} |\mathbf{S}|^{\nu/2}}{r_c^{Q/2} |\mathbf{S}_c|^{\nu_c/2}} \times \prod_{q=1}^Q \frac{\Gamma(\frac{\nu_c+1-q}{2})}{\Gamma(\frac{\nu+1-q}{2})}, \quad (7.6)$$

where N_c is the number of data points assigned to the c^{th} component, $\Gamma(\cdot)$ is the Gamma function, and

$$r_c = r + N_c, \quad \nu_c = \nu + N_c, \quad \mathbf{u}_c = \frac{r\mathbf{u} + \sum_{n:z_n=c} \mathbf{x}_n}{r + N_c},$$

$$\mathbf{S}_c = \mathbf{S} + \sum_{n:z_n=c} \mathbf{x}_n \mathbf{x}_n^\top + r \mathbf{u} \mathbf{u}^\top - r_c \mathbf{u}_c \mathbf{u}_c^\top, \quad (7.7)$$

are the posterior Gaussian-Wishart parameters of the c^{th} component. We use a Dirichlet process with concentration parameter η for infinite mixture modeling (MacEachern and Müller, 1998) in the latent space. Then, the probability of \mathbf{Z} is given as follows:

$$p(\mathbf{Z}|\eta) = \frac{\eta^C \prod_{c=1}^C (N_c - 1)!}{\eta(\eta + 1) \cdots (\eta + N - 1)}, \quad (7.8)$$

where C is the number of components for which $N_c > 0$. The joint distribution is given by

$$p(\mathbf{Y}, \mathbf{X}, \mathbf{Z}|\boldsymbol{\theta}, \mathbf{S}, \nu, \mathbf{u}, r, \eta) = p(\mathbf{Y}|\mathbf{X}, \boldsymbol{\theta})p(\mathbf{X}|\mathbf{Z}, \mathbf{S}, \nu, \mathbf{u}, r)p(\mathbf{Z}|\eta), \quad (7.9)$$

where factors in the right hand side can be calculated by (7.1), (7.6) and (7.8), respectively.

In summary, the infinite warped mixture model generates observations \mathbf{Y} according to the following generative process:

1. Draw mixture weights $\boldsymbol{\lambda} \sim \text{GEM}(\eta)$
2. For each component $c = 1, 2, \dots, \infty$
 - (a) Draw precision $\mathbf{R}_c \sim \mathcal{W}(\mathbf{S}^{-1}, \nu)$
 - (b) Draw mean $\boldsymbol{\mu}_c \sim \mathcal{N}(\mathbf{u}, (r\mathbf{R}_c)^{-1})$
3. For each observed dimension $d = 1, 2, \dots, D$
 - (a) Draw function $f_d(\mathbf{x}) \sim \text{GP}(m(\mathbf{x}), k(\mathbf{x}, \mathbf{x}'))$

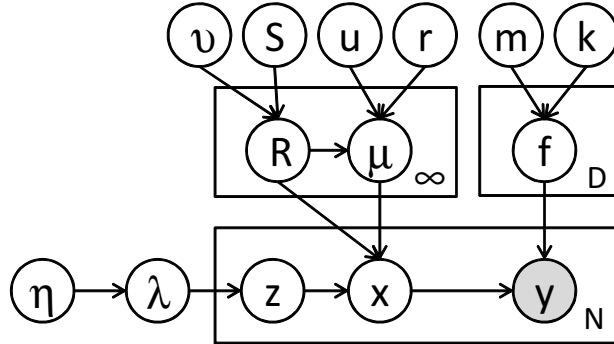


Fig. 7.4 A graphical model representation of the infinite warped mixture model, where the shaded and unshaded nodes indicate observed and latent variables, respectively, and plates indicate repetition.

4. For each observation $n = 1, 2, \dots, N$
 - (a) Draw latent assignment $z_n \sim \text{Mult}(\boldsymbol{\lambda})$
 - (b) Draw latent coordinates $\mathbf{x}_n \sim \mathcal{N}(\boldsymbol{\mu}_{z_n}, \mathbf{R}_{z_n}^{-1})$
 - (c) For each observed dimension $d = 1, 2, \dots, D$
 - i. Draw feature $y_{nd} \sim \mathcal{N}(f_d(\mathbf{x}_n), \beta^{-1})$

Here, $\text{GEM}(\eta)$ is the stick-breaking process (Sethuraman, 1994) that generates mixture weights for a Dirichlet process with parameter η , $\text{Mult}(\boldsymbol{\lambda})$ represents a multinomial distribution with parameter $\boldsymbol{\lambda}$, $m(\mathbf{x})$ is the mean function of the Gaussian process, and $\mathbf{x}, \mathbf{x}' \in \mathbb{R}^Q$. Figure 7.4 shows the graphical model representation of the proposed model. Here, we assume a Gaussian for the mixture component, although we could in principle use other distributions such as Student's t-distribution or the Laplace distribution.

The iWMM can be seen as a generalization of either the GP-LVM or the infinite Gaussian mixture model (iGMM). To be precise, the iWMM with a single fixed spherical Gaussian density on the latent coordinates corresponds to the GP-LVM, while the iWMM with fixed direct mapping function $f_d(\mathbf{x}) = x_d$ and $Q = D$ corresponds to the iGMM.

The iWMM offers attractive properties that do not exist in other probabilistic models; principally, the ability to model clusters with nonparametric densities, and to infer a separate dimension for manifold.

7.3 Inference

We infer the posterior distribution of the latent coordinates \mathbf{X} and cluster assignments \mathbf{Z} using Markov chain Monte Carlo (MCMC). In particular, we alternate collapsed Gibbs sampling of \mathbf{Z} , and Hamiltonian Monte Carlo sampling of \mathbf{X} . Given \mathbf{X} , we can efficiently sample \mathbf{Z} using collapsed Gibbs sampling, integrating out the mixture parameters. Given \mathbf{Z} , we can calculate the gradient of the un-normalized posterior distribution of \mathbf{X} , integrating over warping functions. This gradient allows us to sample \mathbf{X} using Hamiltonian Monte Carlo.

First, we explain collapsed Gibbs sampling for \mathbf{Z} . Given a sample of \mathbf{X} , $p(\mathbf{Z}|\mathbf{X}, \mathbf{S}, \nu, \mathbf{u}, r, \eta)$ does not depend on \mathbf{Y} . This lets us resample cluster assignments, integrating out the iGMM likelihood in closed form. Given the current state of all but one latent component z_n , a new value for z_n is sampled with the following probability:

$$p(z_n = c|\mathbf{X}, \mathbf{Z}_{\setminus n}, \mathbf{S}, \nu, \mathbf{u}, r, \eta) \propto \begin{cases} N_{c \setminus n} \cdot p(\mathbf{x}_n|\mathbf{X}_{c \setminus n}, \mathbf{S}, \nu, \mathbf{u}, r) & \text{existing components} \\ \eta \cdot p(\mathbf{x}_n|\mathbf{S}, \nu, \mathbf{u}, r) & \text{a new component} \end{cases} \quad (7.10)$$

where $\mathbf{X}_c = \{\mathbf{x}_n | z_n = c\}$ is the set of latent coordinates assigned to the c^{th} component, and $\setminus n$ represents the value or set when excluding the n^{th} data point. We can analytically calculate $p(\mathbf{x}_n|\mathbf{X}_{c \setminus n}, \mathbf{S}, \nu, \mathbf{u}, r)$ as follows:

$$p(\mathbf{x}_n|\mathbf{X}_{c \setminus n}, \mathbf{S}, \nu, \mathbf{u}, r) = \pi^{-\frac{N_{c \setminus n} Q}{2}} \frac{r_{c \setminus n}^{Q/2} |\mathbf{S}_{c \setminus n}|^{\nu_{c \setminus n}/2}}{r_{c \setminus n}'^{Q/2} |\mathbf{S}'_{c \setminus n}|^{\nu'_{c \setminus n}/2}} \prod_{d=1}^Q \frac{\Gamma(\frac{\nu'_{c \setminus n} + 1 - d}{2})}{\Gamma(\frac{\nu_{c \setminus n} + 1 - d}{2})}, \quad (7.11)$$

where r'_c , ν'_c , \mathbf{u}'_c and \mathbf{S}'_c represent the posterior Gaussian-Wishart parameters of the c^{th} component when the n^{th} data point is assigned to the c^{th} component. We can efficiently calculate the determinant by using the rank one Cholesky update. In the same way, we can analytically calculate the likelihood for a new component $p(\mathbf{x}_n|\mathbf{S}, \nu, \mathbf{u}, r)$.

Hamiltonian Monte Carlo (HMC) sampling of \mathbf{X} from posterior $p(\mathbf{X}|\mathbf{Z}, \mathbf{Y}, \boldsymbol{\theta}, \mathbf{S}, \nu, \mathbf{u}, r)$, requires computing the gradient of the log of the unnormalized posterior

$$\log p(\mathbf{Y}|\mathbf{X}, \boldsymbol{\theta}) + \log p(\mathbf{X}|\mathbf{Z}, \mathbf{S}, \nu, \mathbf{u}, r) \quad (7.12)$$

The first term of the gradient can be calculated by

$$\frac{\partial \log p(\mathbf{Y}|\mathbf{X}, \boldsymbol{\theta})}{\partial \mathbf{K}} = -\frac{1}{2} D \mathbf{K}^{-1} + \frac{1}{2} \mathbf{K}^{-1} \mathbf{Y} \mathbf{Y}^T \mathbf{K}^{-1}, \quad (7.13)$$

and

$$\frac{\partial k(\mathbf{x}_n, \mathbf{x}_m)}{\partial \mathbf{x}_n} = -\frac{\alpha}{\ell^2} \exp\left(-\frac{1}{2\ell^2}(\mathbf{x}_n - \mathbf{x}_m)^\top (\mathbf{x}_n - \mathbf{x}_m)\right) (\mathbf{x}_n - \mathbf{x}_m), \quad (7.14)$$

using the chain rule. The second term can be calculated as follows:

$$\frac{\partial \log p(\mathbf{X}|\mathbf{Z}, \mathbf{S}, \nu, \mathbf{u}, r)}{\partial \mathbf{x}_n} = -\nu_{z_n} \mathbf{S}_{z_n}^{-1} (\mathbf{x}_n - \mathbf{u}_{z_n}). \quad (7.15)$$

We also infer kernel parameters $\boldsymbol{\theta} = \{\alpha, \beta, \ell\}$ via HMC, using the gradient of the log unnormalized posterior with respect to the kernel parameters. The complexity of each iteration of HMC is dominated by the $\mathcal{O}(N^3)$ computation of \mathbf{K}^{-1} . This complexity could be improved by making use of an inducing-point approximation such as (Quiñonero-Candela and Rasmussen, 2005; Snelson and Ghahramani, 2006).

In summary, we obtain samples from the posterior $p(\mathbf{X}, \mathbf{Z}|\mathbf{Y}, \boldsymbol{\theta}, \mathbf{S}, \nu, \mathbf{u}, r, \eta)$ by iterating the following steps:

1. For each observation $n = 1, \dots, N$, sample the component assignment z_n by collapsed Gibbs sampling (7.10).
2. Sample latent coordinates \mathbf{X} and kernel parameters $\boldsymbol{\theta}$ using Hamiltonian Monte Carlo.

7.3.1 Posterior Predictive Density

In the GP-LVM, the predictive density of at test point \mathbf{y}_* is usually computed by finding the point \mathbf{x}_* which which is most likely to be mapped to \mathbf{y}_* , then using the density of $p(\mathbf{x}_*)$ and the Jacobian of the warping at that point to approximately compute the density at \mathbf{y}_* . When inference is done by simply optimizing the location of the latent points, this estimation method simply requires solving a single optimization for each \mathbf{y}_* .

For our model, we use approximate integration to estimate $p(\mathbf{y}_*)$. This is done for two reasons: First, multiple latent points (possibly from different clusters) can map to the same observed point, meaning the standard method can underestimate $p(\mathbf{y}_*)$. Second, because we do not optimize the latent coordinates but rather sample them, we would

need to perform optimizations for each $p(\mathbf{y}_*)$ separately for each sample. Our method gives estimates for all $p(\mathbf{y}_*)$ at once, but may not be accurate in very high dimensions.

The posterior density in the observed space given the training data is simply:

$$\begin{aligned} p(\mathbf{y}_* | \mathbf{Y}) &= \iint p(\mathbf{y}_*, \mathbf{x}_*, \mathbf{X} | \mathbf{Y}) d\mathbf{x}_* d\mathbf{X} \\ &= \iint p(\mathbf{y}_* | \mathbf{x}_*, \mathbf{X}, \mathbf{Y}) p(\mathbf{x}_* | \mathbf{X}, \mathbf{Y}) p(\mathbf{X} | \mathbf{Y}) d\mathbf{x}_* d\mathbf{X}. \end{aligned} \quad (7.16)$$

We approximate $p(\mathbf{X} | \mathbf{Y})$ using the samples from the Gibbs and Hamiltonian Monte Carlo samplers. We approximate $p(\mathbf{x}_* | \mathbf{X}, \mathbf{Y})$ by sampling points from the latent mixture and warping them, using the following procedure:

1. Draw latent assignments $z_* \sim \text{Mult}(\frac{N_1}{N+\eta}, \dots, \frac{N_C}{N+\eta}, \frac{\eta}{N+\eta})$
2. Draw precision matrix $\mathbf{R}_* \sim \mathcal{W}(\mathbf{S}_{z_*}^{-1}, \nu_{z_*})$
3. Draw mean $\boldsymbol{\mu}_* \sim \mathcal{N}(\mathbf{u}_{z_*}, (r_{z_*} \mathbf{R}_*)^{-1})$
4. Draw latent coordinates $\mathbf{x}_* \sim \mathcal{N}(\boldsymbol{\mu}_*, \mathbf{R}_*^{-1})$

When a new component $C + 1$ is assigned to z_* , the prior Gaussian-Wishart distribution is used for sampling in steps 2 and 3. The first factor of (7.16) can be calculated by

$$p(\mathbf{y}_* | \mathbf{x}_*, \mathbf{X}, \mathbf{Y}) = \mathcal{N}(\mathbf{k}_*^\top \mathbf{K}^{-1} \mathbf{Y}, k(\mathbf{x}_*, \mathbf{x}_*) - \mathbf{k}_*^\top \mathbf{K}^{-1} \mathbf{k}_*), \quad (7.17)$$

where $\mathbf{k}_* = (k(\mathbf{x}_*, \mathbf{x}_1), \dots, k(\mathbf{x}_*, \mathbf{x}_N))^\top$. Each step of this sampling procedure draws from the exact conditional distribution, so the Monte Carlo estimate of the predictive density $p(\mathbf{y}_* | \mathbf{X}, \mathbf{Y})$ will converge to the true marginal distribution. Since the observations \mathbf{y}_* are conditionally normally distributed, each one adds a smooth contribution to the empirical Monte Carlo estimate of the posterior density, as opposed to a collection of point masses. This procedure was used to generate the plots of posterior density in figures 7.1, 7.6, and 7.8.

7.4 Related Work

The GP-LVM is effective as a nonlinear latent variable model in a wide variety of applications (Lawrence, 2004; Lawrence and Urtasun, 2009; Salzmann et al., 2008). The latent positions \mathbf{X} in the GP-LVM are typically obtained by maximum a posteriori estimation or variational Bayesian inference (Titsias and Lawrence, 2010), placing a single fixed

spherical Gaussian prior on \mathbf{x} . A prior which penalizes a high-dimensional latent space was introduced by Geiger et al. (2009), in which the latent variables and their intrinsic dimensionality are simultaneously optimized. The iWMM can also infer the intrinsic dimensionality of nonlinear manifolds: inferring the Gaussian covariance for each latent cluster allows the variance of irrelevant dimensions to become small. Because each latent cluster has a different set of parameters, the effective dimension of each cluster can vary, allowing manifolds of differing dimension in the observed space. This ability is demonstrated in figure 7.6b.

The iWMM can also be viewed as a generalization of the mixture of probabilistic principle component analyzers (Tipping and Bishop, 1999), or mixture of factor analyzers (Ghahramani and Beal, 2000), where the linear mapping of the mixtures is generalized to a nonlinear mapping by Gaussian processes, and number of components is infinite.

There exist non-probabilistic clustering methods which can find clusters with complex shapes, such as spectral clustering (Ng et al., 2002) and nonlinear manifold clustering (Cao and Haralick, 2006; Elhamifar and Vidal, 2011). Spectral clustering finds clusters by first forming a similarity graph, then finding a low-dimensional latent representation using the graph, and finally, clustering the latent coordinates via k-means. The performance of spectral clustering depends on parameters which are usually set manually, such as the number of clusters, the number of neighbors, and the variance parameter used for constructing the similarity graph. In contrast, the iWMM infers such parameters automatically. One of the main advantages of the iWMM over these methods is that there is no need to construct a similarity graph.

The kernel Gaussian mixture model (Wang et al., 2003) can also find non-Gaussian shaped clusters. This model estimates a GMM in the implicit high-dimensional feature space defined by the kernel mapping of the observed space. However, the kernel GMM uses a fixed nonlinear mapping function, with no guarantee that the latent points will be well-modeled by a GMM. In contrast, the iWMM infers the mapping function such that the latent co-ordinates will be well-modeled by a mixture of Gaussians.

7.5 Experimental Results

7.5.1 Clustering Faces

We first examined our model’s ability to model images without pre-processing. We constructed a dataset consisting of 50 greyscale 32x32 pixel images of two individuals from the UMIST faces dataset (Graham and Allinson, 1998). Both series of images capture a person turning his head to the right.

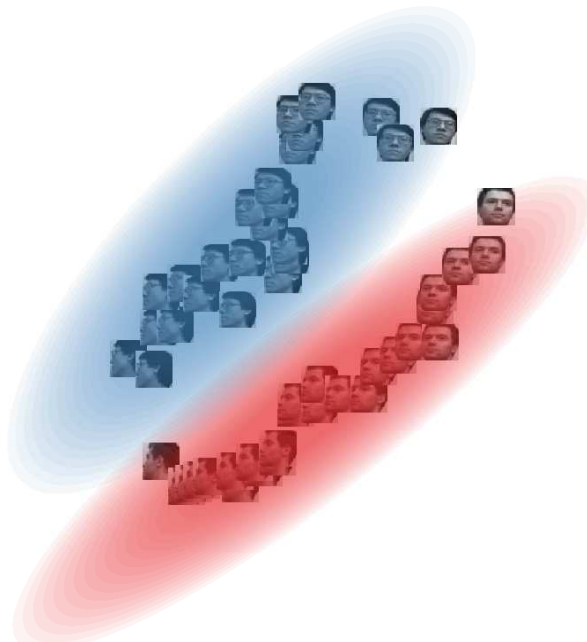


Fig. 7.5 A sample from the 2-dimensional latent space when modeling a series of 32x32 face images. Our model correctly discovers that the data consists of two separate manifolds, both approximately one-dimensional, which share the same head-turning structure.

Figure 7.5 shows a sample from the posterior over the latent coordinates, as well as the density model. The model has recovered three relevant, interpretable features of the dataset. First, that there are two distinct faces. Second, that each set of images lies approximately along a smooth one-dimensional manifold. Third, that the two manifolds share roughly the same structure: the front-facing images of both individuals lie close to one another, as do the side-facing images.

7.5.2 Synthetic Datasets

Next, we demonstrate the proposed model on the four synthetic datasets shown in Figure 7.6. None of these four datasets can be appropriately clustered by Gaussian

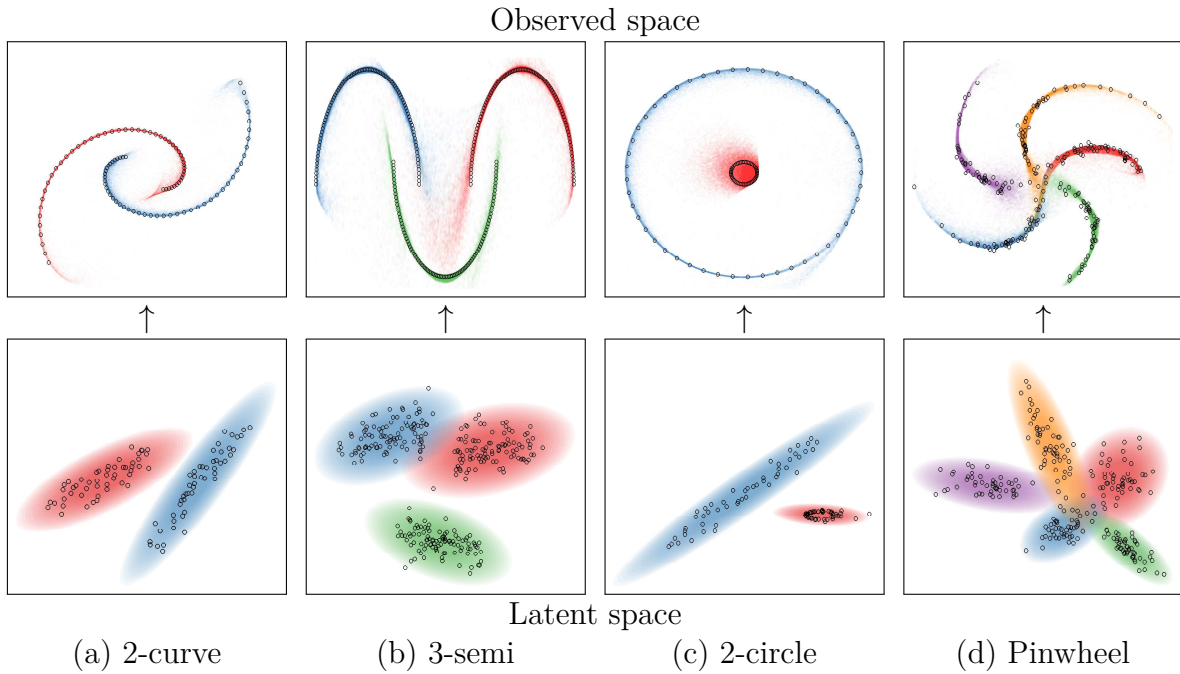


Fig. 7.6 Top row: The observed, unlabeled data points, and the clusters inferred by the iWMM. Bottom row: Latent coordinates and Gaussian components, shown for a single sample from the posterior. Each point in the latent space corresponds to a point in the observed space. This figure is best viewed in color.

mixture models (GMM). For example, consider the 2-curve data shown in Figure 7.6 (a), where 100 data points lie in one of two curved lines in a two-dimensional observed space. A GMM with two components cannot separate the two curved lines, while a GMM with many components could separate the two lines only by breaking each line into many clusters. In contrast, with the iWMM, the two non-Gaussian-shaped clusters in the observed space were represented by two Gaussian-shaped clusters in the latent space, as shown at the bottom row of Figure 7.6 (a). The iWMM separated the two curved lines by nonlinearly warping two Gaussians from the latent space to the observed space.

Figure 7.6 (c) shows an interesting manifold learning challenge: a dataset consisting of two circles. The outer circle is modeled in the latent space by a Gaussian with effectively one degree of freedom. This linear topology fits the outer circle in the observed

space by bending the two ends until they overlap. In contrast, the sampler fails to discover the 1D topology of the inner circle, modeling it with a 2D manifold instead. This example demonstrates that each cluster in the iWMM manifold can have a different effective dimension.

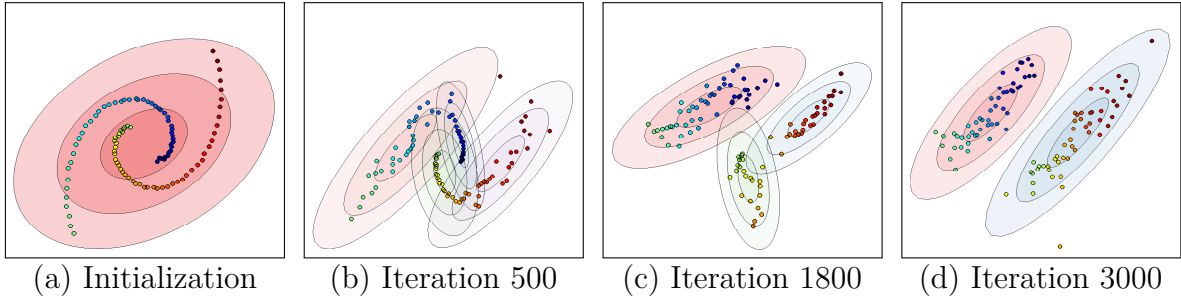


Fig. 7.7 The inferred infinite GMMs over iterations in the two-dimensional latent space with the iWMM using the 2-curve data. Labels indicate the number of iterations of the sampler, and the color of each point represents its ordering in the observed coordinates.

7.5.3 Mixing

An interesting side-effect of learning the number of latent clusters is that this added flexibility can help the sampler escape local minima, helping the sampler to mix properly. Figure 7.7 shows the samples of the latent coordinates and clusters of the iWMM over time, when modeling the 2-curve data. 7.7(a) shows the latent coordinates initialized at the observed coordinates, starting with one latent component. At the 500th iteration 7.7(b), each curved line is modeled by two components. At the 1800th iteration 7.7(c), the left curved line is modeled by a single component. At the 3000th iteration 7.7(d), the right curved line is also modeled by a single component, and the dataset is appropriately clustered. This configuration was relatively stable, and a similar state was found at the 5000th iteration.

7.5.4 Density Estimation

Figure 7.8(a) shows the posterior density in the observed space inferred by the iWMM on the 2-curve data, computed using 1000 samples from the Markov chain. The two separate manifolds of high density implied by the two curved lines was recovered by the iWMM. Note also that the density along the manifold varies with the density of data shown in Figure 7.6(a).

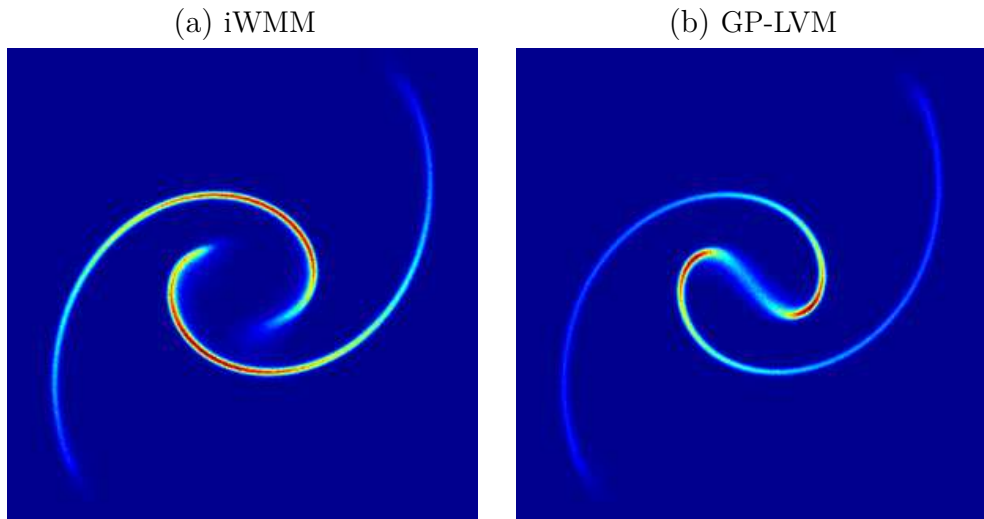


Fig. 7.8 *Left*: The posterior density in the observed space with the 2-curve data inferred by the iWMM. *Right*: The posterior inferred by the iWMM with one component, a model equivalent to the GP-LVM.

This result can be compared to a special case of our model, which uses only a single Gaussian to model the latent coordinates instead of an infinite GMM. Figure 7.8(b) shows that the single-cluster variant of the iWMM posterior is forced to place significant density connecting the two clusters, since it has to reproduce the observed density manifold by warping a single Gaussian.

7.5.5 Visualization

Next, we briefly investigate the potential of the iWMM for low-dimensional visualization of data. Figure 7.9 (a) shows the latent coordinates obtained by averaging over 1000

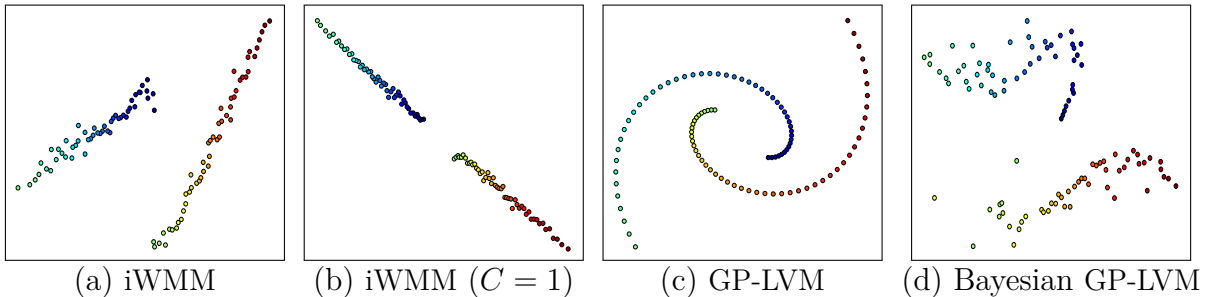


Fig. 7.9 Latent coordinates of the 2-curve data, estimated by four different methods.

samples from the posterior of the iWMM. Because rotating the latent coordinates does

not change their probability, averaging may not be an adequate way to summarize the posterior. However, we show this result in order to show the characteristics of latent coordinates obtained by the iWMM. The estimated latent coordinates are clearly separated, and they form two straight lines. This result indicates that in some cases, the iWMM can recover the topology of the data before it has been warped into a manifold. For comparison, Figure 7.9 (b) shows the latent coordinates estimated by the iWMM when forced to use a single cluster: the latent coordinates lie in two sections of a single straight line. Figure 7.9 (c) and (d) show the latent coordinates estimated by the GP-LVM when optimizing or integrating out the latent coordinates, respectively. Recall that the iWMM ($C = 1$) is a more flexible model than the GP-LVM, since the GP-LVM enforces a spherical covariance in the latent space. These methods did not unfold the two curved lines, since the effective dimension of their latent representation is fixed beforehand. In contrast, the iWMM effectively formed a low-dimensional representation in the latent space.

Regardless of the dimension of the latent space, the iWMM will tend to model each cluster with as low-dimensional a Gaussian as possible. This is because, if the data in a cluster can be made to lie in a low-dimensional plane, a narrowly-shaped Gaussian will assign the latent coordinates much higher likelihood than a spherical Gaussian.

7.5.6 Clustering Performance

We more formally evaluated the density estimation and clustering performance of the proposed model using four real datasets: iris, glass, wine and vowel, obtained from LIBSVM multi-class datasets (Chang and Lin, 2011), in addition to the four synthetic datasets shown above: 2-curve, 3-semi, 2-circle and Pinwheel (Adams and Ghahramani, 2009). The statistics of these datasets are summarized in Table 7.1. In each experiment,

Table 7.1 Statistics of the datasets used for evaluation.

	2-curve	3-semi	2-circle	Pinwheel	Iris	Glass	Wine	Vowel
samples: N	100	300	100	250	150	214	178	528
dimension: D	2	2	2	2	4	9	13	10
num. clusters: C	2	3	2	5	3	7	3	11

we show the results of ten-fold cross-validation. Results in bold are not significantly different from the best performing method in each column according to a paired t-test.

Table 7.2 compares the clustering performance of the iWMM with the iGMM, quan-

Table 7.2 Average Rand index for evaluating clustering performance.

	2-curve	3-semi	2-circle	Pinwheel	Iris	Glass	Wine	Vowel
iGMM	0.52	0.79	0.83	0.81	0.78	0.60	0.72	0.76
iWMM($Q=2$)	0.86	0.99	0.89	0.94	0.81	0.65	0.65	0.50
iWMM($Q=D$)	0.86	0.99	0.89	0.94	0.77	0.62	0.77	0.76

tified by the Rand index (Rand, 1971), which measures the correspondence between inferred clusters and true clusters. The iGMM is another probabilistic generative model commonly used for clustering, which can be seen as a special case of the iWMM in which the Gaussian clusters are not warped. These experiments demonstrate the extent to which nonparametric cluster shapes allow a mixture model to recover more meaningful clusters.

Table 7.3 lists average test log likelihood, comparing the proposed models with kernel density estimation (KDE), and the infinite Gaussian mixture model (iGMM). In KDE, the kernel width is estimated by maximizing the leave-one-out log densities. Since the manifold on which the observed data lies can be at most D -dimensional, we set the latent dimension Q equal to the observed dimension D in iWMMs. We also include the $Q = 2$ case in an attempt to characterize how much modeling power is lost by forcing the latent representation to be visualizable. The proposed models achieved high test likelihoods compared with the KDE and the iGMM.

Table 7.3 Average test log-likelihood for evaluating density estimation performance.

	2-curve	3-semi	2-circle	Pinwheel	Iris	Glass	Wine	Vowel
KDE	-2.47	-0.38	-1.92	-1.47	-1.87	1.26	-2.73	6.06
iGMM	-3.28	-2.26	-2.21	-2.12	-1.91	3.00	-1.87	-0.67
iWMM($Q=2$)	-0.90	-0.18	-1.02	-0.79	-1.88	5.76	-1.96	5.91
iWMM($Q=D$)	-0.90	-0.18	-1.02	-0.79	-1.71	5.70	-3.14	-0.35

Source Code

Code to reproduce all the above experiments is available at github.com/duvenaud/warped-mixtures.

7.6 Future Work

The Dirichlet process mixture of Gaussians in the latent space of our model could easily be replaced by a more sophisticated density model, such as a hierarchical Dirichlet process (Teh et al., 2006), or a Dirichlet diffusion tree (Neal, 2003). Another straightforward extension of our model would be making inference more scalable by using sparse Gaussian processes (Quiñonero-Candela and Rasmussen, 2005; Snelson and Ghahramani, 2006) or more advanced Hamiltonian Monte Carlo methods (Zhang and Sutton, 2011). An interesting but more complex extension of the iWMM would be a semi-supervised version of the model. The iWMM could allow label propagation along regions of high density in the latent space, even if those regions were stretched along low-dimensional manifolds in the observed space. Another natural extension would be to allow a separate warping for each cluster, which would also improve inference speed.

7.7 Conclusion

In this chapter, we introduced a simple generative model of non-Gaussian density manifolds which can infer nonlinearly separable clusters, low-dimensional representations of varying dimension per cluster, and density estimates which smoothly follow data contours. We then introduced an efficient sampler for this model which integrates out both the cluster parameters and the warping function exactly. We further demonstrated that allowing non-parametric cluster shapes improves clustering performance over the Dirichlet process Mixture of Gaussians.

Many methods have been proposed which can perform some combination of clustering, manifold learning, density estimation and visualization. We demonstrated that a simple but flexible probabilistic generative model can perform well at all these tasks.

Appendix A

Gaussian Conditionals

A standard result shows how to condition on knowing a subset of the dimensions \mathbf{y}_B of a vector \mathbf{y} having a multivariate Gaussian distribution. If

$$\mathbf{y} = \begin{bmatrix} \mathbf{y}_A \\ \mathbf{y}_B \end{bmatrix} \sim \mathcal{N}\left(\begin{bmatrix} \boldsymbol{\mu}_A \\ \boldsymbol{\mu}_B \end{bmatrix}, \begin{bmatrix} \boldsymbol{\Sigma}_{AA} & \boldsymbol{\Sigma}_{AB} \\ \boldsymbol{\Sigma}_{BA} & \boldsymbol{\Sigma}_{BB} \end{bmatrix}\right) \quad (\text{A.1})$$

then

$$\mathbf{y}_A | \mathbf{y}_B \sim \mathcal{N}(\boldsymbol{\mu}_A + \boldsymbol{\Sigma}_{AB} \boldsymbol{\Sigma}_{BB}^{-1} (\mathbf{x}_B - \boldsymbol{\mu}_B), \boldsymbol{\Sigma}_{AA} - \boldsymbol{\Sigma}_{AB} \boldsymbol{\Sigma}_{BB}^{-1} \boldsymbol{\Sigma}_{BA}). \quad (\text{A.2})$$

This result can be used in the context of Gaussian process regression, where $\mathbf{y}_B = [f(\mathbf{x}_1), f(\mathbf{x}_2), \dots, f(\mathbf{x}_N)]$ represents a set of function values observed at some subset of locations $[\mathbf{x}_1, \mathbf{x}_2, \dots, \mathbf{x}_N]$, while $\mathbf{y}_A = [f(\mathbf{x}_1^*), f(\mathbf{x}_2^*), \dots, f(\mathbf{x}_N^*)]$ represents test points whose predictive distribution we'd like to know. In this case, the necessary covariance matrices are given by:

$$\boldsymbol{\Sigma}_{AA} = k(\mathbf{X}, \mathbf{X}) \quad (\text{A.3})$$

$$\boldsymbol{\Sigma}_{AB} = k(\mathbf{X}, \mathbf{X}^*) \quad (\text{A.4})$$

$$\boldsymbol{\Sigma}_{BA} = k(\mathbf{X}^*, \mathbf{X}) \quad (\text{A.5})$$

$$\boldsymbol{\Sigma}_{BB} = k(\mathbf{X}^*, \mathbf{X}^*) \quad (\text{A.6})$$

and similarly for the mean vectors.

Appendix B

Kernel Definitions

Here we give the formulas for all one-dimensional base kernels mentioned in the thesis. Each of these formulas is multiplied by a scale factor σ_f^2 , which we omit for clarity.

$$C(x, x') = 1 \quad (\text{B.1})$$

$$\text{WN}(x, x') = \delta(x - x') \quad (\text{B.2})$$

$$\text{Lin}(x, x') = (x - c)(x' - c) \quad (\text{B.3})$$

$$\text{SE}(x, x') = \exp\left(-\frac{(x - x')^2}{2\ell^2}\right) \quad (\text{B.4})$$

$$\text{RQ}(x, x') = \left(1 + \frac{(x - x')^2}{2\alpha\ell^2}\right)^{-\alpha} \quad (\text{B.5})$$

$$\text{Per}(x, x') = \sigma_f^2 \frac{\exp\left(\frac{1}{\ell^2} \cos 2\pi \frac{(x-x')}{p}\right) - I_0\left(\frac{1}{\ell^2}\right)}{\exp\left(\frac{1}{\ell^2}\right) - I_0\left(\frac{1}{\ell^2}\right)} \quad (\text{B.6})$$

$$\cos(x, x') = \cos\left(\frac{2\pi(x - x')}{p}\right) \quad (\text{B.7})$$

$$\text{CP}(k_1, k_2)(x, x') = \sigma(x)k_1(x, x')\sigma(x') + (1 - \sigma(x))k_2(x, x')(1 - \sigma(x')) \quad (\text{B.8})$$

$$\boldsymbol{\sigma} = \sigma(x)\sigma(x') \quad (\text{B.9})$$

$$\bar{\boldsymbol{\sigma}} = (1 - \sigma(x))(1 - \sigma(x')) \quad (\text{B.10})$$

where $\delta_{x,x'}$ is the Kronecker delta function, I_0 is the modified Bessel function of the first kind of order zero, and other symbols are kernel parameters. Equations (B.3), (B.4) and (B.6) are plotted in table 2.1, and equations (B.2), (B.5) and (B.7) are plotted in table 3.1. Draws from GP priors with changepoint kernels are shown in figure 2.7.

The Generalized Periodic Kernel

Lloyd (2013a) showed that the standard periodic kernel due to MacKay (1998) can be decomposed into a periodic and a constant component. He derived the equivalent periodic kernel without any constant component, shown in equation (B.6). He further showed that its limit as the lengthscale grows is the cosine kernel:

$$\lim_{\ell \rightarrow \infty} \text{Per}(x, x') = \cos\left(\frac{2\pi(x - x')}{p}\right). \quad (\text{B.11})$$

Separating out the constant component allows us to express negative prior covariance, as well as increasing the interpretability of the resulting models.

Appendix C

Search Operators

The model construction phase of ABCD starts with the noise kernel, WN. New kernel expressions are generated by applying search operators to the current kernel, which replace some part of the existing kernel expression with a new kernel expression.

The search used in the multidimensional regression experiments in sections 3.8.4 and 6.5 used only the following search operators:

$$\mathcal{S} \rightarrow \mathcal{S} + \mathcal{B} \tag{C.1}$$

$$\mathcal{S} \rightarrow \mathcal{S} \times \mathcal{B} \tag{C.2}$$

$$\mathcal{B} \rightarrow \mathcal{B}' \tag{C.3}$$

where \mathcal{S} represents any kernel subexpression and \mathcal{B} is any base kernel within a kernel expression. These search operators represent addition, multiplication and replacement. When the multiplication operator is applied to a subexpression which includes a sum of subexpressions, parentheses () are introduced. For instance, if rule (C.2) is applied to the subexpression $k_1 + k_2$, the resulting expression is $(k_1 + k_2) \times \mathcal{B}$.

Afterwards, we added several more search operators in order to speed up the search. These new operators do not change the set of possible models.

To accommodate changepoints and changewindows, we introduced the following additional operators to our search:

$$\mathcal{S} \rightarrow \text{CP}(\mathcal{S}, \mathcal{S}) \tag{C.4}$$

$$\mathcal{S} \rightarrow \text{CW}(\mathcal{S}, \mathcal{S}) \tag{C.5}$$

$$\mathcal{S} \rightarrow \text{CW}(\mathcal{S}, \mathcal{C}) \tag{C.6}$$

$$\mathcal{S} \rightarrow \text{CW}(\mathcal{C}, \mathcal{S}) \tag{C.7}$$

where C is the constant kernel. The last two operators result in a kernel only applying outside, or within, a certain region.

To allow the search to simplify existing expressions, we introduced the following operators:

$$\mathcal{S} \rightarrow \mathcal{B} \quad (\text{C.8})$$

$$\mathcal{S} + \mathcal{S}' \rightarrow \mathcal{S} \quad (\text{C.9})$$

$$\mathcal{S} \times \mathcal{S}' \rightarrow \mathcal{S} \quad (\text{C.10})$$

where \mathcal{S}' represents any other kernel expression. We also introduced the operator

$$\mathcal{S} \rightarrow \mathcal{S} \times (\mathcal{B} + \text{C}) \quad (\text{C.11})$$

Which allows a new base kernel to be added along with the constant kernel, for cases when multiplying by a base kernel by itself would restrict the model too much.

Appendix D

Example Report

The following pages of this appendix contain an entire automatically-generated report, run on a dataset measuring annual solar irradiation data from 1610 to 2011. This dataset was previously analyzed by [Lean et al. \(1995\)](#).

Other example reports can be found at mlg.eng.cam.ac.uk/Lloyd/abcdoutput/

1 Executive summary

The raw data and full model posterior with extrapolations are shown in figure 1.

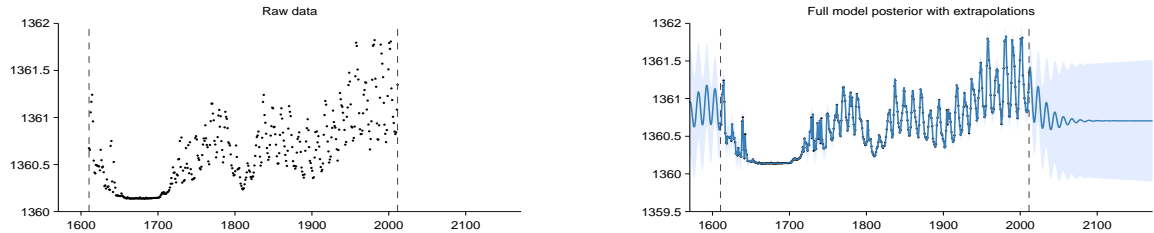


Figure 1: Raw data (left) and model posterior with extrapolation (right)

The structure search algorithm has identified nine additive components in the data. The first 4 additive components explain 92.3% of the variation in the data as shown by the coefficient of determination (R^2) values in table 1. The first 8 additive components explain 99.2% of the variation in the data. After the first 5 components the cross validated mean absolute error (MAE) does not decrease by more than 0.1%. This suggests that subsequent terms are modelling very short term trends, uncorrelated noise or are artefacts of the model or search procedure. Short summaries of the additive components are as follows:

- A constant.
- A constant. This function applies from 1644 until 1713.
- A smooth function. This function applies until 1644 and from 1719 onwards.
- An approximately periodic function with a period of 10.8 years. This function applies until 1644 and from 1719 onwards.
- A rapidly varying smooth function. This function applies until 1644 and from 1719 onwards.
- Uncorrelated noise.
- A rapidly varying smooth function with marginal standard deviation increasing linearly away from 1843. This function applies from 1751 onwards.
- A rapidly varying smooth function. This function applies until 1644 and from 1719 until 1751.
- A constant. This function applies from 1713 until 1719.

#	R^2 (%)	ΔR^2 (%)	Residual R^2 (%)	Cross validated MAE	Reduction in MAE (%)
-	-	-	-	1360.65	-
1	0.0	0.0	0.0	0.33	100.0
2	35.3	35.3	35.3	0.23	29.4
3	72.5	37.2	57.5	0.18	20.7
4	92.3	19.9	72.2	0.15	16.4
5	97.8	5.5	71.4	0.15	0.4
6	97.8	0.0	0.2	0.15	0.0
7	98.4	0.5	24.8	0.15	-0.0
8	99.2	0.8	50.7	0.15	-0.0
9	100.0	0.8	100.0	0.15	-0.0

Table 1: Summary statistics for cumulative additive fits to the data. The residual coefficient of determination (R^2) values are computed using the residuals from the previous fit as the target values; this measures how much of the residual variance is explained by each new component. The mean absolute error (MAE) is calculated using 10 fold cross validation with a contiguous block design; this measures the ability of the model to interpolate and extrapolate over moderate distances. The model is fit using the full data so the MAE values cannot be used reliably as an estimate of out-of-sample predictive performance.

2 Detailed discussion of additive components

2.1 Component 1 : A constant

This component is constant.

This component explains 0.0% of the total variance. The addition of this component reduces the cross validated MAE by 100.0% from 1360.6 to 0.3.

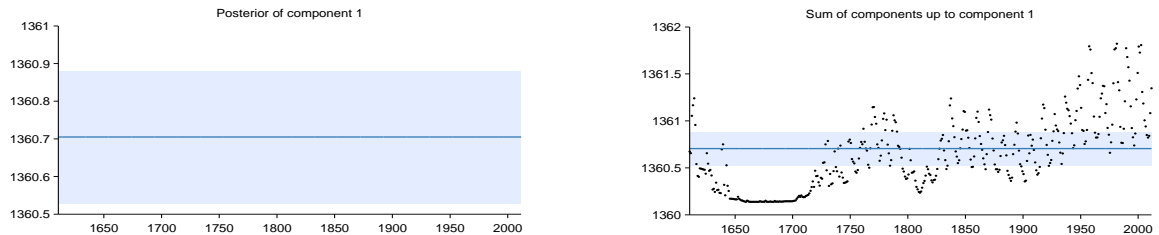


Figure 2: Posterior of component 1 (left) and the posterior of the cumulative sum of components with data (right)

2.2 Component 2 : A constant. This function applies from 1644 until 1713

This component is constant. This component applies from 1644 until 1713.

This component explains 35.3% of the residual variance; this increases the total variance explained from 0.0% to 35.3%. The addition of this component reduces the cross validated MAE by 29.42% from 0.33 to 0.23.

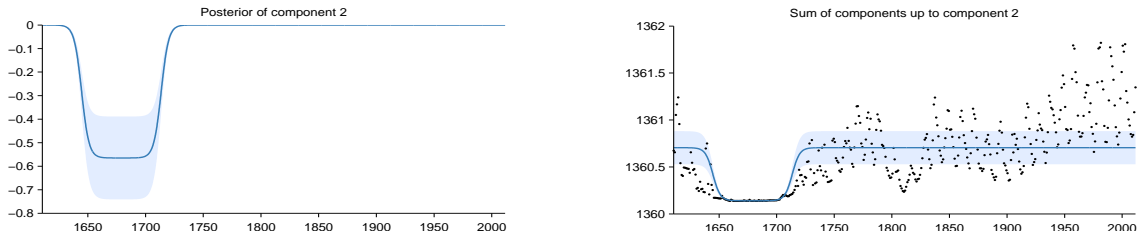


Figure 3: Posterior of component 2 (left) and the posterior of the cumulative sum of components with data (right)

2.3 Component 3 : A smooth function. This function applies until 1644 and from 1719 onwards

This component is a smooth function with a typical lengthscale of 21.9 years. This component applies until 1644 and from 1719 onwards.

This component explains 57.5% of the residual variance; this increases the total variance explained from 35.3% to 72.5%. The addition of this component reduces the cross validated MAE by 20.66% from 0.23 to 0.18.

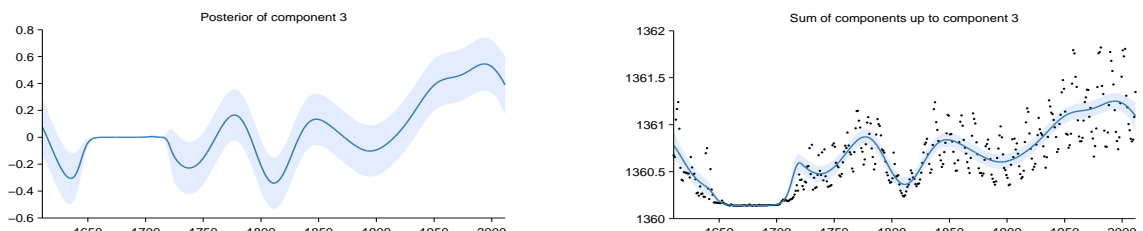


Figure 4: Posterior of component 3 (left) and the posterior of the cumulative sum of components with data (right)

2.4 Component 4 : An approximately periodic function with a period of 10.8 years. This function applies until 1644 and from 1719 onwards

This component is approximately periodic with a period of 10.8 years. Across periods the shape of the function varies smoothly with a typical lengthscale of 33.2 years. The shape of the function within each period has a typical lengthscale of 12.6 years. This component applies until 1644 and from 1719 onwards.

This component explains 72.2% of the residual variance; this increases the total variance explained from 72.5% to 92.3%. The addition of this component reduces the cross validated MAE by 16.42% from 0.18 to 0.15.

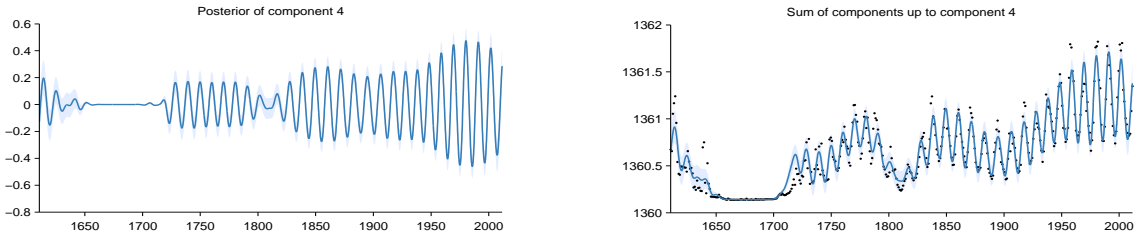


Figure 5: Posterior of component 4 (left) and the posterior of the cumulative sum of components with data (right)

2.5 Component 5 : A rapidly varying smooth function. This function applies until 1644 and from 1719 onwards

This function is a rapidly varying but smooth function with a typical lengthscale of 1.2 years. This component applies until 1644 and from 1719 onwards.

This component explains 71.4% of the residual variance; this increases the total variance explained from 92.3% to 97.8%. The addition of this component reduces the cross validated MAE by 0.41% from 0.15 to 0.15.

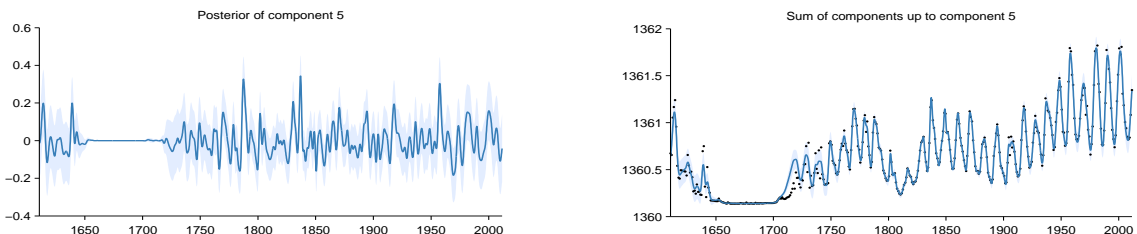


Figure 6: Posterior of component 5 (left) and the posterior of the cumulative sum of components with data (right)

2.6 Component 6 : Uncorrelated noise

This component models uncorrelated noise.

This component explains 0.2% of the residual variance; this increases the total variance explained from 97.8% to 97.8%. The addition of this component reduces the cross validated MAE by 0.00% from 0.15 to 0.15. This component explains residual variance but does not improve MAE which suggests that this component describes very short term patterns, uncorrelated noise or is an artefact of the model or search procedure.

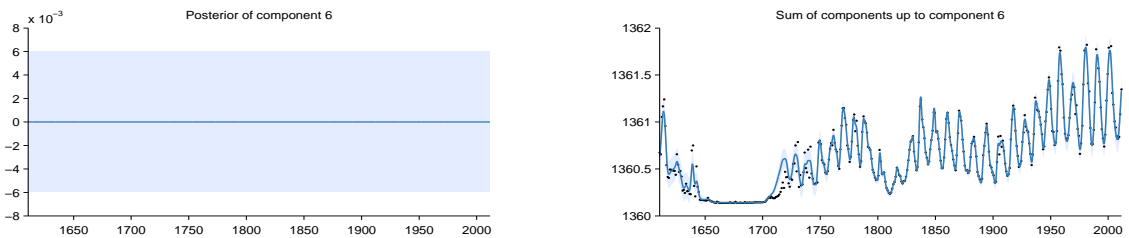


Figure 7: Posterior of component 6 (left) and the posterior of the cumulative sum of components with data (right)

2.7 Component 7 : A rapidly varying smooth function with marginal standard deviation increasing linearly away from 1843. This function applies from 1751 onwards

This function is a rapidly varying but smooth function with a typical lengthscale of 3.1 months. The marginal standard deviation of the function increases linearly away from 1843. This component applies from 1751 onwards.

This component explains 24.8% of the residual variance; this increases the total variance explained from 97.8% to 98.4%. The addition of this component increases the cross validated MAE by 0.00% from 0.15 to 0.15. This component explains residual variance but does not improve MAE which suggests that this component describes very short term patterns, uncorrelated noise or is an artefact of the model or search procedure.

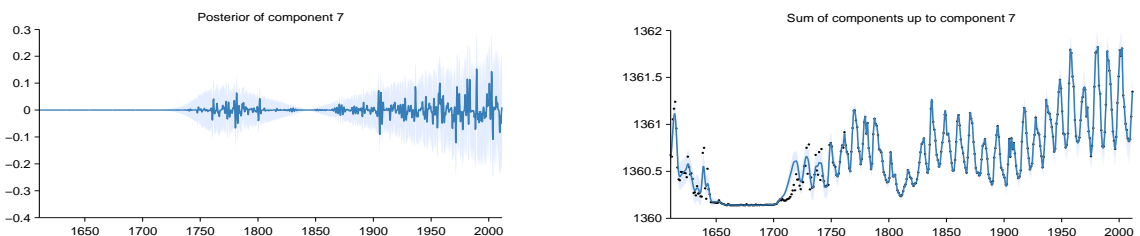


Figure 8: Posterior of component 7 (left) and the posterior of the cumulative sum of components with data (right)

2.8 Component 8 : A rapidly varying smooth function. This function applies until 1644 and from 1719 until 1751

This function is a rapidly varying but smooth function with a typical lengthscale of 3.1 months. This component applies until 1644 and from 1719 until 1751.

This component explains 50.7% of the residual variance; this increases the total variance explained from 98.4% to 99.2%. The addition of this component increases the cross validated MAE by 0.00% from 0.15 to 0.15. This component explains residual variance but does not improve MAE which suggests that this component describes very short term patterns, uncorrelated noise or is an artefact of the model or search procedure.

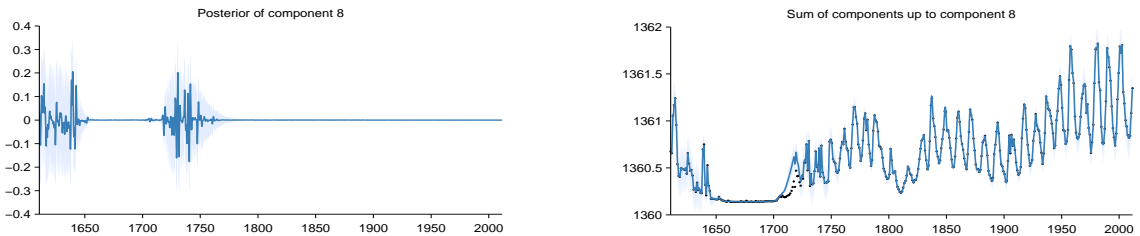


Figure 9: Posterior of component 8 (left) and the posterior of the cumulative sum of components with data (right)

2.9 Component 9 : A constant. This function applies from 1713 until 1719

This component is constant. This component applies from 1713 until 1719.

This component explains 100.0% of the residual variance; this increases the total variance explained from 99.2% to 100.0%. The addition of this component increases the cross validated MAE by 0.01% from 0.15 to 0.15. This component explains residual variance but does not improve MAE which suggests that this component describes very short term patterns, uncorrelated noise or is an artefact of the model or search procedure.

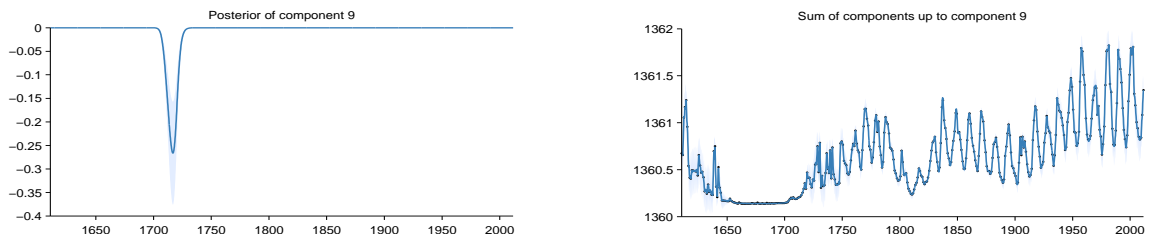


Figure 10: Posterior of component 9 (left) and the posterior of the cumulative sum of components with data (right)

3 Extrapolation

Summaries of the posterior distribution of the full model are shown in figure 11. The plot on the left displays the mean of the posterior together with pointwise variance. The plot on the right displays three random samples from the posterior.

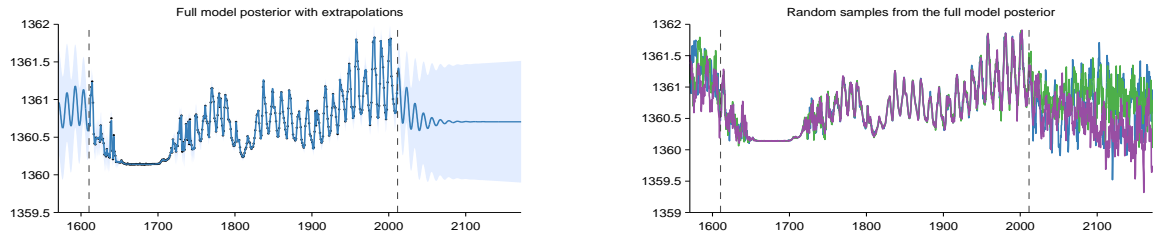


Figure 11: Full model posterior. Mean and pointwise variance (left) and three random samples (right)

References

R.P. Adams and Z. Ghahramani. Archipelago: nonparametric Bayesian semi-supervised learning. In *Proceedings of the 26th Annual International Conference on Machine Learning*. ACM, 2009. (page 106)

Ryan P Adams, Hanna M Wallach, and Zoubin Ghahramani. Learning the structure of deep sparse graphical models. In *International Conference on Artificial Intelligence and Statistics*, pages 1–8, 2010. (page 74)

F. Bach. Exploring large feature spaces with hierarchical multiple kernel learning. In *Advances in Neural Information Processing Systems*, pages 105–112. 2009a. (page 39)

Francis Bach. High-dimensional non-linear variable selection through hierarchical kernel learning. *CoRR*, abs/0909.0844, 2009b. (pages 84, 87, and 89)

Francis R Bach, Gert RG Lanckriet, and Michael I Jordan. Multiple kernel learning, conic duality, and the SMO algorithm. In *Proceedings of the twenty-first international conference on Machine learning*, page 6. ACM, 2004. (pages 32, 40, and 41)

K. Bache and M. Lichman. UCI machine learning repository, 2013. URL <http://archive.ics.uci.edu/ml>. (page 87)

Pierre Baldi and Peter J Sadowski. Understanding dropout. In *Advances in Neural Information Processing Systems*, pages 2814–2822, 2013. (page 82)

A Barbu, A Bridge, Z Burchill, D Coroian, S Dickinson, S Fidler, A Michaux, S Mussman, S Narayanaswamy, D Salvi, L Schmidt, J Shangguan, JM Siskind, J Waggoner, S Wang, J Wei, Y Yin, and Z Zhang. Video in sentences out. In *Conference on Uncertainty in Artificial Intelligence*, 2012. (page 53)

Richard Bellman. Dynamic programming and lagrange multipliers. *Proceedings of the National Academy of Sciences of the United States of America*, 42(10):767, 1956. (page 12)

Yoshua Bengio, Patrice Simard, and Paolo Frasconi. Learning long-term dependencies with gradient descent is difficult. *Neural Networks, IEEE Transactions on*, 5(2):157–166, 1994. (page 74)

- Yoshua Bengio, Olivier Delalleau, and Nicolas Le Roux. The curse of highly variable functions for local kernel machines. *Advances in neural information processing systems*, 18:107–114, 2006. ISSN 1049-5258. (pages 71 and 81)
- W. Bing, Z. Wen-qiong, C. Ling, and L. Jia-hong. A GP-based kernel construction and optimization method for RVM. In *International Conference on Computer and Automation Engineering (ICCAE)*, volume 4, pages 419–423, 2010. (page 40)
- Salomon Bochner. *Lectures on Fourier integrals*, volume 42. Princeton University Press, 1959. (pages 20 and 40)
- George EP Box, Gwilym M Jenkins, and Gregory C Reinsel. *Time series analysis: forecasting and control*. Wiley. com, 2013. (page 42)
- G.E.P. Box, G.M. Jenkins, and G.C. Reinsel. *Time series analysis: forecasting and control*. 1976. (page 36)
- W. Cao and R. Haralick. Nonlinear manifold clustering by dimensionality. In *International Conference on Pattern Recognition (ICPR)*, volume 1, pages 920–924. IEEE, 2006. (page 101)
- Chih-Chung Chang and Chih-Jen Lin. Libsvm: A library for support vector machines. *ACM Trans. Intell. Syst. Technol.*, 2(3):27:1–27:27, 2011. (page 106)
- Youngmin Cho. *Kernel methods for deep learning*. PhD thesis, University of California, San Diego, 2012. (page 71)
- M. Christoudias, R. Urtasun, and T. Darrell. Bayesian localized multiple kernel learning. *Technical report, EECS Department, University of California, Berkeley*, 2009. (pages 39 and 84)
- Wikimedia Commons. Stereographic projection of a Sudanese Möbius band, 2005. URL <http://commons.wikimedia.org/wiki/File:MobiusSnail2B.png>. (page 27)
- Corinna Cortes and Vladimir Vapnik. Support-vector networks. *Machine learning*, 20(3):273–297, 1995. (page 17)
- Andreas Damianou and Neil Lawrence. Deep Gaussian processes. In *Artificial Intelligence and Statistics*, pages 207–215, 2013. (pages 56 and 73)
- Eyal Dechter, Jon Malmaud, Ryan P Adams, and Joshua B Tenenbaum. Bootstrap learning via modular concept discovery. In *Proceedings of the Twenty-Third international joint conference on Artificial Intelligence*, pages 1302–1309. AAAI Press, 2013. (page 41)
- L. Diosan, A. Rogozan, and J.P. Pecuchet. Evolving kernel functions for SVMs by genetic programming. In *Machine Learning and Applications, 2007*, pages 19–24. IEEE, 2007. (page 40)

- Nicolas Durrande, David Ginsbourger, and Olivier Roustant. Additive kernels for gaussian process modeling. *arXiv preprint arXiv:1103.4023*, 2011. (page 84)
- David Duvenaud, Hannes Nickisch, and Carl Edward Rasmussen. Additive Gaussian processes. In *Advances in Neural Information Processing Systems 24*, pages 226–234, Granada, Spain, 2011. (page 77)
- David Duvenaud, James Robert Lloyd, Roger Grosse, Joshua B. Tenenbaum, and Zoubin Ghahramani. Structure discovery in nonparametric regression through compositional kernel search. In *Proceedings of the 30th International Conference on Machine Learning*, June 2013. (page 29)
- David Duvenaud, Oren Rippel, Ryan P. Adams, and Zoubin Ghahramani. Avoiding pathologies in very deep networks. Reykjavik, Iceland, April 2014. URL <http://arxiv.org/pdf/1402.5836.pdf>. (page 57)
- D. Eaton and K. Murphy. Bayesian structure learning using dynamic programming and MCMC. 2007. URL <http://www.cs.ubc.ca/~murphyk/Papers/eaton-uai07.pdf>. (page 30)
- Ehsan Elhamifar and René Vidal. Sparse manifold clustering and embedding. In *Advances in Neural Information Processing Systems*, pages 55–63, 2011. (page 101)
- E.B. Fox and D.B. Dunson. Multiresolution Gaussian Processes. In *Neural Information Processing Systems 25*. MIT Press, 2013. (page 41)
- N. Friedman and D. Koller. Being Bayesian about Network Structure: A Bayesian Approach to Structure Discovery in Bayesian Networks. *Machine Learning*, 50:95–126, 2003. (page 30)
- M. Ganesalingam and W. T. Gowers. A fully automatic problem solver with human-style output. *CoRR*, abs/1309.4501, 2013. (page 53)
- Roman Garnett, Michael A Osborne, Steven Reece, Alex Rogers, and Stephen J Roberts. Sequential bayesian prediction in the presence of changepoints and faults. *The Computer Journal*, 53(9):1430–1446, 2010. (pages 32 and 41)
- A. Geiger, R. Urtasun, and T. Darrell. Rank priors for continuous non-linear dimensionality reduction. In *IEEE Conference on Computer Vision and Pattern Recognition (CVPR)*, pages 880–887. IEEE, 2009. (page 101)
- Andrew Gelman. Why waste time philosophizing?, 2013. URL <http://andrewgelman.com/2013/02/11/why-waste-time-philosophizing/>. (page 30)
- Andrew Gelman and Cosma Rohilla Shalizi. Philosophy and the practice of bayesian statistics. *British Journal of Mathematical and Statistical Psychology*, 2012. (page 30)

- Robert Gens and Pedro Domingos. Learning the structure of sum-product networks. In *International Conference on Machine learning*, 2013. (page 75)
- Z. Ghahramani and M.J. Beal. Variational inference for Bayesian mixtures of factor analysers. *Advances in Neural Information Processing Systems*, 12:449–455, 2000. (page 101)
- Elad Gilboa, Yunus Saatçi, and J Cunningham. Scaling multidimensional inference for structured Gaussian processes. In *Proceedings of the 30th International Conference on Machine Learning*, 2013. (page 83)
- D. Ginsbourger, O. Roustant, and N. Durrande. Invariances of random fields paths, with applications in Gaussian process regression. Technical Report arXiv:1308.1359 [math.ST], August 2013. (pages 22 and 23)
- David Ginsbourger, Xavier Bay, Olivier Roustant, and Laurent Carraro. Argumentwise invariant kernels for the approximation of invariant functions. In *Annales de la Faculté de Sciences de Toulouse*, number 3, 2012. (page 22)
- Noah D Goodman, Tomer D Ullman, and Joshua B Tenenbaum. Learning a theory of causality. *Psychological review*, 118(1):110, 2011. (page 12)
- Daniel B Graham and Nigel M Allinson. Characterizing virtual eigensignatures for general purpose face recognition. *Face Recognition: From Theory to Applications*, 163:446–456, 1998. (page 102)
- Roger B. Grosse, Ruslan Salakhutdinov, William T. Freeman, and Joshua B. Tenenbaum. Exploiting compositionality to explore a large space of model structures. In *Uncertainty in Artificial Intelligence*, 2012. (pages 30 and 41)
- C. Gu. *Smoothing spline ANOVA models*. Springer Verlag, 2002. ISBN 0387953531. (page 39)
- T.J. Hastie and R.J. Tibshirani. *Generalized additive models*. Chapman & Hall/CRC, 1990. (pages 15 and 76)
- James Hensman, Nicolo Fusi, and Neil D Lawrence. Gaussian processes for big data. *arXiv preprint arXiv:1309.6835*, 2013. (page 5)
- James Hensman, Andreas Damianou, and Neil Lawrence. Deep Gaussian processes for large datasets. In *Artificial Intelligence and Statistics Late-breaking Posters*, 2014. (page 56)
- Michiel Hermans and Benjamin Schrauwen. Recurrent kernel machines: Computing with infinite echo state networks. *Neural Computation*, 24(1):104–133, 2012. (page 74)
- Geoffrey E Hinton, Nitish Srivastava, Alex Krizhevsky, Ilya Sutskever, and Ruslan R Salakhutdinov. Improving neural networks by preventing co-adaptation of feature detectors. *arXiv preprint arXiv:1207.0580*, 2012. (page 81)

- Rob J. Hyndman. Time series data library, Accessed July 2013. URL <http://data.is/TSDLdemo>. (page 41)
- Tomoharu Iwata, David Duvenaud, and Zoubin Ghahramani. Warped mixtures for nonparametric cluster shapes. Bellevue, Washington, July 2013. URL <http://arxiv.org/pdf/1206.1846.pdf>. (page 92)
- E. T. Jaynes. Highly informative priors. In *Proceedings of the Second International Meeting on Bayesian Statistics*, 1985. (page 29)
- C.G. Kaufman and S.R. Sain. Bayesian functional anova modeling using Gaussian process prior distributions. *Bayesian Analysis*, 5(1):123–150, 2010. (page 84)
- C. Kemp and J.B. Tenenbaum. The discovery of structural form. *Proceedings of the National Academy of Sciences*, 105(31):10687–10692, 2008. (page 40)
- E.D. Klenske, M.N. Zeilinger, B. Scholkopf, and P. Hennig. Nonparametric dynamics estimation for time periodic systems. In *Communication, Control, and Computing (Allerton), 2013 51st Annual Allerton Conference on*, pages 486–493, Oct 2013. (page 37)
- Imre Risi Kondor. *Group theoretical methods in machine learning*. PhD thesis, Columbia University, 2008. (pages 22 and 25)
- Gabriel Kronberger and Michael Kommenda. Evolution of covariance functions for gaussian process regression using genetic programming. *arXiv preprint arXiv:1305.3794*, 2013. (page 40)
- N. Lawrence. Probabilistic non-linear principal component analysis with gaussian process latent variable models. *The Journal of Machine Learning Research*, 6:1783–1816, 2005. (page 26)
- N.D. Lawrence. Gaussian process latent variable models for visualisation of high dimensional data. *Advances in Neural Information Processing Systems*, 16:329–336, 2004. (page 100)
- N.D. Lawrence and R. Urtasun. Non-linear matrix factorization with Gaussian processes. In *Proceedings of the 26th Annual International Conference on Machine Learning*, pages 601–608. ACM, 2009. (page 100)
- Neil D Lawrence and Andrew J Moore. Hierarchical Gaussian process latent variable models. In *Proceedings of the 24th international conference on Machine learning*, pages 481–488. ACM, 2007. (page 73)
- Miguel Lázaro-Gredilla, Joaquin Quiñonero-Candela, Carl Edward Rasmussen, and Aníbal R Figueiras-Vidal. Sparse spectrum gaussian process regression. *The Journal of Machine Learning Research*, 99:1865–1881, 2010. (pages 32 and 39)
- J. Lean, J. Beer, and R. Bradley. Reconstruction of solar irradiance since 1610: Implications for climate change. *Geophysical Research Letters*, 22(23):3195–3198, 1995. (pages 50, 52, and 114)

- Yann LeCun and Yoshua Bengio. Convolutional networks for images, speech, and time series. *The handbook of brain theory and neural networks*, 3361, 1995. (page 25)
- Honglak Lee, Chaitanya Ekanadham, and Andrew Ng. Sparse deep belief net model for visual area v2. In *Advances in neural information processing systems*, pages 873–880, 2007. (page 75)
- D. Lerner and D. Asimov. The Sudanese Möbius band. In *SIGGRAPH Electronic Theatre*, 1984. (page 27)
- Percy Liang, Michael I Jordan, and Dan Klein. Learning programs: A hierarchical bayesian approach. In *Proceedings of the 27th International Conference on Machine Learning (ICML-10)*, pages 639–646, 2010. (page 41)
- Douglas A Lind, William G Marchal, Samuel Adam Wathen, and Business Week Magazine. *Basic statistics for business and economics*. McGraw-Hill/Irwin Boston, 2006. (pages 32 and 42)
- James Robert Lloyd. personal communication, 2013a. (pages 32 and 111)
- James Robert Lloyd. GEFCom2012 hierarchical load forecasting: Gradient boosting machines and gaussian processes. *International Journal of Forecasting*, 2013b. (page 37)
- James Robert Lloyd, David Duvenaud, Roger Grosse, Joshua B. Tenenbaum, and Zoubin Ghahramani. Automatic construction and natural-language description of nonparametric regression models. Technical Report arXiv:1402.4304 [stat.ML], 2014. (pages 29, 40, 45, and 53)
- I.G. Macdonald. *Symmetric functions and Hall polynomials*. Oxford University Press, USA, 1998. ISBN 0198504500. (page 79)
- S.N. MacEachern and P. Müller. Estimating mixture of Dirichlet process models. *Journal of Computational and Graphical Statistics*, pages 223–238, 1998. (page 96)
- David JC MacKay. *Bayesian methods for adaptive models*. PhD thesis, California Institute of Technology, 1992. (page 3)
- David J.C. MacKay. Introduction to gaussian processes. *NATO ASI Series F Computer and Systems Sciences*, 168:133–166, 1998. (pages 24 and 111)
- David JC MacKay. *Information theory, inference, and learning algorithms*. Cambridge University press, 2003. (page 3)
- James Martens. Deep learning via Hessian-free optimization. In *Proceedings of the 27th International Conference on Machine Learning*, pages 735–742, 2010. (page 75)
- JH Maunsell and David C van Essen. The connections of the middle temporal visual area (mt) and their relationship to a cortical hierarchy in the macaque monkey. *The Journal of neuroscience*, 3(12):2563–2586, 1983. (page 68)

- James Mercer. Functions of positive and negative type, and their connection with the theory of integral equations. *Philosophical Transactions of the Royal Society of London. Series A, Containing Papers of a Mathematical or Physical Character*, pages 415–446, 1909. (page 20)
- Charles A Micchelli, Yuesheng Xu, and Haizhang Zhang. Universal kernels. *The Journal of Machine Learning Research*, 7:2651–2667, 2006. (page 12)
- Ha Quang Minh, Partha Niyogi, and Yuan Yao. Mercer’s theorem, feature maps, and smoothing. In *Learning theory*, pages 154–168. Springer, 2006. (page 20)
- T.P. Minka. Expectation propagation for approximate bayesian inference. In *Uncertainty in Artificial Intelligence*, volume 17, pages 362–369. Citeseer, 2001. (page 87)
- @ML_Hipster. “... essentially, all models are wrong, but yours are stupid too.” – G.E.P. Box in a less than magnanimous mood., 2013. URL https://twitter.com/ML_Hipster/status/394577463990181888. (page 1)
- Grégoire Montavon, Dr Braun, and Klaus-Robert Müller. Layer-wise analysis of deep networks with Gaussian kernels. *Advances in Neural Information Processing Systems*, 23:1678–1686, 2010. (page 75)
- Radford M Neal. *Bayesian learning for neural networks*. PhD thesis, University of Toronto, 1995. (pages 17, 57, 68, 73, and 74)
- R.M. Neal. Density modeling and clustering using dirichlet diffusion trees. *Bayesian Statistics*, 7:619–629, 2003. (page 108)
- J.A. Nelder and R.W.M. Wedderburn. Generalized linear models. *Journal of the Royal Statistical Society. Series A (General)*, 135(3):370–384, 1972. (page 76)
- A.Y. Ng, M.I. Jordan, and Y. Weiss. On spectral clustering: Analysis and an algorithm. *Advances in Neural Information Processing Systems*, 2:849–856, 2002. (page 101)
- H. Nickisch and C. Rasmussen. Gaussian mixture modeling with Gaussian process latent variable models. *Pattern Recognition*, pages 272–282, 2010. (page 93)
- J. Nocedal. Updating quasi-newton matrices with limited storage. *Mathematics of computation*, 35(151):773–782, 1980. (page 87)
- Nutonian. Eureqa, 2011. URL <http://www.nutonian.com/>. (pages 40 and 41)
- Razvan Pascanu, Tomas Mikolov, and Yoshua Bengio. Understanding the exploding gradient problem. *arXiv preprint arXiv:1211.5063*, 2012. (page 74)
- T.A. Plate. Accuracy versus interpretability in flexible modeling: Implementing a trade-off using Gaussian process models. *Behaviormetrika*, 26:29–50, 1999. ISSN 0385-7417. (pages 32, 39, and 84)
- Daniel Preotiuc-Pietro and Trevor Cohn. A temporal model of text periodicities using Gaussian processes. In *EMNLP*, pages 977–988. ACL, 2013. (page 37)

- J. Quiñonero-Candela and C.E. Rasmussen. A unifying view of sparse approximate Gaussian process regression. *The Journal of Machine Learning Research*, 6:1939–1959, 2005. (pages 5, 99, and 108)
- Herschel Rabitz and Ömer F Aliş. General foundations of high-dimensional model representations. *Journal of Mathematical Chemistry*, 25(2-3):197–233, 1999. (page 86)
- W.M. Rand. Objective criteria for the evaluation of clustering methods. *Journal of the American Statistical association*, pages 846–850, 1971. (page 107)
- Carl Edward Rasmussen and Zoubin Ghahramani. Occam’s razor. *Advances in neural information processing systems*, pages 294–300, 2001. (pages 3 and 34)
- Carl Edward Rasmussen and Hannes Nickisch. Gaussian processes for machine learning (gpml) toolbox. *J. Mach. Learn. Res.*, 11:3011–3015, December 2010. ISSN 1532-4435. URL <http://dl.acm.org/citation.cfm?id=1756006.1953029>. (page 5)
- C.E. Rasmussen. The infinite Gaussian mixture model. *Advances in Neural Information Processing Systems*, 12(5.2):2, 2000. (page 92)
- C.E. Rasmussen and C.K.I. Williams. *Gaussian Processes for Machine Learning*, volume 38. The MIT Press, Cambridge, MA, USA, 2006. (pages 1, 5, 36, 37, and 92)
- Salah Rifai, Grégoire Mesnil, Pascal Vincent, Xavier Muller, Yoshua Bengio, Yann Dauphin, and Xavier Glorot. Higher order contractive auto-encoder. In *Machine Learning and Knowledge Discovery in Databases*, pages 645–660. Springer, 2011a. (page 64)
- Salah Rifai, Pascal Vincent, Xavier Muller, Xavier Glorot, and Yoshua Bengio. Contractive auto-encoders: Explicit invariance during feature extraction. In *Proceedings of the 28th International Conference on Machine Learning*, pages 833–840, 2011b. (page 64)
- Oren Rippel and Ryan Prescott Adams. High-dimensional probability estimation with deep density models. *arXiv preprint arXiv:1302.5125*, 2013. (page 74)
- D. Ruppert, M.P. Wand, and R.J. Carroll. *Semiparametric regression*, volume 12. Cambridge University Press, 2003. (pages 32 and 39)
- Yunus Saatçi, Ryan D Turner, and Carl E Rasmussen. Gaussian process change point models. In *Proceedings of the 27th International Conference on Machine Learning (ICML-10)*, pages 927–934, 2010. (page 42)
- Ruslan Salakhutdinov and Geoffrey Hinton. Using deep belief nets to learn covariance kernels for Gaussian processes. *Advances in Neural information processing systems*, 20:1249–1256, 2008. (page 39)

- M. Salzmann, R. Urtasun, and P. Fua. Local deformation models for monocular 3D shape recovery. In *IEEE Conference on Computer Vision and Pattern Recognition, CVPR*, pages 1–8, 2008. (page 100)
- Andrew Saxe, Pang W Koh, Zhenghao Chen, Maneesh Bhand, Bipin Suresh, and Andrew Y Ng. On random weights and unsupervised feature learning. In *Proceedings of the 28th International Conference on Machine Learning (ICML-11)*, pages 1089–1096, 2011. (page 75)
- Andrew M Saxe, James L McClelland, and Surya Ganguli. Dynamics of learning in deep linear neural networks. 2013. (page 75)
- Michael Schmidt and Hod Lipson. Distilling free-form natural laws from experimental data. *Science*, 324(5923):81–85, April 2009. ISSN 1095-9203. doi: 10.1126/science.1165893. (page 40)
- G. Schwarz. Estimating the dimension of a model. *The Annals of Statistics*, 6(2):461–464, 1978. (page 35)
- Jayaram Sethuraman. A constructive definition of Dirichlet priors. *Statistica Sinica*, 4:639–650, 1994. (page 97)
- E. Snelson and Z. Ghahramani. Sparse Gaussian processes using pseudo-inputs. *Advances in Neural Information Processing Systems*, 2006. (pages 5, 99, and 108)
- Ercan Solak, Roderick Murray-Smith, E. Solak, William Leithead, Carl Rasmussen, and Douglas Leith. Derivative observations in Gaussian process models of dynamic systems, 2003. (page 63)
- Nitish Srivastava. *Improving neural networks with dropout*. PhD thesis, University of Toronto, 2013. (page 81)
- Christian Steinruecken. *Lossless Data Compression*. PhD thesis, Cavendish Laboratory, University of Cambridge, 2014. (page 41)
- M. Stitson, A. Gammerman, V. Vapnik, V. Vovk, C. Watkins, and J. Weston. Support vector regression with ANOVA decomposition kernels. *Advances in kernel methods: Support vector learning*, pages 285–292, 1999. (page 85)
- Y.W. Teh, M.I. Jordan, M.J. Beal, and D.M. Blei. Hierarchical dirichlet processes. *Journal of the American Statistical Association*, 101(476):1566–1581, 2006. (page 108)
- M.E. Tipping and C.M. Bishop. Mixtures of probabilistic principal component analyzers. *Neural computation*, 11(2):443–482, 1999. (page 101)
- M. Titsias and N. Lawrence. Bayesian Gaussian process latent variable model. *AISTATS*, 2010. (page 100)

- L. Todorovski and S. Dzeroski. Declarative bias in equation discovery. In *International Conference on Machine Learning*, pages 376–384, 1997. (page 40)
- Jarno Vanhatalo, Jaakko Riihimaki, Jouni Hartikainen, Pasi Jylanki, Ville Tolvanen, and Aki Vehtari. Gpstuff, 2014. <http://mloss.org/software/view/451/>. (page 5)
- V.N. Vapnik. *Statistical learning theory*, volume 2. Wiley New York, 1998. (page 85)
- G. Wahba. *Spline models for observational data*. Society for Industrial Mathematics, 1990. ISBN 0898712440. (pages 39 and 86)
- J. Wang, J. Lee, and C. Zhang. Kernel trick embedded Gaussian mixture model. In *Algorithmic Learning Theory*, pages 159–174. Springer, 2003. (page 101)
- Sida Wang and Christopher Manning. Fast dropout training. In *Proceedings of the 30th International Conference on Machine Learning (ICML-13)*, pages 118–126, 2013. (page 82)
- T. Washio, H. Motoda, Y. Niwa, et al. Discovering admissible model equations from observed data based on scale-types and identity constraints. In *International Joint Conference On Artifical Intelligence*, volume 16, pages 772–779, 1999. (page 40)
- Andrew Wilson, David A Knowles, and Zoubin Ghahramani. Gaussian process regression networks. In *Proceedings of the 29th International Conference on Machine Learning*, pages 599–606, 2012. (page 74)
- Andrew Gordon Wilson and Ryan Prescott Adams. Gaussian process covariance kernels for pattern discovery and extrapolation. *arXiv: 1302.4245*, June 2013. (pages 32, 39, and 42)
- I-C Yeh. Modeling of strength of high-performance concrete using artificial neural networks. *Cement and Concrete research*, 28(12):1797–1808, 1998. (page 15)
- Y. Zhang and C. Sutton. Quasi-Newton Markov chain Monte Carlo. *Advances in Neural Information Processing Systems*, pages 2393–2401, 2011. (page 108)